

AEC RESEARCH AND
DEVELOPMENT REPORT

RESEARCH REPORTS

HW-84573

HW-84573

**QUARTERLY PROGRESS REPORT
METALLURGY RESEARCH OPERATION
OCTOBER, NOVEMBER, DECEMBER, 1964**

JANUARY 15, 1965

HANFORD LABORATORIES

HANFORD ATOMIC PRODUCTS OPERATION
RICHLAND, WASHINGTON

GENERAL  ELECTRIC

metadc100542

OF
ARY
Documents Collection
Jun 3 1965

LEGAL NOTICE

This report was prepared as an account of Government sponsored work. Neither the United States, nor the Commission, nor any person acting on behalf of the Commission:

A. Makes any warranty or representation, expressed or implied, with respect to the accuracy, completeness, or usefulness of the information contained in this report, or that the use of any information, apparatus, method, or process disclosed in this report may not infringe privately owned rights; or

B. Assumes any liabilities with respect to the use of, or for damages resulting from the use of any information, apparatus, method, or process disclosed in this report.

As used in the above, "person acting on behalf of the Commission" includes any employee or contractor of the Commission, or employee of such contractor, to the extent that such employee or contractor of the Commission, or employee of such contractor prepares, disseminates, or provides access to, any information pursuant to his employment or contract with the Commission, or his employment with such contractor.

HW-84573
UC-25, Metals, Ceramics
and Materials
(TID-4500, 37th Ed.)

QUARTERLY PROGRESS REPORT
METALLURGY RESEARCH OPERATION
OCTOBER, NOVEMBER, DECEMBER, 1964

By
Staff of Metallurgy Research Operation

FIRST UNRESTRICTED
DISTRIBUTION MADE

APR 27 '65

J. J. Cadwell	Manager
J. C. Tobin	Manager, Reactor Metals Research
T. K. Bierlein	Manager, Physical Metallurgy
R. L. Dillon	Manager, Chemical Metallurgy
R. G. Wheeler	Manager, Materials Engineering

January 15, 1965

HANFORD ATOMIC PRODUCTS OPERATION
RICHLAND, WASHINGTON

Work performed under Contract No. AT(45-1)-1350 between
the Atomic Energy Commission and General Electric Company

WARNING - PRELIMINARY REPORT

This report contains information of a preliminary nature and is prepared
primarily for the use of Hanford Atomic Products Operation personnel.
It is subject to revision on further checking or collection of additional data.

Printed by/for the U. S. Atomic Energy Commission

Printed in USA. Price \$5.00. Available from the Clearinghouse for Federal
Scientific and Technical Information, National Bureau of Standards,
U. S. Department of Commerce, Springfield, Virginia

Previous Reports in this series:

HW-76228	October, November, December, 1962
HW-77052	January, February, March, 1963
HW-77954	April, May, June, 1963
HW-78962	July, August, September, 1963
HW-79766	October, November, December, 1963
HW-81269	January, February, March, 1964
HW-82651	April, May, June, 1964
HW-84281	July, August, September, 1964

TABLE OF CONTENTS

SUMMARY	2.1
PHYSICAL METALLURGY	3.1
RADIATION EFFECTS ON METALS - J. L. Brimhall, H. E. Kissinger, J. J. Laidler, B. Mastel, and K. R. Merckx	3.1
Transmission Electron Microscopy	3.1
Electron Diffraction Contrast	3.5
X-Ray Diffraction Studies	3.6
Mechanical Properties	3.10
Slip Line Studies	3.12
SWELLING OF IRRADIATED FISSIONABLE MATERIALS - R. D. Leggett, J. L. Brimhall, B. Mastel, and H. A. Taylor	3.17
Irradiation Program	3.17
Postirradiation Examination	3.19
Supplemental Studies	3.53
Thin Foils	3.53
Line Broadening	3.56
PLUTONIUM PHYSICAL METALLURGY - R. D. Nelson, F. E. Bowman, H. E. Kissinger, and B. Mastel.	3.59
Phase Transformation Studies	3.59
Crystallographic Studies	3.72
REACTOR METALS RESEARCH	4.1
ALLOY SELECTION - T. T. Claudson	4.1
Mechanical Property Testing	4.1
IN-REACTOR MEASUREMENTS OF MECHANICAL PROPERTIES - J. A. Williams, D. H. Nyman, and J. W. Carter	4.3
In-Reactor Measurements	4.3
Capsule Development	4.6
Creep-Rupture Tests	4.8
IRRADIATION FACILITIES OPERATION - J. E. Irvin	4.11
Facilities Operation	4.11

IRRADIATION DAMAGE TO ZIRCALOY-2 -	
J. E. Irvin	4.15
Surveillance of NPR Tubing	4.15
FRACTURE STUDIES - R. G. Hoagland	4.22
DAMAGE MECHANISMS - F. A. Smidt	4.28
CHEMICAL METALLURGY	5.1
ENVIRONMENTAL EFFECTS	5.1
Water Environment with Hydrogen Addition -	
W. A. Burns	5.1
ATR GAS LOOP SUPPORT	5.10
Corrosion Studies - L. A. Charlot and	
R. E. Westerman	5.10
Corrosion of Super Alloys in High Temperature,	
High Velocity Helium - R. A. Thiede and	
R. E. Westerman	5.13
Equipment Status	5.13
ZrO ₂ - Oxygen Probe - D. W. Shannon	5.16
PRP MATERIALS DEVELOPMENT	5.18
In-Reactor Corrosion of PRTR Fuel Sheathing -	
H. C. Bowen and B. Griggs	5.18
PRODUCTION REACTOR CORROSION AND COATING	
STUDIES	5.19
Corrosion of High Silicon Aluminum	
Alloys - H. C. Bowen	5.19
N-REACTOR CORROSION AND HYDRIDING	5.21
Nickel-Plated Aluminum for High Temperature	
Aqueous Environments - A. B. Johnson	5.21
MATERIALS ENGINEERING	6.1
GAS LOOP DEVELOPMENT	6.1
Model Gas Loop Heater and Piping Redesign -	
D. R. Doman	6.1
Helium Purification System - J. H. Hoage	6.2
Weld Embrittlement - D. R. Ireland	6.3
PRTR PRESSURE TUBES	6.4
In-Reactor Monitoring - P. J. Pankaskie	6.4

Properties of Irradiated PRTR Pressure Tubes - M. C. Fraser	6.5
Irradiated Tube Testing Facility - P. M. Jackson	6.6
Movement of Zirconium Hydride in Zircaloy-2 - R. J. Evans	6.7
N-REACTOR PRESSURE TUBES	6.10
Zr-Nb Pressure Tubing - L. J. Defferding	6.10
PROPERTIES OF IRRADIATED STEEL STRUCTURES	6.11
Low Alloy Steel Pressure Vessels - D. R. Ireland	6.11

SUMMARYPHYSICAL METALLURGYRADIATION EFFECTS ON METALS

Foils of molybdenum irradiated to 10^{20} nvt contain defect clusters associated with complex interconnecting dislocation networks and rings, which at this high irradiation level are independent of carbon concentration. The dislocation rings have Burgers vectors $\frac{a}{2} \langle 111 \rangle$ and lie on $\{111\}$. Large loops which form during annealing at 750 C are interstitial in character and in general lie on $\{321\}$. Dislocations with Burgers vector $a[100]$ were detected. The development of a computer program aimed at predicting diffraction contrast effects and intensities has been initiated.

The lattice parameter of polycrystalline molybdenum undergoes a decrease in the exposure range of 10^{19} to 10^{20} nvt, but the X-ray line width continues to increase. Annealing of polycrystalline molybdenum irradiated to 10^{20} nvt results in recovery of line width, but not lattice parameter. Coalescence of defects into stable clusters at a temperature near 1000 C is presumably responsible for the line sharpening. Unit length increases of 0.00024 and unit lattice parameter increases of 0.00016 were measured in single crystals of molybdenum irradiated to 7×10^{18} nvt. These changes imply a high concentration of vacancies.

The effective activation volumes, V^* , for unirradiated and irradiated (1×10^{17} and 1×10^{18} nvt) molybdenum have been determined from strain-rate change experiments conducted at several temperatures, and the effect of postirradiation annealing has been investigated. V^* increases with temperature from a value of $10b^3$ at 295 K, and for low strains, V^* is much higher in the irradiated specimens. Annealing at 550 and 875 K restores V^* to the unirradiated value; annealing at 460 K only partially restores it.

Slip lines formed on the surface of single crystals of high purity molybdenum which had been bent after irradiation to 10^{19} nvt have been correlated with channels observed in the crystal by transmission microscopy.

Studies on a similar crystal, which contained approximately 450 ppm C as intentional impurity, has shown that slip line density is higher in the crystal containing carbon; carbides appear to be dislocation sources and barriers.

SWELLING OF IRRADIATED FISSIONABLE MATERIALS

The effects and interactions of burnup, burnup rate, temperature, external pressure, composition, metallurgical state, and geometry on the behavior of uranium during capsule irradiations have been investigated. The first controlled pressure (1000 psi) and temperature (450 C) capsule containing high purity and alloy uranium specimens was discharged from the reactor and disassembled for examination. A second controlled pressure (1000 psi) and temperature (575 C) capsule was charged in a reactor and is operating successfully. A third controlled pressure capsule is being assembled for in-reactor operation at a higher temperature of irradiation, 625 C.

Radiometallurgical examination of specimens irradiated in controlled temperature capsules corroborates that alloy additives of Fe + Si and Fe + Al reduce the swelling of uranium. Also, quenching alloy specimens from the gamma phase and reheating to high alpha or beta phase temperatures promotes additional irradiation stability. In general, the stability of U + Fe-Al specimens is superior to U + Fe-Si specimens.

Postirradiation density values of high-purity and alloy specimens from the first controlled pressure-temperature capsule show markedly the effectiveness of pressure in reducing swelling of uranium. Metallographic examination confirms the very small changes noted in density.

The development of a technique to thin dilute Fe-Si alloys of uranium for transmission electron microscopy has also yielded a semiquantitative method for determining the number of particles per unit volume in these alloys. The value of high resolution transmission electron microscopy in the determination of particle density is significant, particularly for observing particles with diameters smaller than 800 Å.

The breadth of (111) and (112) X-ray diffraction peaks in irradiated uranium has been determined as a function of postirradiation annealing.

Breadth decreases at temperatures to approximately 450 C, increases significantly in the range 450 to 500 C, and decreases again within the range of 500 to 650 C.

PLUTONIUM PHYSICAL METALLURGY

Information concerning the mechanism of the $\beta \rightarrow \alpha$ transformation of plutonium has been derived from experiments on the effect of compressive stresses and transformation rates on this transformation. Because the unit length is only slightly affected by transformation rate and reaches a constant value of 0.09 for stresses in the range of 9000 to 17,000 psi, it has been concluded that this transformation is probably diffusionless.

Banding of alpha grains and grain size effects due to compressive loading during the $\beta \rightarrow \alpha$ transformation have been further investigated: as little as 2000 psi can cause oriented banding; large alpha grains have formed in the matrix subjected to multiple transformations. Volume changes associated with transformation of a highly textured rod are extremely anisotropic.

Unit length changes during transformation of $\gamma \rightarrow \beta$ have been determined as a function of compressive stress, and transformation rate. This transformation is more strongly affected by transformation rate than is the $\beta \rightarrow \alpha$.

The effect of plastic deformation of (1) the parent beta and (2) parent gamma on the subsequent transformation to the phase stable at lower temperatures indicates that $\beta \rightarrow \alpha$ transformation is retarded and $\gamma \rightarrow \beta$ is accelerated.

Crystallographic relationships which arise as a consequence of phase transformations in plutonium are being derived by means of elevated temperature X-ray diffractometry. Considerable evidence has been obtained which indicates that repeated $\alpha \rightarrow \beta \rightarrow \alpha$ cycling does not significantly alter a strong 010 fiber texture initially present in a specimen, and that it does introduce a strong texture in a randomly oriented specimen. It is concluded at this time that the increased strength of beta phase plutonium prepared by transformation from gamma as compared with transformation from alpha is related to crystallographic orientation differences.

REACTOR METALS RESEARCH

ALLOY SELECTION

Several nickel-base alloys are being irradiated and tested to determine the effects of irradiation environment upon their mechanical properties. Specimens of Hastelloy X-280 irradiated at 280 C to exposures of 8.3×10^{20} nvt fast have been tested at 650 C. Results from these tests show a marked reduction in ductility. Uniform elongation values of about 5% were found as compared to values of 30% for similar specimens tested at room temperature.

Specimens of Inconel 625 have been irradiated at temperatures of 740, 280, and 50 C and tested at room temperatures. Data from these tests show that the higher irradiation temperature reduces the ductility of this material.

Specimens of Inconel 625 irradiated to 1×10^{20} nvt fast were tested at room temperature, 300 C, and 650 C. The yield and ultimate strengths at the highest test temperature were about 50% of the room temperature values. Marked reductions in ductility were also found.

IN-REACTOR MEASUREMENTS OF MECHANICAL PROPERTIES

Two in-reactor creep tests on annealed AISI 304 SS were started during the past quarter. At 550 C, 30,000 psi, the in-reactor creep rate was 2.8×10^{-5} /hr after 300 hr as compared to the out-of-reactor rate of 2.7×10^{-5} /hr. At 650 C, 20,000 psi, the in-reactor creep rate was 5.7×10^{-4} /hr after 60 hr, which decreased during a reactor outage to 3.6×10^{-4} /hr at 120 hr. No minimum rate was obtained during neutron irradiation. The out-of-reactor test produced a creep rate of 7.8×10^{-4} /hr at 60 hr and 3.9×10^{-4} /hr at 380 hr. In-reactor elongation on breaking was about 8 to 9% after 145 hr, while out-of-reactor elongation was 29% after 480 hr.

Out-of-reactor activation energies are 95,000 cal/mole from Hanford data and 100,000 cal/mole for data from the literature. In-reactor activation energies range from 60 to 70 Kcal/mole to 145 Kcal/mole and exhibit stress and temperature dependency.

An irradiated in-reactor test capsule was sent to Radiometallurgy for examination. The overall appearance of the capsule was very good.

The prototype design of a high temperature in-reactor creep capsule has been completed. The capsule will utilize molybdenum or tungsten heaters to achieve operating temperatures of 1900 C.

A high temperature creep-rupture apparatus has been developed. It can operate at temperatures of up to 1300 C. Creep-rupture tests on Haynes 25 and Hastelloy X tested in this apparatus, in vacuum, at 2100 F have been made. The Haynes 25 results indicate a more pessimistic rupture time with lower stress than was found in an earlier study.

IRRADIATION FACILITIES OPERATION

With the conclusion of ETR Cycles 66, 67, and 68, over 145 specimens were discharged from ETR core positions. The majority of these specimens were irradiated in the G-7 Hot Water Loop at approximately 550 F. Materials irradiated and discharged include Zircaloy-2, stainless steels, nickel-base alloys, and refractory metal alloys.

Two of the four special quadrants containing Inconel 600-Zircaloy-2 transition tensile specimens were discharged from the G-7 loop after exposures of approximately 1.0×10^{20} nvt (> 1 Mev). Two quadrants containing 12 control specimens were loaded into the out-of-reactor loop to receive exposures similar to that obtained in the G-7 loop. Special testing fixtures are being fabricated to test both the irradiated and unirradiated specimens at room temperature and at 550 F. This study is being performed in support of the "Advanced BONUS Core Development Program" being conducted by Combustion Engineering, Inc.

IRRADIATION DAMAGE TO ZIRCALOY-2

Tensile specimens fabricated from Zircaloy-2 tubing supplied for the N-Reactor at Hanford were used to determine weight gain and hydrogen pickup as a function of time, temperature, and integrated neutron exposure. The corrosion rate of the irradiated material was found to be a factor of 10 greater than that of the same material exposed under identical conditions in

an out-of-reactor loop. A flux dependence was also observed when two experiments were irradiated for the same time at different flux rates. The experiment in the higher flux zone exhibited a 50% greater weight gain than that of the test in the lower flux. Corrosion rates of the tubing material appear to be the same as those observed for rolled plate. Preliminary results indicate a theoretical corrosion hydrogen pickup of 50% or greater for each tube after an exposure of only 1.11×10^{20} nvt (> 1 Mev) or approximately 21 days at greater than 280 C. Additional data from long term exposures in both the in-reactor and out-of-reactor hot water loops will be obtained from specimens which are currently being tested. Tensile tests on these specimens are being conducted at room temperature and at 300 C.

FRACTURE STUDIES

Studies have been underway to determine the feasibility of using the double cantilever beam (DCB) specimen for evaluating the effects of in-reactor environments on the fracture properties of candidate reactor materials.

Due to the nature of the DCB specimen, a relatively large number of data, concerning both crack initiation and crack arrest fracture toughness, may be determined from a single specimen.

Preliminary test results using the DCB technique have been obtained on A302-B and Zircaloy-2. The crack initiation fracture toughness values for A302-B show a strong temperature dependence between -165 and -120 C. This contrasts with the crack arrest fracture toughness values which are nearly temperature independent in this temperature range. The crack initiation and crack arrest fracture toughness values for Zircaloy-2 possess nearly the same degree of temperature dependence between -130 and -90 C.

DAMAGE MECHANISMS

The present status of the theory of thermally activated flow which deals with the relationship between the effective stress and the activation energy is reviewed and compared with the experimental results determined in this study. It is found that the data fit several of the theoretical relations over a limited range but deviate markedly in other ranges.

An empirical relation, $U/c = 1 - (\tau^*/\tau_p)^{\frac{1}{2}}$, is found to give the best fit to most of the data. It satisfies the boundary conditions, and the observed temperature and strain rate dependence over a wider range than any of the theoretical relations.

CHEMICAL METALLURGY

ENVIRONMENTAL EFFECTS

Detailed analyses of zirconium alloy specimens discharged from the ETR G-7 loop following 16.5 days' exposure to the low-oxygen 280 C water of Cycle 65 were continued and comparisons have been made with control coupons exposed to deoxygenated water in an out-of-reactor autoclave. Materials included in this test are Irradiation Effects Program Zircaloy-2 from plate stocks 6515 and 6497, NPR Zircaloy-2, Zircaloy-4, nickel-free Zircaloy-2, and Zr-3 wt% Nb-1 wt% Sn heat treated for maximum corrosion resistance. Zircaloy-2 specimens were present in the annealed, 10, 20, 40, and 86% cold-worked condition, and the Zircaloy-4 and nickel-free Zircaloy-2 were exposed in the annealed condition only.

Comparisons of the behavior of these materials based upon incomplete analytical data available to date indicate that the weight gains of all alloys tested are comparable at each flux position and there is no effect of extent of cold work or of cold work versus annealing on weight gains. The ratio of weight gain in-reactor to weight gain out-of-reactor increased from about two to one at the lowest fast flux intensity ($< 6 \times 10^{12}$ nv) to about five to one at the highest fast flux position ($\sim 6 \times 10^{13}$ nv) except for the Zr-3 wt% Nb-1 wt% Sn alloy which showed no significant effect of flux on weight gain below about 6×10^{13} nv (> 1 Mev) and a maximum weight gain ratio of two to one at the highest flux position.

Hydrogen pickup fractions were generally higher for all irradiated specimens. No consistent or significant effect of flux intensity on hydrogen pickup was observed in the case of Zircaloy-2 specimens, but the Zircaloy-4 and nickel-free Zircaloy-2 alloys showed marked increases in pickup fractions with increasing flux intensity. Zr-3 wt% Nb-1 wt% Sn proved to be the

best alloy in this respect also, with no significant change in the hydrogen pickup fraction of about 15%. In-reactor hydrogen pickup fractions for the other alloys exceeded 34% in most cases.

ATR GAS LOOP SUPPORT

Hastelloy X-280 and Haynes 25 have been thermally cycled in 25 torr oxygen from room temperature to 2048 F. After 9 cycles (450 hr at 2048 F) Hastelloy X-280 was found far more resistant to oxidation, under conditions of thermal cycling than Haynes 25.

Samples of Haynes 25 and Hastelloy X have been exposed to helium (nominally "Grade A") at 350 psi and 2050 F, at velocities of the order of 525 fps. Following an oil leak in the compressor diaphragm, a sample of Haynes 25 was carburized clear through its 0.25-in. diam. Upon reexposure to the gas, after system cleanup, decarburization was rapid. Oxidation rates of both Haynes 25 and Hastelloy X in the high helium flow compare favorably with oxidation rates in a static system at equivalent oxygen pressures.

A revised zirconium electrolytic oxygen probe has been designed which uses air as a reference oxygen partial pressure. The new probe follows the theoretical voltage from below 1 ppm to 21% oxygen.

PRP MATERIALS DEVELOPMENT

Zircaloy corrosion coupons attached to a PRTR fuel element have been successfully irradiated for 2000 hr. The irradiation is continuing.

PRODUCTION REACTOR CORROSION AND COATING STUDIES

Aluminum alloys containing 7 to 10% silicon plus nickel and/or magnesium are being compared to 8001 aluminum for corrosion in 140 and 50 C process water and in high-purity, high-temperature water. In tests to date the 10% silicon alloy containing nickel and magnesium has corroded about 30% less than 8001 in nonisothermal loop experiments (140-70 C) at 25 fps velocity. In 360 C water all the silicon-containing alloys corrode more rapidly than 8001, especially those alloys containing magnesium. The nickel-containing

silicon alloys are more resistant to 400 C steam than 8001. All the silicon alloys pitted when galvanically coupled to stainless steel. No evidence of stress corrosion on any of the alloys has been seen to date.

N-REACTOR CORROSION AND HYDRIDING

Nickel-Plated Aluminum for High Temperature Aqueous Environments

Three nickel-plated Pu-Al fuel elements and five plated 8001 aluminum dummy elements were exposed in the C-1 in-reactor loop for approximately 1 month in pH 5.5 to 7.3 water at a water temperature of 260 C. The nickel plate was chemically deposited in thicknesses of 0.4 and 0.8 mils; the plated elements were subjected to heat treatments of 2.5, 10, and 40 hr at 400 C. Postirradiation metallography shows that the plate was retained, with relatively little corrosion on dummy elements (0.8 mil plate); attack on fueled elements was more pronounced, but was contained by nickel/aluminum diffusion layers.

MATERIALS ENGINEERING

GAS LOOP DEVELOPMENT

Model Gas Loop Heater and Piping Redesign

Two design modifications are being made on the model gas loop to investigate designs proposed for use in the ATR gas loop; (1) use of a compact two-stage heater, and (2) use of metallic foil internally insulated piping.

Helium Purification System

Helium gas purities of less than 0.1 ppm for gaseous impurities and less than 2 ppm moisture were achieved using an Engelhard, Inc., purification system. A bypass cleanup system was installed on the Gas Loop with excellent results in all remaining species but hydrogen.

Weld Embrittlement

The relative age embrittlement or loss in ductility of Hastelloy X and Hastelloy W weld filler metals is currently being investigated. The ductility is being measured from "free-bend" tests of longitudinal weld

samples of AISI 316 SS to Hastelloy X and Haynes 25 to Hastelloy X. The unaged properties have been determined and the aging is currently in progress.

PRTR PRESSURE TUBES

In-Reactor Monitoring

During this quarter 43 inspections of the PRTR pressure tubes were made. These inspections disclosed a new 15 mils deep fretted area in the tube in Process Channel 1653.

An analysis of inspection data during 1964 was made and resulted in the proposal of a new inspection schedule of about one-half the magnitude employed in the past several years.

Properties of Irradiated PRTR Pressure Tubes

The third report of information on postirradiation evaluation of Zircaloy-2 PRTR pressure tubes has been written. The data presented indicate that the PRTR Zircaloy-2 pressure tubes have high strength with ductility, are resistant to crack propagation, have low notch sensitivity, and, generally, have low hydride concentration.

Irradiated Tube Testing Facility

The Irradiation Tube Testing Facility has operated continuously during the past quarter on a program for evaluating irradiated Zircaloy-2 pressure tubing sections.

Movement of Zirconium Hydride in Zircaloy-2

A hydrided strip of Zircaloy-2 was connected to a direct current power supply to determine the effects of a direct current on zirconium hydride.

Metallographic studies indicate a small amount of hydride movement toward the negative end and a large movement of hydride from the hot center to the cool ends.

N-REACTOR PRESSURE TUBES

Zr-Nb Pressure Tubing

An order of 84 ft of 2.375 in. OD by 0.180 in. wall, Zr-2.5 wt% Nb pressure has been received. One-half of the tubing has 33% cold work, and the remainder has 50% cold work. The tubing will be used to determine burst and crack propagation properties.

PROPERTIES OF IRRADIATED STEEL STRUCTURES

Low Alloy Steel Pressure Vessels

This part of the program will determine the effects of irradiation on the crack propagation and burst test properties of ASTM A212 B. The irradiation of tube specimens will begin during the first half of 1965. The unirradiated properties and procedures for obtaining multiple data points from a single specimen are currently being investigated.

PHYSICAL METALLURGY

RADIATION EFFECTS ON METALS - J. L. Brimhall, H. E. Kissinger,
J. J. Laidler, B. Mastel, and K. R. Merckx

This program is directed toward establishing the combined effect of impurities and neutron irradiation on the properties and structure of specific metals, and deducing from thermally-activated recovery processes how the damage state can be altered. Present studies involve single and polycrystalline specimens of molybdenum, nickel, and rhenium. Work to date has been concentrated on molybdenum, with the efforts on nickel and rhenium confined to sample preparation and preliminary experiments.

Transmission Electron Microscopy

Foils of molybdenum containing < 10, 150, and 450 ppm carbon have been examined by transmission electron microscopy after an exposure of 10^{20} nvt ($E > 1$ Mev). Defect clusters were observed in all the samples and were generally associated with complex interconnecting dislocation networks and rings. The microstructure of all samples irradiated to this high exposure appears to be similar. This observation is in contrast to those made on specimens which received lower exposures, where a difference exists between the samples containing low and high amounts of carbon. Figure 3.1 is a micrograph of irradiated molybdenum containing 150 ppm carbon and shows the complex nature of the damage. An estimate of the number of spots gives an approximate concentration of 1×10^{16} /cc, about the same as observed in identical material after an exposure of only 10^{19} nvt. This apparent discrepancy can be explained if it is assumed that the spot defects are unresolved prismatic loops. As more defects are formed and migrate to the loops during the higher exposure, the loops grow. Adjacent loops find themselves close enough together that the attractive force between them results in coalescence of the loops into a single larger one. Interactions between growing loops of unlike Burgers vectors would result in complex network formation. These processes account for the reduction in the extrapolated density of spot defects. The Burgers vectors of the observed dislocation rings have been determined to be

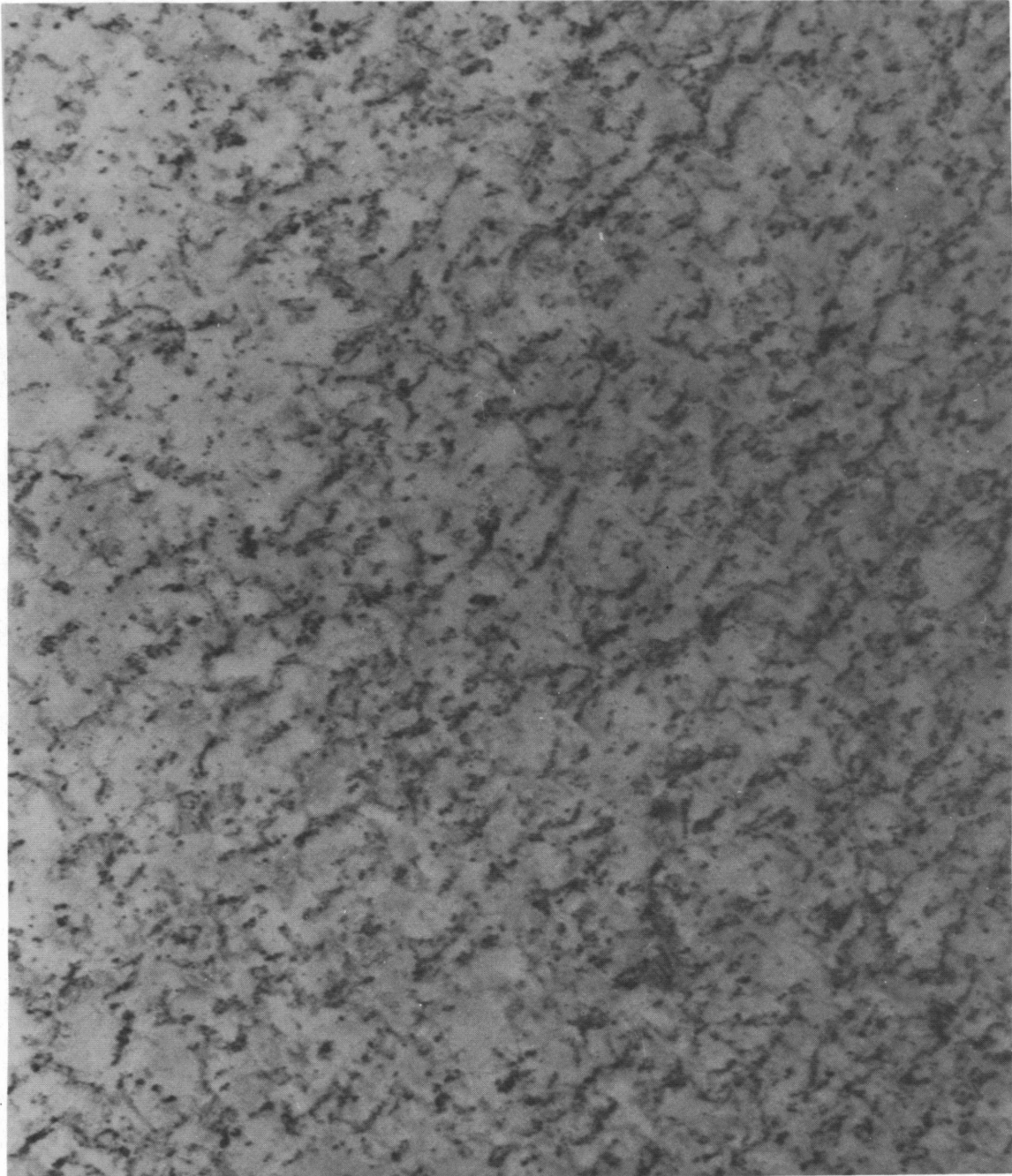


FIGURE 3.1

Defect Structures and Dislocation Networks Present in Molybdenum
Containing 150 ppm Carbon After Irradiation to 10^{20} nvt ($E > 1$ Mev)
(145,000X)

Neg. 2867A

$\frac{a}{2} \langle 111 \rangle$; the rings are uniformly distributed on all four (111) planes. Dislocations having other Burgers vectors were not observed in the "as-irradiated" state. Electron diffraction patterns of these foils revealed several anomalies. Forbidden reflections and pronounced streaking of spots parallel to $\langle 110 \rangle$ has been observed. The origin of the streaking may be associated with thin twins, stacking faults, or large point defect clusters. However, the microstructure did not disclose the presence of such features, and the true nature of the anomaly requires further investigation. The electron diffraction patterns of similar foils after annealing at 750 C for 2 hr did not show forbidden reflections or streaking.

Foils similar to those described above were deformed in tension and subsequently studied by microscopy. Fracture occurred across the diameter of the circular foil after very little deformation. Optical examination of the foil showed that the fracture path followed grain boundaries. Transmission microscopy failed to show dislocations or channels which could be ascribed to the deformation process. Obviously the energy for the formation and motion of a dislocation through the mass of irradiation-produced defects is extremely high and grain boundary cracking occurs preferentially.

The behaviour of the defect structures was further studied by annealing the irradiated foils at 750 C for 2 hr. The microstructure of the carbon-free and carbon-bearing molybdenum samples had several features in common. Small defect clusters (approximately $10^{15}/\text{cc}$) and dislocation loops of various sizes were present in both types of foils. Some of the larger loops are irregular in shape, which indicates that they were formed by coalescences of smaller loops. A number of the large loops has been identified as being interstitial in character and for the most part lie on $\{321\}$ planes. In addition to features described above, the molybdenum foils containing carbon contained irregular dislocation networks. Figure 3.2 shows the microstructure of a sample containing 450 ppm carbon after annealing at 750 C for 2 hr. Shown are loops, dislocation segments and nodes. Three different orientations of the same area are presented which permits assignment of Burgers vectors to dislocations making up a node. The reflection producing

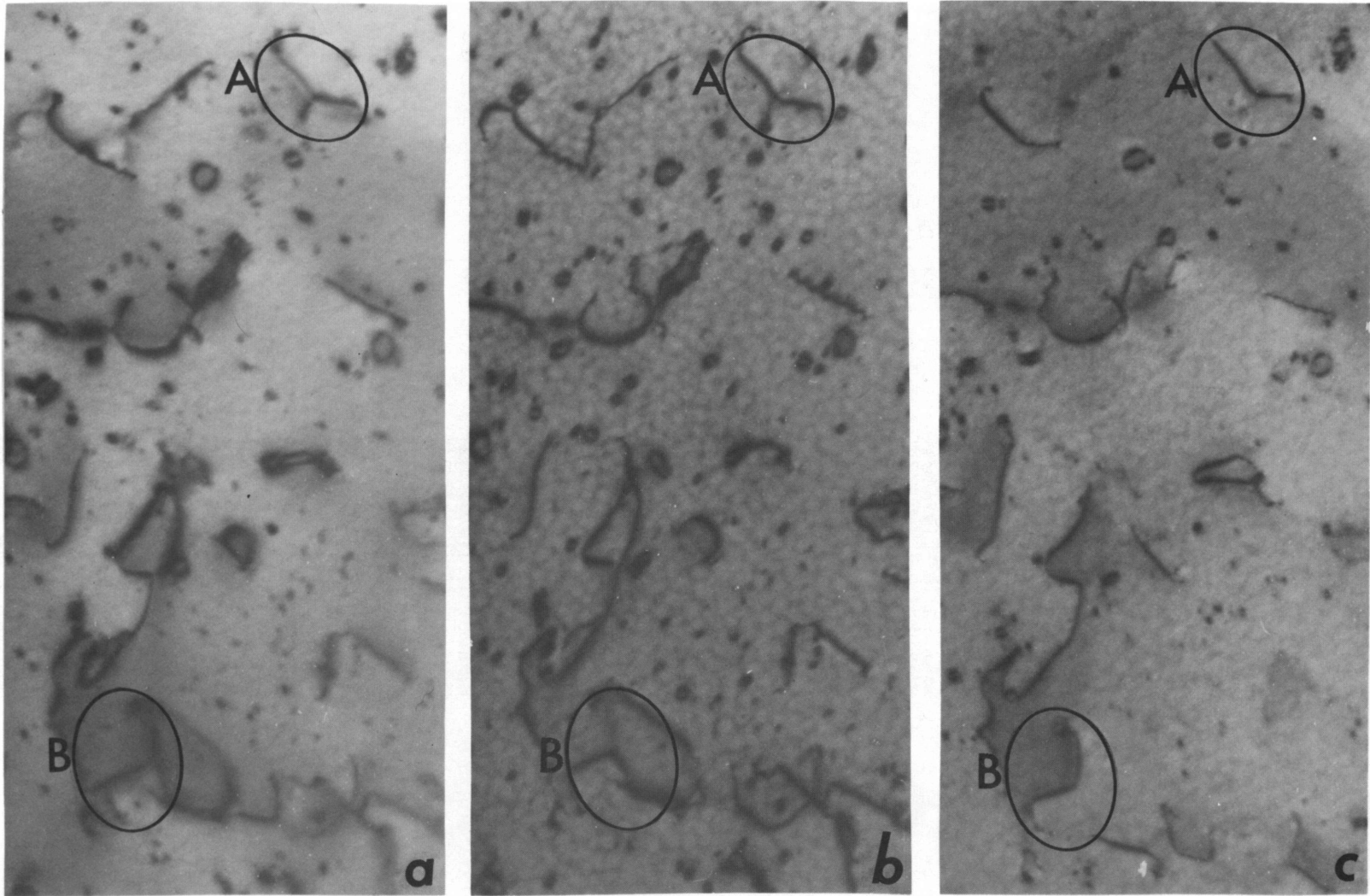
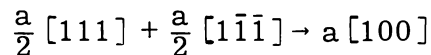


FIGURE 3.2

Dislocation Nodes Formed in Molybdenum Containing 450 ppm Carbon
Irradiated to 10^{20} nvt ($E > 1$ Mev) and Annealed at 750 C for 2 hr. Shown is the Same Area
with Three Different Reflections, (a) $(21\bar{1})$, (b) (002) , and (c) (011) Giving Contrast
(123, 000X)

contrast in micrograph (a) is $(21\bar{1})$, in (b) is (002) , and in (c) is (011) . The micrographs show that two dislocations of the node marked A appear in all three micrographs. However, the third dislocation disappears when the sample is orientated for the (011) reflection. From the invisibility criterion, Burgers vectors $\frac{a}{2} [\bar{1}11]$ and $\frac{a}{2} [002]$ may be assigned to those dislocations present in all three orientations and $\frac{a}{2} [1\bar{1}1]$ may be assigned to that dislocation which goes out of contrast when the (011) orientation is operating.

These Burgers vectors were chosen on the basis that $\sum_i b_i = 0$ at the node. Similarly, dislocations of the node designated at B which are present in all three micrographs will have a Burgers vector $\frac{a}{2} [\bar{1}11]$. Dislocations which are present only when the operating reflections are $(21\bar{1})$ and (002) have Burgers vectors $\frac{a}{2} [11\bar{1}]$ and dislocations having Burgers vectors $a [020]$ will give contrast when the reflections $(21\bar{1})$ and (011) are operating. From these analyses it is apparent that dislocations with Burgers vectors of $\frac{a}{2} \langle 111 \rangle$ and $a \langle 100 \rangle$ are present. These networks form during annealing when loops having different $\frac{a}{2} \langle 111 \rangle$ Burgers vectors interact. A reaction of the type



would explain the presence of dislocations having a $\langle 100 \rangle$ Burgers vectors.

The presence of the networks discussed above is evidence that the radiation damage sustained by the two types of samples, with and without carbon, is different. This conclusion is in agreement with observations made from samples irradiated to 10^{19} nvt in which dislocation loops were detected only in molybdenum containing carbon.

Electron Diffraction Contrast

A report⁽¹⁾ has been written which describes a computer program, its input data, and its method of evaluation. The computer program evaluates the change of intensity of an electron beam diffracted through a foil

1. K. R. Merckx. Computer Program for Electron Diffraction Intensities, HW-SA-3779, November 1964.

with a general straight dislocation. The "Two-Beam Dynamical Theory" was used to describe the conditions of diffraction through the foil. This program can also be used to describe diffraction around defect structures other than dislocations once the appropriate displacement functions due to the defect structures are derived. The derivations of the displacement equations around a dislocation loop are being developed in form suitable for application with this diffraction program. Modifications of the existing program's output are expected so that parameters having direct correlation with experimental measurements are reported. The preceding program utilizes a subroutine which determines the diffraction conditions through a foil without a fault. This subroutine has been incorporated into a program from which numerical results useful for evaluating foil thickness can be obtained. A suitable form of presentation is being sought for correlation with measurements of foil rotation and electron intensity made on the Philips EM-200. A check on the numerical results of the program is being made with an approximation reported in a paper by Howie and Whelan.⁽¹⁾ Since the electron intensity variation with foil rotation is dependent upon both the foil thickness and absorption parameter, a method of separating this dependence has yet to be devised. At the present time, the value for the absorption parameter must be known.

X-Ray Diffraction Studies

A series of molybdenum foils with three controlled carbon contents have been examined by X-ray diffraction after irradiation to 1×10^{20} nvt ($E > 1$ Mev). The three carbon levels are as follows: high-purity, less than 10 ppm C; medium carbon, ~ 150 ppm C, and high carbon, ~ 450 ppm C. Results of the X-ray measurements for the high-purity sample (< 10 ppm C) were reported in the previous Quarterly Report (HW-84281). The samples having higher carbon content have now been examined. Lattice parameters

1. A. Howie and M. J. Whelan. "Diffraction Contrast of Electron Microscope Images of Crystal Lattice Defects," Proc. Roy. Soc., London, series A, vol. 263, pp. 217-237, 1961, and vol. 267, pp. 206-230, 1962.

after 1×10^{20} nvt ($E > 1$ Mev) tended to be slightly lower for higher carbon contents. Lattice parameters for these samples, and for similar samples irradiated to 1×10^{18} nvt, 1×10^{19} nvt, and unirradiated, are summarized in Table 3.1. The significant feature in Table 3.1 is that the lattice parameter values after 1×10^{20} nvt are decreased from the values after 1×10^{19} nvt.

TABLE 3.1
LATTICE PARAMETERS OF MOLYBDENUM CONTAINING CARBON

<u>Carbon Content</u>	<u>Unirradiated</u>	<u>1×10^{18}</u>	<u>1×10^{19}</u>	<u>1×10^{20}</u>
< 10 ppm	$3.1471 \pm 0.0001 \text{ \AA}$	3.1476 \AA	$3.1481 \pm 0.0001 \text{ \AA}$	$3.1480 \pm 0.0003 \text{ \AA}$
150 ppm	3.1471 \AA	3.1476 \AA	$3.1481 \pm 0.0001 \text{ \AA}$	$3.1476 \pm 0.0002 \text{ \AA}$
450 ppm	3.1471 \AA	--	$3.1480 \pm 0.0001 \text{ \AA}$	$3.1476 \pm 0.0003 \text{ \AA}$

The X-ray lines were much broadened after 1×10^{20} nvt, making the lattice parameter measurements much less precise. Line profiles for the high-purity (< 10 ppm C) samples after irradiation are shown in Figure 3.3. These observations, together with the change in character of the spot defects seen in transmission electron microscopy, indicate that the type of damage accumulation is modified by some as yet unknown mechanism.

Samples of these molybdenum foils irradiated to 1×10^{20} nvt have been subjected to 2-hr anneals at 750 and 1000 C, after which the lattice parameters and line breadths were remeasured. The results are summarized in Table 3.2. It appears that the lattice parameter values will not return to the preirradiation value (3.1471 \AA) unless the annealing temperature is further increased. The line width, particularly for the high carbon (400 to 500 ppm C), is essentially completely recovered after the anneal at 1000 C. This is taken to indicate that the annealing coalesces the defects into quite stable clusters separated by regions of relatively perfect material, so that the line breadths are but slightly affected.

Four single-crystal molybdenum rods whose lengths and lattice parameters were carefully measured prior to irradiation have been received

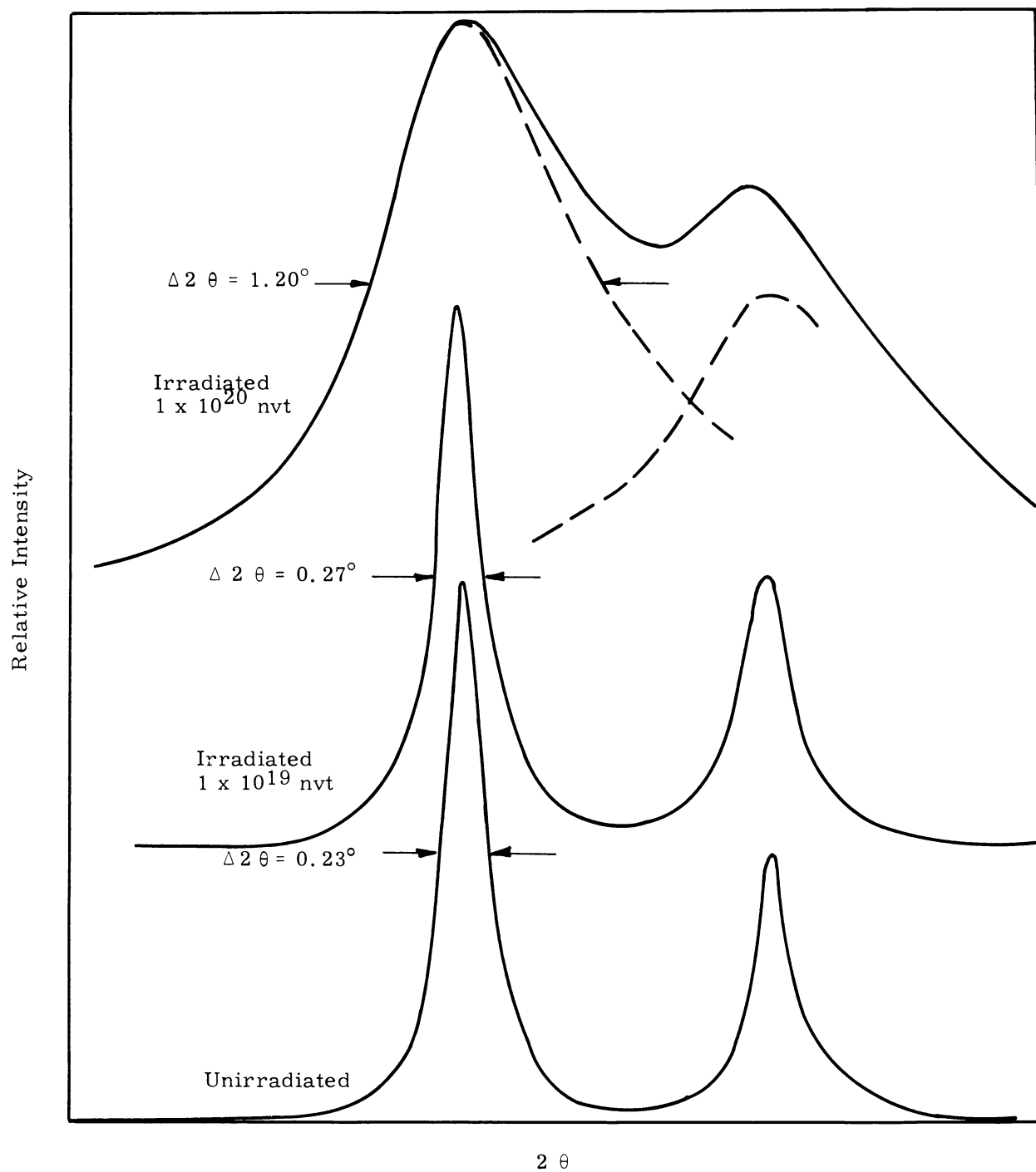


FIGURE 3.3

Effect of Irradiation Exposure on Breadth of 400 Line of Molybdenum
Cu K α Radiation

TABLE 3.2

EFFECT OF ANNEALING AFTER IRRADIATION TO 1×10^{20} nvt

Sample	750 C Anneal		1000 C Anneal	
	a_o	Width 400 Line	a_o	Width 400 Line
< 10 ppm C	3.1476 Å	0.512°	3.1474 Å	0.29°
150 ppm C	3.1474 Å	0.537°	---	---
450 ppm C	3.1474 Å	0.583°	3.1474 Å	0.25°

after an exposure of 7×10^{18} nvt ($E > 1$ Mev). Lengths were remeasured to 1 part in 10^5 , using the same technique as was used for the preirradiation measurements. One crystal was found to have a black or dark brown deposit on one end after irradiation which was easily removed by immersing in a NaOH solution. The measured length values were, therefore, made uncertain by this treatment. The results of length measurements are given in Table 3.3.

TABLE 3.3

LENGTH CHANGES
IN IRRADIATED SINGLE-CRYSTAL MOLYBDENUM RODS

(Length, cm)

Sample	Preirradiation	Postirradiation	% Change
1 A	5.23380	5.23502	+ 0.023
2 A	5.25325	5.25447	+ 0.023
3 A	5.24403	5.24520	+ 0.022
4 A*	5.25407	5.25455	+ 0.009

* Deposit removed from one end

Lattice parameters proved to be more difficult to measure. Despite the fact that the crystals were carefully annealed prior to irradiation, post-irradiation measurements made at different points on the same crystal showed considerable variation. All four samples yielded about the same

value of lattice parameter, $3.14765 \pm 0.00005 \text{ \AA}$, uncorrected for refraction. The corresponding preirradiation value was $3.14715 \pm 0.00003 \text{ \AA}$, making the irradiation-induced lattice parameter increase approximately 0.016%. This is lower than the length increase by a considerable amount. This is considered⁽¹⁾ a result of an excess of isolated vacancy defects; in fact, the vacancy concentration can be calculated. If $\Delta L/L$ is the fractional increase in length and $\Delta a/a$ is the fractional increase in lattice parameter, then

$$(\Delta L/L) - (\Delta a/a) = 1/3 C_v \quad (1)$$

where C_v is the vacancy concentration. Substituting the measured values:

$$0.00024 - 0.00016 = 1/3 C_v \quad (2)$$

$$C_v = 2.4 \times 10^{-4} \quad (3)$$

Since there are about 7×10^{22} lattice sites per cubic centimeter, the above concentration corresponds to 1.7×10^{19} vacancies/cc. This seems to be a rather large number considering the relatively low exposure given these samples.

These samples will be annealed at successively higher temperatures, and lengths and lattice parameters will be remeasured. If the vacancy concentration is as high as indicated, the annealing behaviour should provide a means for studying the motion of vacancy defects.

Mechanical Properties

Studies on the temperature and rate-dependence of the flow stress in unirradiated and irradiated polycrystalline molybdenum are now in progress. The experimental approach employs differential tensile tests conducted at various temperatures and strain rates. The polycrystalline molybdenum used for the tensile specimens is the source material used in the preparation

1. R. W. Baluffi and R. O. Simmons. J. Appl. Phys. vol. 31, p. 2284, 1960.

of single crystals for the purposes of this program, and is believed to have a purity of 99.98-99.99%, according to the manufacturer's analysis. Specimens were irradiated to 1×10^{17} and 1×10^{18} nvt ($E > 1$ Mev) at 60 C and were subjected to various postirradiation annealing treatments. These annealing treatments were conducted for 2 hr at temperatures of 460, 550, and 875 K, which correspond to the various recovery reactions known to occur in molybdenum. Although the experiments are by no means complete, a sufficient number of strain-rate change tests have been performed to give an insight into the nature of the defects serving as obstacles to thermally-activated dislocation motion. In the strain-rate change experiment, conducted at a constant temperature T , the effective activation volume, V^* , is given by the relation

$$V^* = kT \frac{\partial \ln \dot{\gamma}}{\partial \tau} \quad T ,$$

where $\dot{\gamma}$ is the strain rate, τ the flow stress, and k is Boltzmann's constant. In both the irradiated and unirradiated conditions, V^* was found to increase drastically on going from 295 to 323 K. At temperatures of 295 K and lower (i. e., $< 0.1 T_m$), the effective activation volume is of such a magnitude, approximately $10b^3$, that the controlling mechanism for thermally-activated deformation is probably one of overcoming the Peierls-Nabarro stress barrier. There is an obvious change in mechanism upon irradiation; at low strains, V^* is much higher than in the unirradiated condition. This is apparently a manifestation of the channeling of dislocations, observed and reported previously. Annealing at 550 and 875 K restores V^* to the unirradiated value, but the 460 K annealing treatment lowers V^* to a value intermediate between the unirradiated and as-irradiated state. It appears to be this reaction which eliminates the high value of V^* at low strains in the as-irradiated specimens and may therefore represent the breakup of small interstitial clusters. Further analysis is in progress.

Slip Line Studies

Sections cut perpendicular to the principle slip direction in a high-purity molybdenum single crystal which was irradiated to 10^{19} nvt and then bent have been thinned and observed in the electron microscope. Channels are observed as shown in Figure 3.4. The width, spacing, and general appearance of the channels is substantial evidence that the dislocation motion producing the channels produces the slip lines. A direct correlation between some lines seen on the polished foil in the optical microscope and the channels seen in the electron microscope has been made.

Crystallographic analysis shows the large channels to be parallel to the (011) or (101) planes. Some of the smaller branching channels are parallel to {112} planes as indicated on Figure 3.4. Islands of spot defects in the channels are also observed analogous to the islands of unslipped material seen in the slip bands.

The observations of these channels are in agreement with the conclusion reached previously on the importance of cross slip in channel formation. ⁽¹⁾ The few dislocations in the channels exist mainly along the edge of the channel. This is evidence that the channels and slip lines grow wider during deformation through dislocations sweeping out defects along the edge of the channel. A wide channel can also form, however, by two closely spaced channels merging. This would result in the formation of the islands of spot defects mentioned earlier.

Sections cut from a deformed unirradiated single crystal of molybdenum have been observed by transmission electron microscopy. Isolated tangles of dislocations are seen, distributed fairly uniformly throughout the matrix. There is no evidence of dislocation motion which would lead to a channeling behaviour.

1. Quarterly Progress Report, Metallurgy Research Operation, July, August, September, 1964, edited by J. J. Cadwell, HW-84281, pp. 3.16-3.22. September 15, 1964.

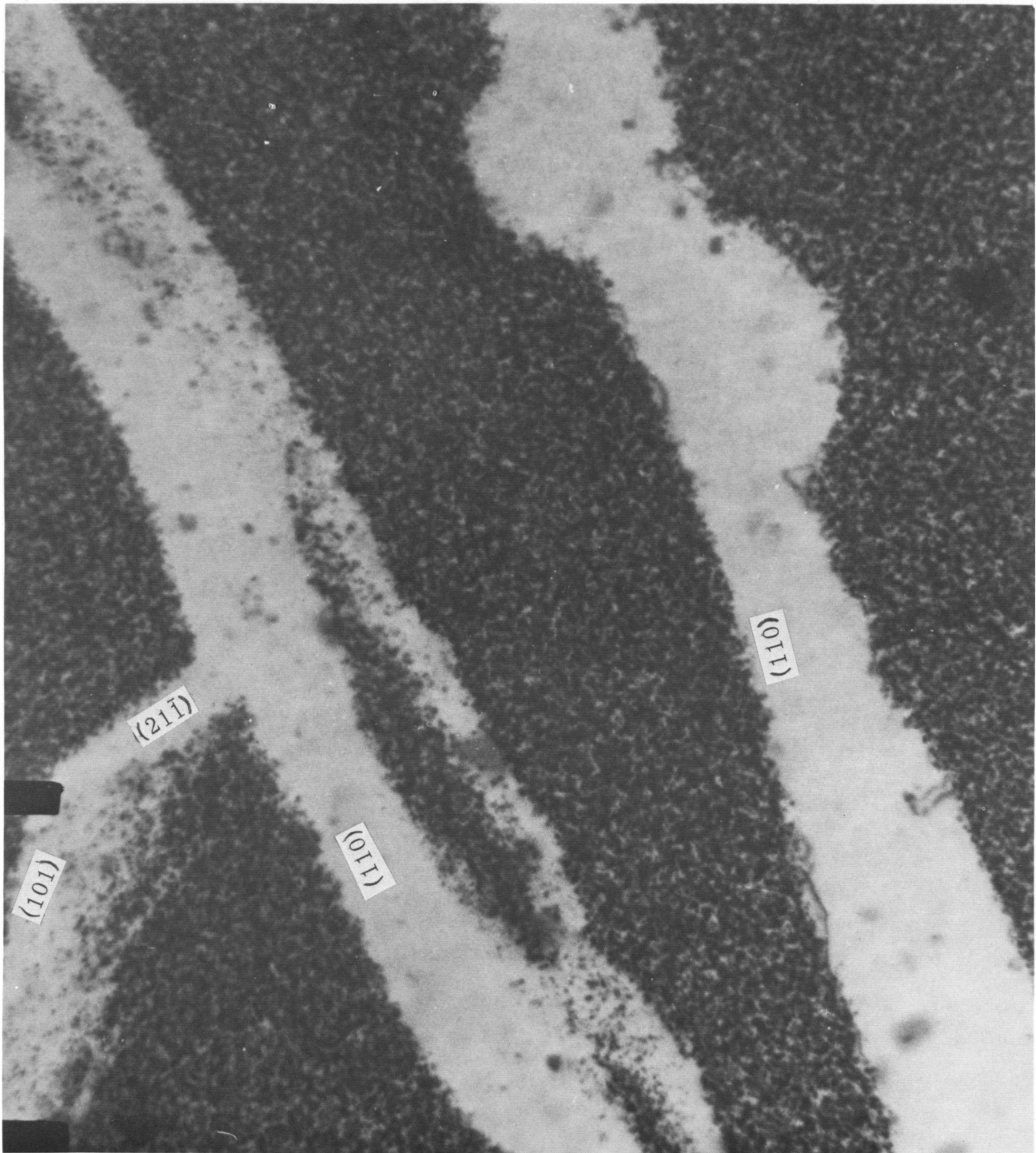


FIGURE 3.4

Dislocation Channels in Bent Irradiated Single Crystal of Molybdenum
(50,000X)

Neg. 90C

Slip line formation in a molybdenum single crystal containing 450-550 ppm carbon which was irradiated to 10^{19} nvt and then bent has also been studied. The orientation of the crystal with respect to the bending loads and the operative slip systems is shown in Figure 3.5.

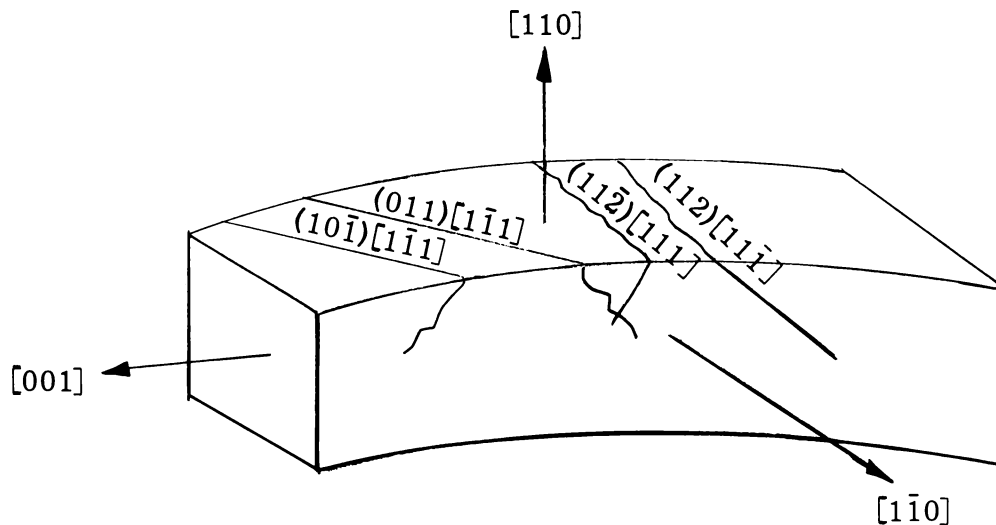


FIGURE 3.5

Orientation of Irradiated Bent Molybdenum Crystal
Containing 450-500 ppm C

There are several distinguishing features of the slip lines in this crystal as compared to the high-purity molybdenum. At least two principle slip directions are active in the initial deformation whereas only one direction is predominant in the high-purity molybdenum. The average width of the lines is less but the density of slip lines is greater in the molybdenum containing carbon. The slip lines were also visibly affected by the presence of the carbides.

When observed by surface replicas, the coarse irregular slip lines have many kinks and appear to "flow around" the carbides as shown in Figure 3.6. These kinks can also be seen where no carbides are present. In this case, a carbide probably lies beneath the surface. Short slip line segments which appear to emanate from carbides are also seen (Figure 3.7).

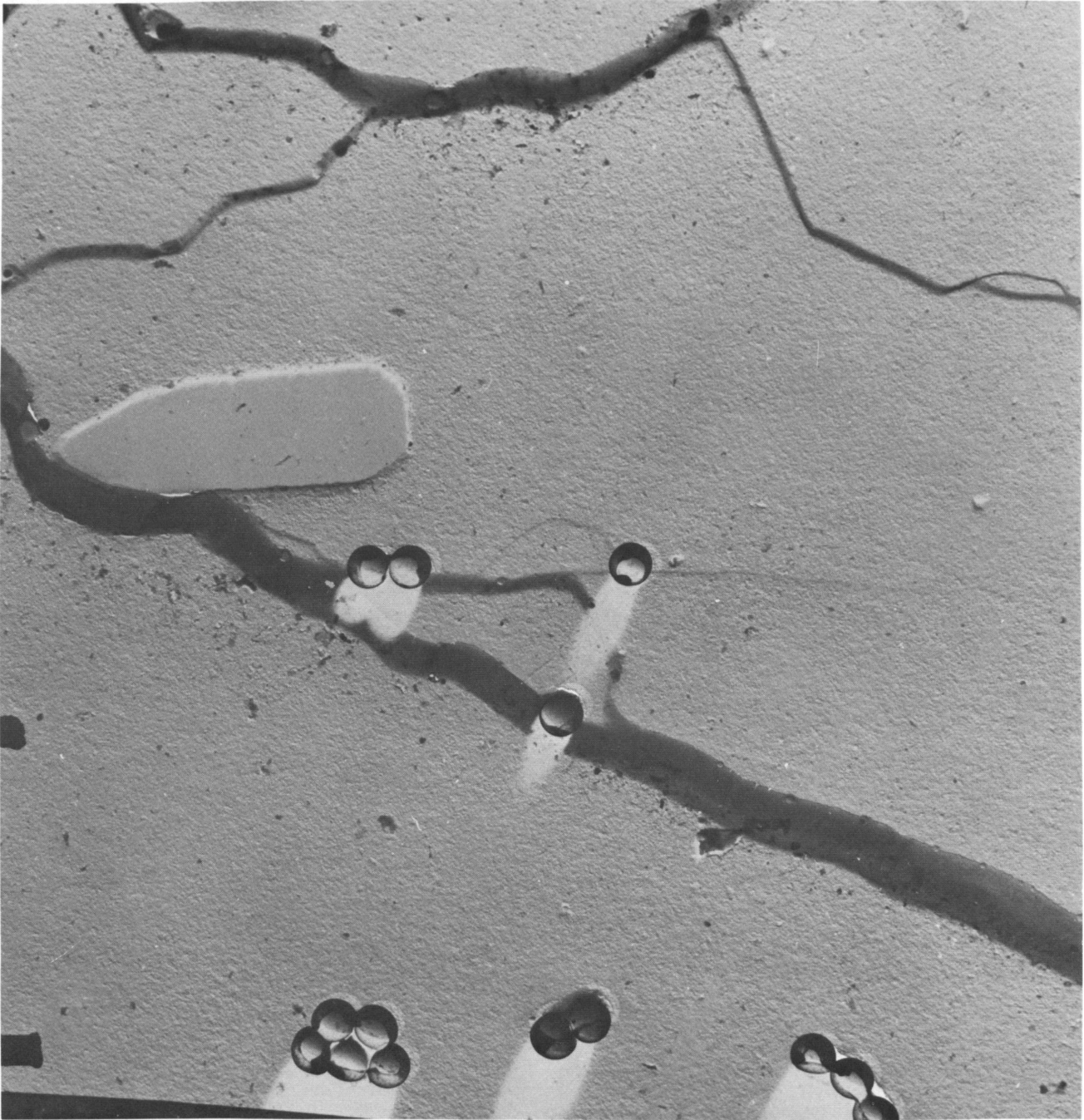


FIGURE 3. 6

Slip Line Structure in Bent Irradiated Molybdenum Single Crystal
Containing 450-550 ppm Carbon Denoting Barrier Affect of Carbides
(5000X)

Neg. 131A

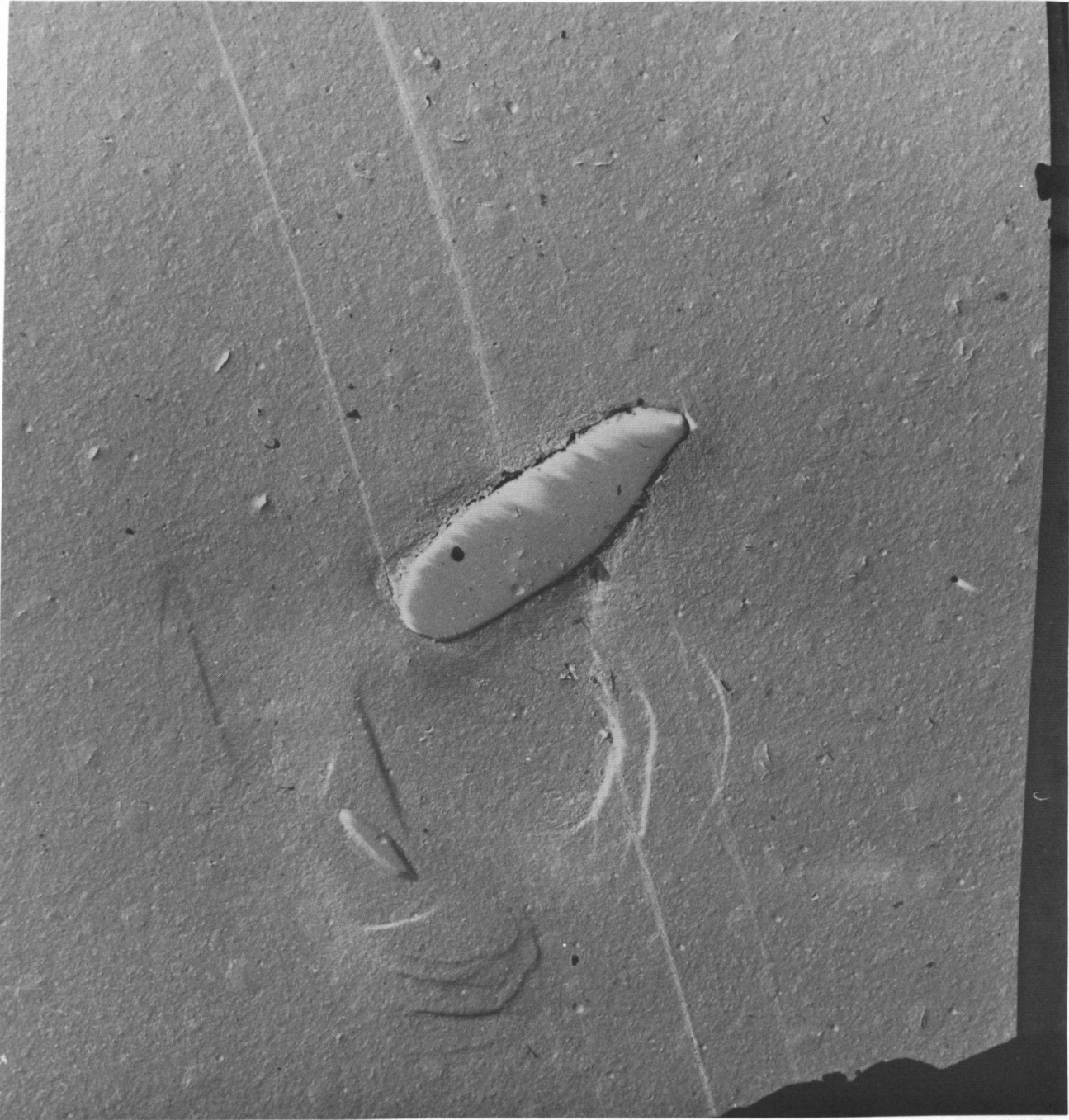


FIGURE 3.7

Slip Line Structure in Bent Irradiated Molybdenum Single Crystal
Containing 450-500 ppm Carbon Denoting the Straight Slip Lines
and Slip Line Segments Around Carbides
(5000X)

Neg. 137D

It appears that the carbides are acting as dislocation sources as well as dislocation barriers. It is difficult to determine if the straight lines curve around the carbides. They appear to fan out or sometimes disappear in the region surrounding the carbide, Figure 3.7.

SWELLING OF IRRADIATED FISSIONABLE MATERIALS - R. D. Leggett,
J. L. Brimhall, B. Mastel, and H. A. Taylor

When fissionable metals are irradiated, the ordered metallic structure is perturbed in a number of ways. High energy neutrons and fission fragments collide with metal atoms, knocking them out of their structural positions. The resultant defects, vacancies, interstitials, dislocation loops, etc., can adversely affect metallic properties. Similarly, the fission products generated, some of which are noble gases, may be incompatible with the structure and so precipitate or coalesce as second phase inclusions or gas pores. Furthermore, the high localized temperatures associated with the fission event can cause anisotropic fissionable metals such as uranium to drastically change shape in accordance with the crystallography of the specimens. These effects and their interactions are being studied with regard to the influence of irradiation variables such as the specimen temperature, burnup, burnup rate, and external pressure, and of metallurgical variables such as composition, structure, and geometry. The primary emphasis to date on this program has been that of determining the basic processes responsible for the behaviour of uranium irradiated at temperatures in the high alpha, where swelling is known to be important. Fundamental information developed by this program will provide a basis for engineering exploitation of the many beneficial attributes of metal fuels for use in reactor applications.

Irradiation Program

The first high pressure swelling capsule (P-2), constructed according to the design of the prototypical controlled pressure-temperature capsule

described in HW-82651, ⁽¹⁾ was discharged from the reactor after reaching goal exposure and disassembled in the Radiometallurgy Laboratory. The capsule operated in-reactor at a control pressure of 1000 psi and a control temperature of 450 C, regardless of the operating state of the reactor. This capsule contained six high-purity uranium specimens, two U + Fe-Al specimens, and two U + Fe-Si specimens representing several metallurgical states. Each specimen is half tubular in shape, being derived from a hollow cylinder 5/8 in. long, 1/2 in. OD, and with 0.030 in. wall thickness.

A second controlled pressure-temperature capsule (P-3) was charged into a reactor and is operating successfully at goal conditions of temperature and pressure, namely 575 C and 1000 psi. It, too, contains high-purity uranium, U + Fe-Al, and U + Fe-Si specimens of the half tubular geometry and several metallurgical states are represented. It is expected that radio-metallurgical examination of the irradiated specimens will provide greater insight into the effect of pressure on "growth" induced, crystallographically aligned tearing.

A sister capsule (P-4) to the previous two pressurized capsules is being assembled for in-reactor operation at 1000 psi and 625 C. The next series of capsules will be made to operate at a lower pressure; 500 psi is contemplated.

Recent swelling capsule irradiations have emphasized the need for precise pre- and postirradiation density values of uranium specimens because of the small amount of swelling being observed. A one-pan analytical substitution type balance, modified to weigh samples in air and in liquid beneath the balance case, is being used to determine density of individual unirradiated specimens to an accuracy of $\pm 0.01 \text{ g/cm}^3$.

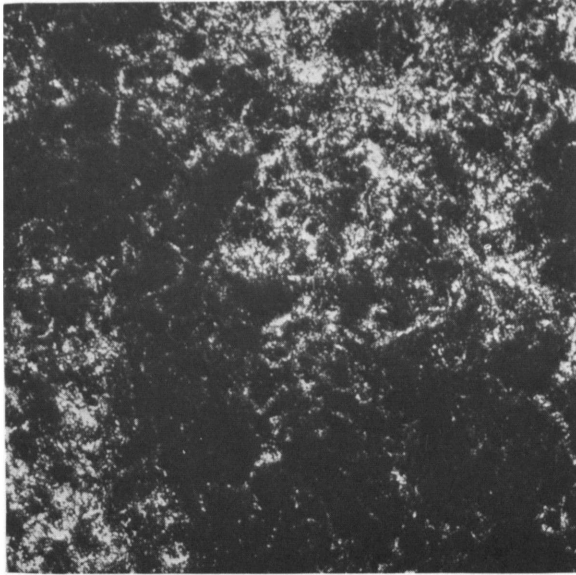
1. Quarterly Progress Report, Metallurgy Research Operation, April, May, June, 1964, edited by J. J. Cadwell, HW-82651, pp. 3.16-3.20, July 15, 1964.

Postirradiation Examination

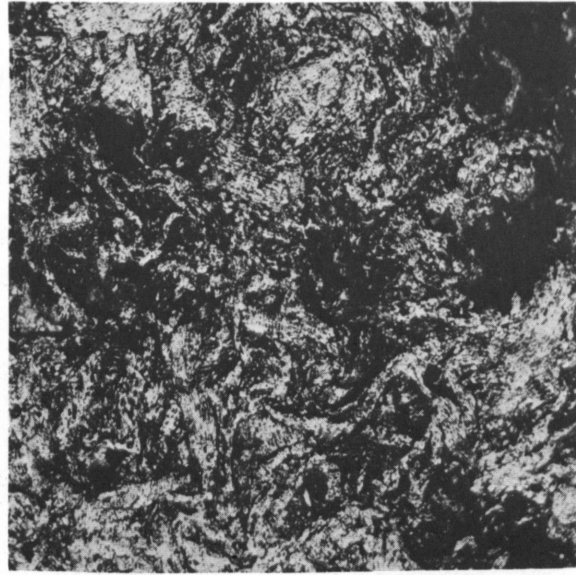
The metallographic examination of the high-purity uranium, U + Fe-Al and U + Fe-Si specimens which were irradiated to 0.16 at. % BU in Capsule No. 28 has been completed. This capsule was not controlled but operated from 400-500 C when the reactor was up and cooled to ambient when the reactor went down. Pertinent irradiation data concerning these samples was reported in HW-84281.⁽¹⁾ Of the five high-purity uranium specimens in this capsule it was only possible to recover and do metallography on the two as-extruded specimens. The others were too badly swollen. Figure 3.8(a) shows the gross tearing that occurred in one of the as-extruded samples. In the electron microscope both grain boundary tears and crystallographically aligned microtears (Figure 3.9) were identified. These observations agree with other data obtained with similar specimens irradiated in this temperature range. The grain boundary tears formed when the temperature was near 400 C and the aligned tears when the temperature was near 500 C. Once formed both would probably continue to grow with additional irradiation at intermediate temperatures.

The swelling observed in the U + 140 Fe-95 Si specimen included in Capsule 28 was but a small fraction of the swelling observed in the high-purity specimens (2% as opposed to 52%). The optical microstructure of the U + Fe-Si specimen depicted in Figure 3.8(b) reveals the "swirled" structure typical of this irradiation temperature but only a very few tears are present as compared with the high-purity specimen shown in Figure 3.8(a). The limited tearing revealed by electron microscopy is shown in Figure 3.10. A still further reduction in swelling was realized by a U + 400 Fe-640 Al specimen that had been quenched from 1000 C and

1. Quarterly Progress Report, Metallurgy Research Operation, July, August, September, 1964, edited by J. J. Cadwell, HW-84281, Table 3.4, p. 3.37. September 15, 1964.

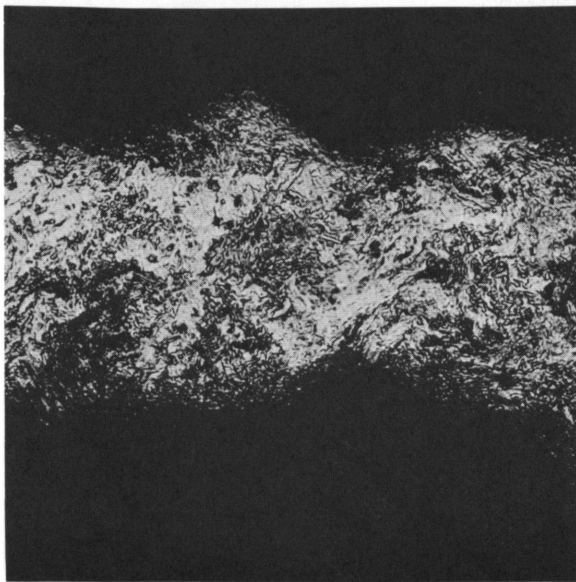


(75X)

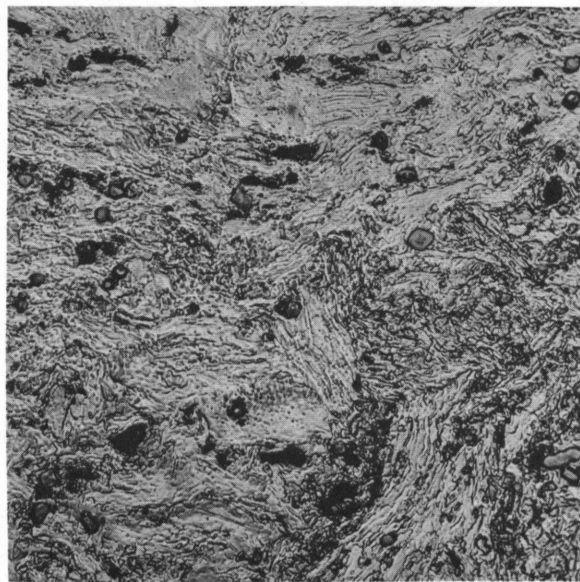


(250X)

(a) High Purity Uranium (28B-1) - As-Extruded $\frac{\Delta V}{V} = 52\%$



(75X)



(250X)

(b) U + 140 Fe-95 Si (28A-2) at 1000 C for 24 hr
Water Quenched + 525 C for 24 hr $\frac{\Delta V}{V} = 2\%$

FIGURE 3.8

Comparison of Tearing in High Purity Uranium and U + Fe-Si Specimens
Irradiated to 0.16 at. % BU at 400-500 C in Capsule No. 28
Neg. C5058, C4738, C5062, C4742

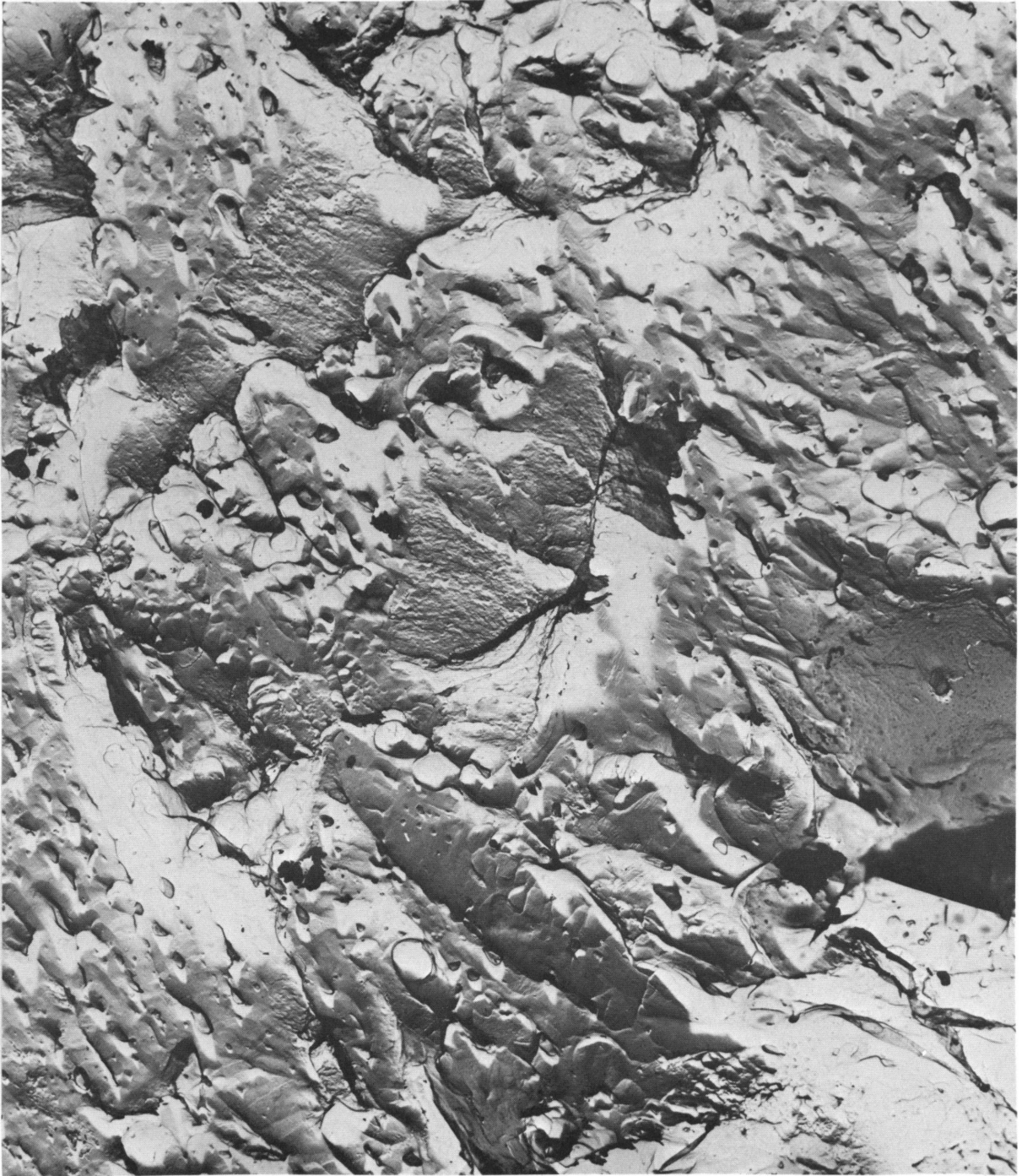


FIGURE 3.9

Grain Boundary Tearing and Crystallographically Aligned Microtearing
in High Purity Uranium Specimen 28B-1 Irradiated to 0.16 at. % BU
at 400-500 C (3500X)

Neg. 2877A

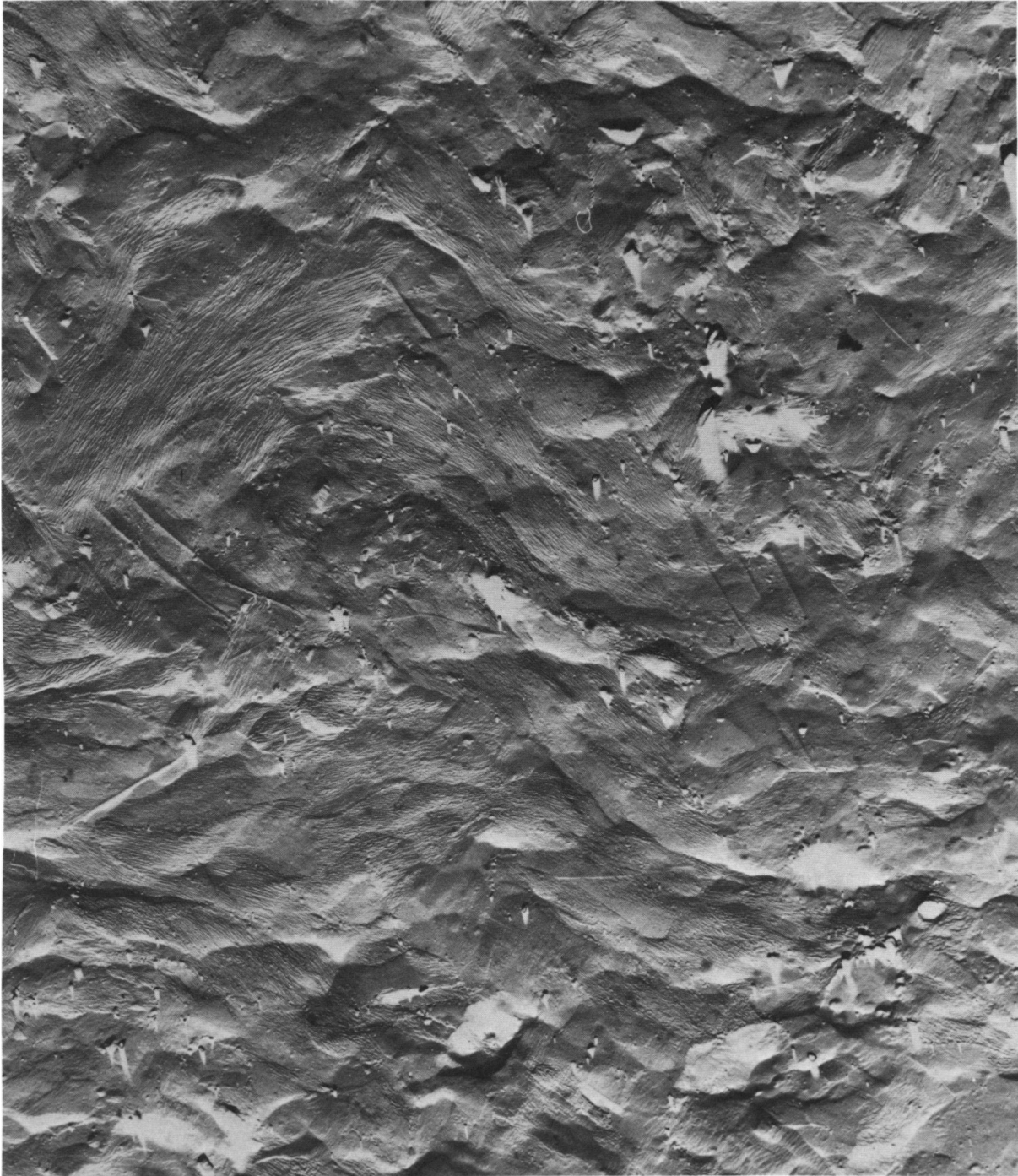


FIGURE 3.10

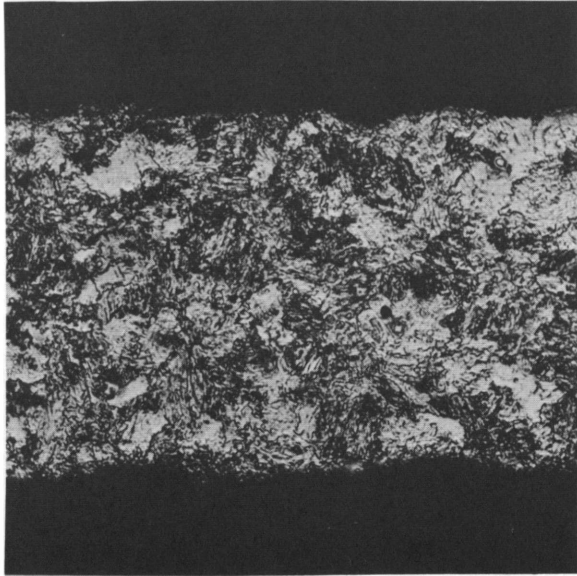
Limited Tearing in U + 140 Fe-95 Si Specimen 28A-2
Irradiated to 0.16 at.% BU at 400-500 C
(3500X)

Neg. 2875A

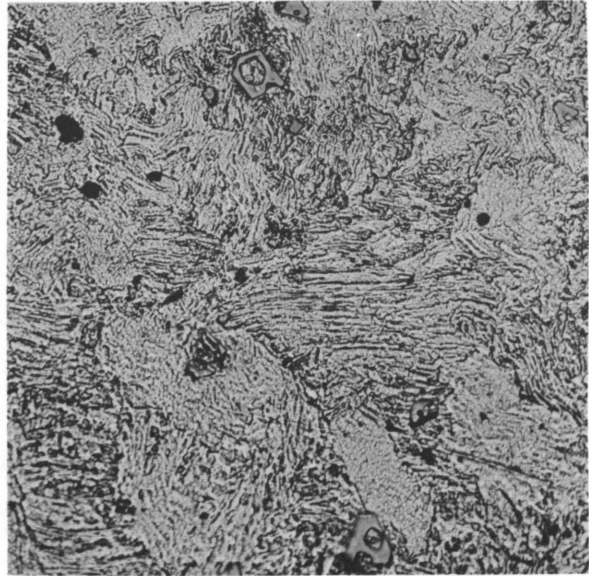
reheated at 525 C for 24 hr prior to irradiation. The optical microstructure is shown in Figure 3. 11(a) and an electron micrograph is shown in Figure 3. 12. There is very little difference in the microstructure of the U + Fe-Si and the U + Fe-Al specimens in spite of the differing amounts of swelling which were measured (2% versus 0. 5%). This is due to a few relatively large tears that existed in a relatively small region of the U + Fe-Si specimen. The beta heat-treated specimen of the U + Fe-Al alloy swelled more than either the gamma-alpha treated U + Fe-Al or U + Fe-Si specimens but of course, swelled considerably less than high-purity uranium. The optical microstructures of the U + Fe-Al specimen in the two heat-treated states are compared in Figure 3. 11. An electron micrograph of the beta treated specimen, Figure 3. 13, shows a moderate amount of tearing commensurate with the measured 4. 5% swelling.

The remaining three general swelling capsules, No. 22, 23, and 27, of the series of six capsules containing dilute uranium alloy specimens in addition to the high-purity uranium specimens were opened in Radiometallurgy, the specimens recovered and their densities determined. The composition, preirradiation heat treatment, irradiation conditions, as-irradiated density and calculated volume change are shown for each sample in Tables 3. 4, 3. 5, and 3. 6, respectively. Similar data for Capsule No. 26 was reported in HW-82651⁽¹⁾ and for Capsules 28 and 29 in HW-84281.⁽²⁾ The macro-appearance of the specimens from Capsules 22, 23, and 27 are illustrated in Figures 3. 14, 3. 15, and 3. 16, respectively. The metallographic examination of these specimens will be initiated shortly.

-
1. Quarterly Progress Report, Metallurgy Research Operation, April, May, June, 1964, edited by J. J. Cadwell, HW-82651, Table 3. 2, p. 3. 22. July 15, 1964.
 2. Quarterly Progress Report, Metallurgy Research Operation, July, August, September, 1964, edited by J. J. Cadwell, HW-84281, Table 3. 4, p. 3. 37, and Table 3. 5, p. 3. 39. September 15, 1964.

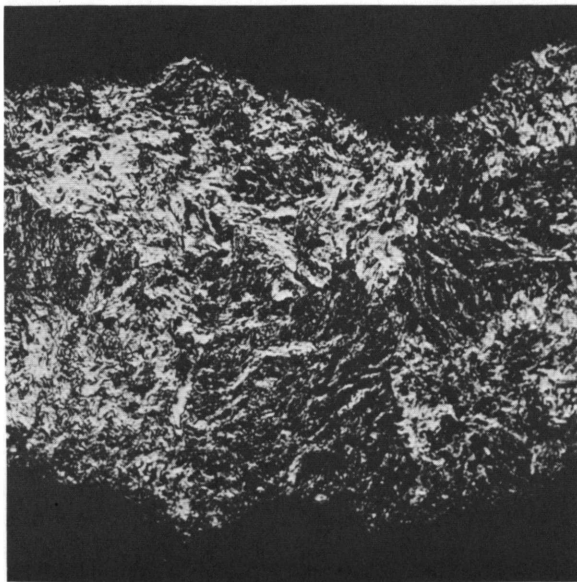


(75X)

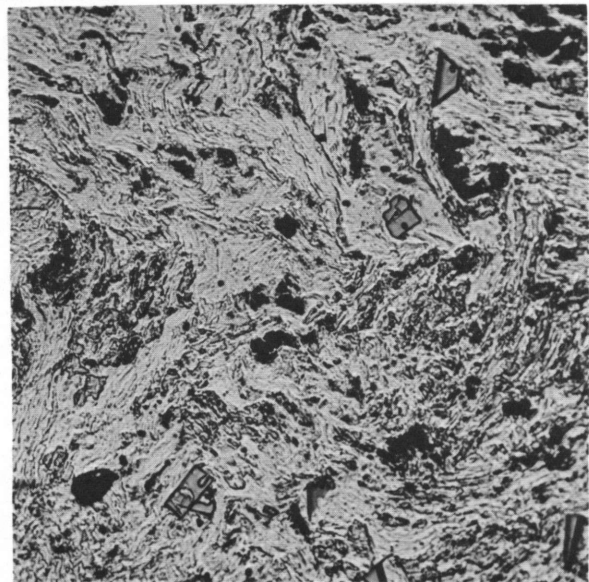


(250X)

(a) 1000 C for 24 hr - Water Quenched + 525 C (28A-1)

for 24 hr $\frac{\Delta V}{V} = 0.5\%$ 

(75X)



(250X)

(b) 730 C for 15 min - Water Quenched (28D-1) in the Bulk

Prior to Specimen Machining. $\frac{\Delta V}{V} = 4.5\%$ FIGURE 3.11Influence of Preirradiation Heat Treatment on Tearing
in Specimens of U + 400 Fe-640 Al

Irradiated in Capsule No. 28 at 400-500 C to 0.16 at.% BU

Neg. C4841, C5264, C-4842, C-5265

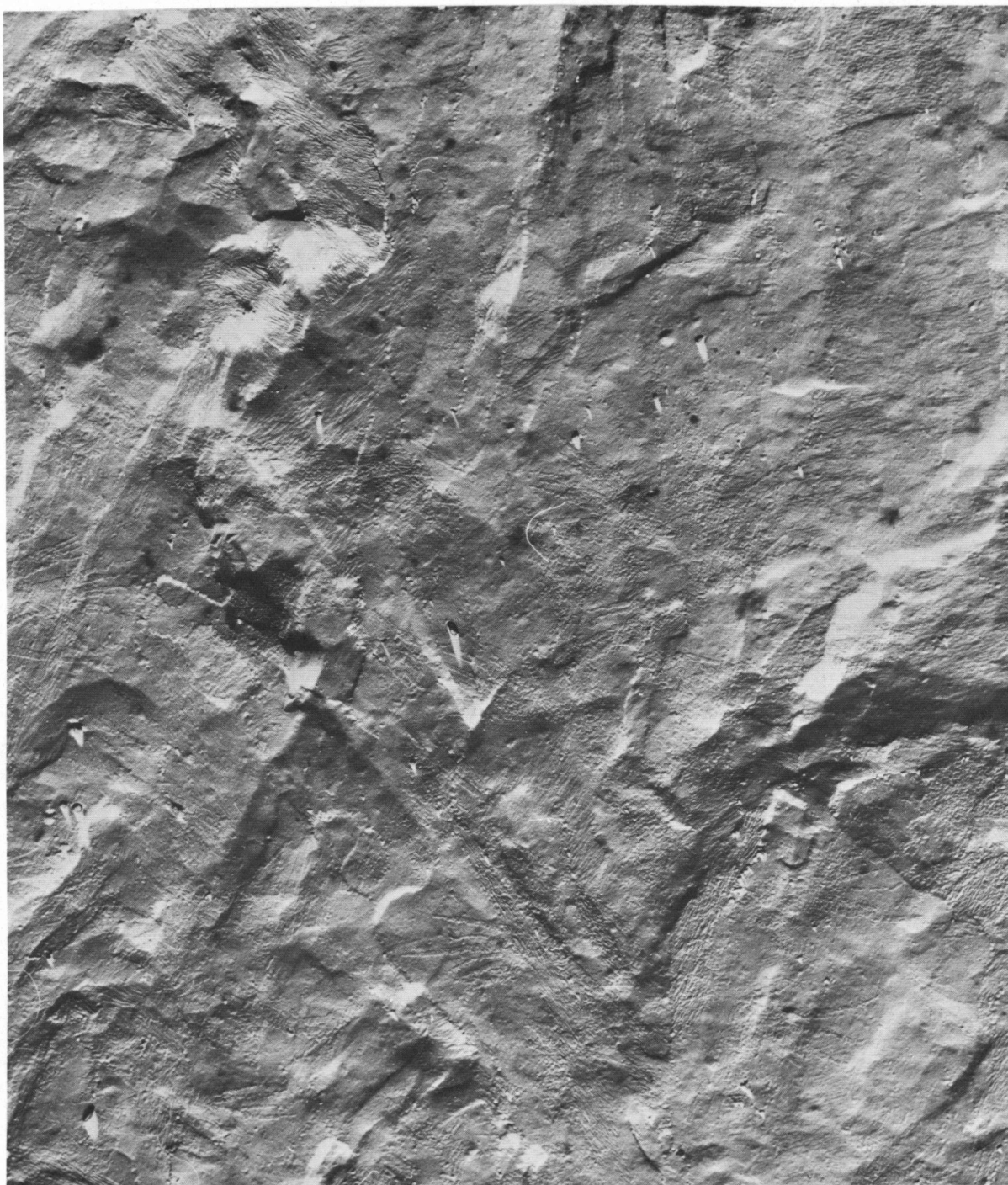


FIGURE 3.12

Limited Tearing in a $\gamma \rightarrow \alpha$ Treated Specimen (28A-1)
of U + 400 Fe-640 Al Irradiated to 0.16 at. % BU at 400-500 C
(5500X)

Neg. 2872-D



FIGURE 3.13

Tearing in a Beta Treated Specimen (28D-1) of U + 400 Fe-640 Al
Irradiated to 0.16 at. % BU at 400-500 C
(5500X)

Neg. 2879B

TABLE 3.4
IRRADIATION HISTORY AND VOLUME CHANGE OF SPECIMENS^(a) IN CAPSULE No. 22

Specimen Number	Type Material ^(b)	Heat Treatment	Irradiation Temperature, C ^(d)		As-Irradiated Density ρ , g/cc	Swelling, % $\frac{\rho_i - \rho_f}{\rho_f} \times 100$	"R" % Swelling ^(e) at. % BU
			First 0.037 at. % BU	Last 0.05 at. % BU			
22-A-1	U + Fe-Si	1000 C - 24 hr Water Quench + 400 C - 3 days	485	185	18.64	1.7	46
22-A-2	U + Fe-Al	1000 C - 24 hr Water Quench + 400 C - 3 days	485	185	18.61	1.6	43
22-B-1	U(T-2)	As-Extruded	535	210	17.41	8.9	240
22-B-2	U(T-2)	730 C - 15 min Oil Quench	535	210	17.26	9.9	270
22-C-1	U(T-2)	640 C - 4 days	525	200	16.14	17	460
22-C-2	U(T-2)	730 C - 15 min Oil Quench + 640 C - 4 days	525	200	17.15	11	300
22-D-1	U + Fe-Si	Beta Quench ^(c) + 400 C - 3 days	485	200	18.67	1.5	41
22-D-2	U + Fe-Al	Beta Quench ^(c) + 400 C - 3 days	485	200	18.72	0.96	26

(a) Specimens were half-hollow cylinders, 1/2 in. OD x 5/8 in. long, 0.030 in. wall thickness

(b) Composition in ppm: U + Fe-Al, 400 Fe, 640 Al, 85 Si, 500 C
U + Fe-Si, 140 Fe, ~25 Al, 95 Si, 400 C
High-Purity U: 65 Fe, < 5 Al, 24 Si, 6 C

(c) Beta Quench: Large bulk specimen heated to 730 C in a salt bath and quenched into water prior to machining specimens.

(d) Capsule was originally controlled at 525 C. After 0.038 at. % BU had been attained, the capsule temperature was reduced to 200 C. The capsule was discharged at a total burnup of 0.087 at. %, (4×10^{19} fissions/cc)

(e) Using 0.037 as the burnup value.

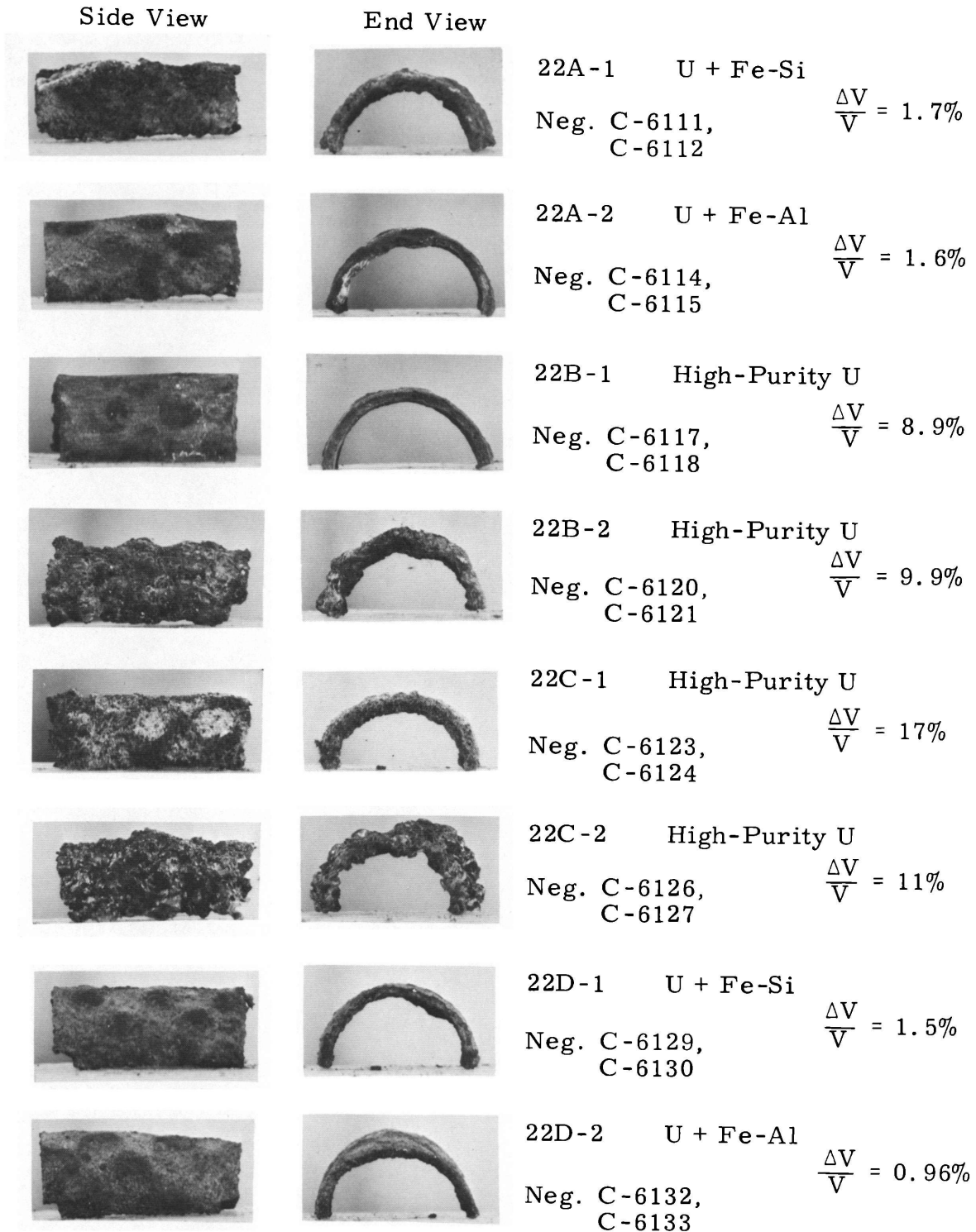


FIGURE 3. 14

As-Irradiated Macroappearance of Specimens Irradiated in Capsule No. 22
(2X)

TABLE 3.5
IRRADIATION HISTORY AND VOLUME CHANGE OF SPECIMENS^(a) IN CAPSULE No. 23

Specimen Number	Type Material ^(b)	Heat Treatment	Irradiation Temperature, C		As-Irradiated Density ρ , g/cc	Swelling, % $\frac{\rho_i - \rho_f}{\rho_f} \times 100$	"R" % Swelling at. % BU
			Reactor Up	Reactor Down			
23-A-1	U + Fe-Si	1000 C - 24 hr Water Quench + 400 C - 3 days	550	585	18.48	2.5	23
23-A-2	U + Fe-Al	1000 C - 24 hr Water Quench + 400 C - 3 days	550	585	18.52	2.0	18
23-A-2	U(T-2)	As-Extruded	610	625	17.94	6.0	55
23-B-2	U(T-2)	730 C - 15 min Oil Quench	610	625	18.45	3.0	27
23-C-1	U(T-2)	640 C - 4 days	625	625	18.02	5.5	50
23-C-2	U(T-2)	720 C - 15 min Oil Quench + 640 C - 4 days	625	625	18.37	3.5	32
23-D-1	U + Fe-Si	Beta Quench ^(c) + 400 C - 3 days	575	595	17.20	10	91
23-D-2	U + Fe-Al	Beta Quench ^(c) + 400 C - 3 days	575	595	18.60	1.6	14

(a) Specimens were half-hollow cylinders, 1/2 in. OD x 5/8 in. long x 0.030 in. wall thickness

(b) Composition in ppm: U + Fe-Al; 400 Fe, 640 Al, 85 Si, 500 C
U + Fe-Si; 140 Fe, ~25 Al, 95 Si, 400 C
High-Purity U: 65 Fe, <5 Al, 24 Si, 6 C

(c) Beta Quench: Large bulk specimen heated to 730 C in a salt bath and quenched into water prior to machining specimens

Exposure: 0.11 at. % BU (0.54×10^{20} fissions/cc)

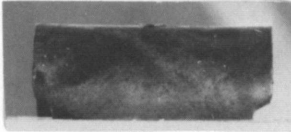
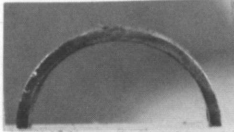
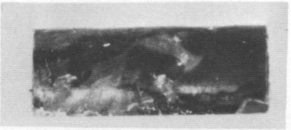
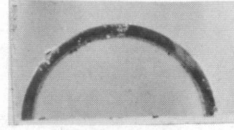
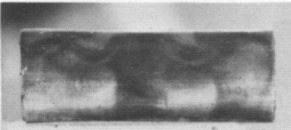
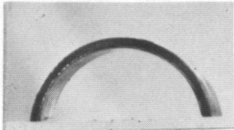
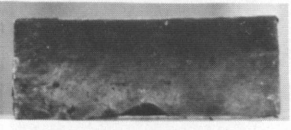
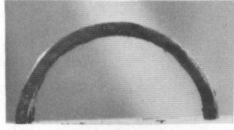
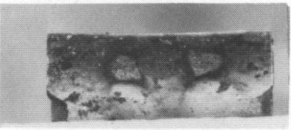
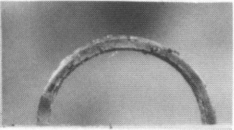
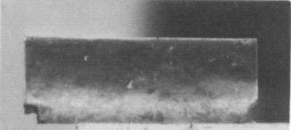
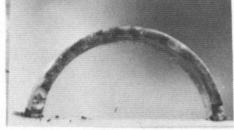
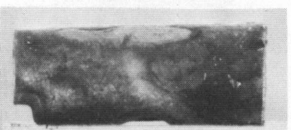
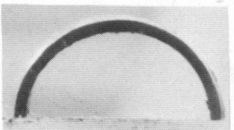
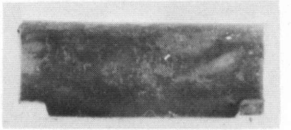
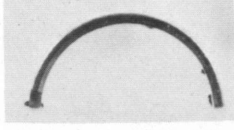
Side View	End View			
		23A-1	U + Fe-Si	$\frac{\Delta V}{V} = 2.5\%$
		Neg. C-6015, C-6016		
		23A-2	U + Fe-Al	$\frac{\Delta V}{V} = 2\%$
		Neg. C-6018, C-6019		
		23B-1	High-Purity U	$\frac{\Delta V}{V} = 6\%$
		Neg. C-6021, C-6022		
		23B-2	High-Purity U	$\frac{\Delta V}{V} = 3\%$
		Neg. C-6024, C-6025		
		23C-1	High-Purity U	$\frac{\Delta V}{V} = 5.5\%$
		Neg. C-6027, C-6028		
		23C-2	High-Purity U	$\frac{\Delta V}{V} = 3.5\%$
		Neg. C-6030, C-6031		
		23D-1	U + Fe-Si	$\frac{\Delta V}{V} = 10\%$
		Neg. C-6033, C-6035		
		23D-2	U + Fe-Al	$\frac{\Delta V}{V} = 1.6\%$
		Neg. C-6036, C-6037		

FIGURE 3.15

As-Irradiated Macroappearance of Specimens Irradiated in Capsule No. 23
(2X)

TABLE 3.6
IRRADIATION HISTORY AND VOLUME CHANGE OF SPECIMENS^(a) IN CAPSULE No. 27

Specimen Number	Type Material ^(b)	Heat Treatment	Irradiation Temperature, C		As-Irradiated Density ρ , g/cc	Swelling, % $\frac{\rho_i - \rho_f}{\rho_f} \times 100$	"R" % Swelling at.% BU
			Reactor Up	Reactor Down			
27-A-1	U + Fe-Al	800 C - 2 hr Furnace Cooled + 730 C - 15 min Oil Quench	435	450	18.75	0.8	7
27-A-2	U + Fe-Si	800 C - 2 hr Furnace Cooled + 730 C - 15 min Oil Quench	435	450	18.68	1.5	14
27-B-1	U(T-3)	As-Extruded	485	480	10.24	85	770
27-B-2	U(T-3)	730 C - 15 min Oil Quench	485	480	12.02	57	520
27-C-1	U(T-3)	730 C - 15 min Furnace Cooled	500	500	Specimens too badly damaged for density measurements		
27-C-2	U(T-3)	900 C - 15 min Furnace Cooled	500	500	Specimens too badly damaged for density measurements		
27-D-1	U + Fe-Al	Beta Quench ^(c)	460	465	18.58	1.7	15
27-D-2	U + Fe-Si	Beta Quench ^(c)	460	465	18.96 - Doesn't agree with macroappearance		

(a) Specimens were half-hollow cylinders, 1/2 in. OD x 5/8 in. long x 0.030 in. wall thickness

(b) Composition in ppm: U + Fe-Al; 400 Fe, 640 Al, 85 Si, 500 C
U + Fe-Si; 140 Fe, ~ 25 Al, 95 Si, 400 C
High-Purity U: 65 Fe, < 5 Al, 24 Si, 6 C

(c) Beta Quench: Large bulk specimen heated to 730 C in a salt bath and quenched into water prior to machining specimens

Exposure: 0.11 at.% BU (0.54×10^{20} fissions/cc)

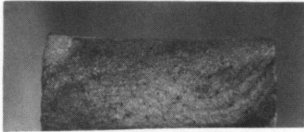
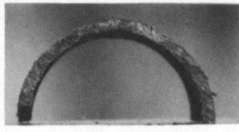
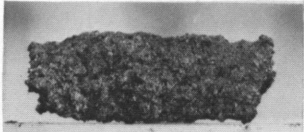

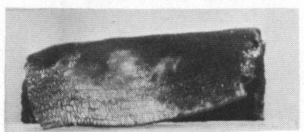
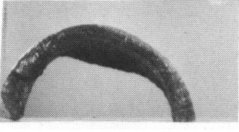


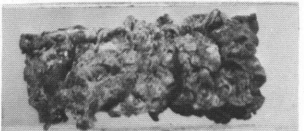

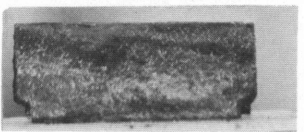
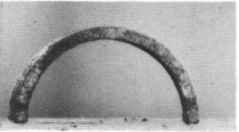
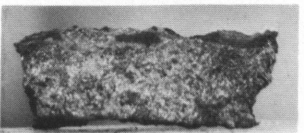
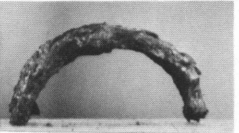
Side View	End View			
		27A-1	U + Fe-Al	
		Neg. C-6090, C-6091		$\frac{\Delta V}{V} = 0.8\%$
		27A-2	U + Fe-Si	
		Neg. C-6093, C-6094		$\frac{\Delta V}{V} = 1.5\%$
		27B-1	High-Purity U	
		Neg. C-6096, C-6097		$\frac{\Delta V}{V} = 85\%$
		27B-2	High-Purity U	
		Neg. C-6099, C-6100		$\frac{\Delta V}{V} = 57\%$
		27C	High-Purity U	
		Neg. C-6102, C-6103		No Density
		27D-1	U + Fe-Al	
		Neg. C-6105, C-6106		$\frac{\Delta V}{V} = 1.7\%$
		27D-2	U + Fe-Si	
		Neg. C-6108, C-6109		$\Delta V = 0\% (?)$

FIGURE 3.16

As-Irradiated Macroappearance of Specimens Irradiated in Capsule No. 27
(2X)

The data from Capsules 22, 23, and 27 corroborate the previous conclusions that (1) both alloy compositions exhibited behavior that was much improved over the behavior of high-purity uranium, and (2) the U + Fe-Al alloy specimens were in general superior to the U + Fe-Si alloy specimens. These data also show conclusively that quenching alloy specimens from the gamma phase and reheating to either beta phase or high alpha phase temperatures results in a still further significant increase in irradiation stability. This effect is more pronounced in the U + Fe-Al alloy. The benefits derived from the $\gamma \rightarrow \beta$ or $\gamma \rightarrow \alpha$ treatments are believed to come about by virtue of the very large number of finely dispersed second-phase particles that are formed by the second anneal. These particles are thought to interfere with the mechanical processes that give rise to swelling in uranium at irradiation temperatures below 600 C. Obviously, more detailed studies are required in order to understand the mechanism by which the additives affect the improvement.

Figure 3.17 depicts the large influence that relatively small alloying additions have on the swelling behavior of uranium. The swelling-temperature relationship that was previously established⁽¹⁾ for high-purity uranium in the as-extruded condition is presented for comparison purposes. The bulk of the data points shown in Figure 3.17 represent high-purity uranium in the as-extruded condition from the present series of six capsules. Part of this latter data is from specimens from the second high-purity extrusion employed in this study. One data point in Figure 3.17 is from a seventh capsule, Number 32, containing only high-purity uranium that operated at beta temperatures. (See subsequent pages.) Tables 3.7 and 3.8 summarize the data obtained from U + Fe-Si specimens and U + Fe-Al specimens, respectively. This data falls into two groups according to heat treatment.

1. R. D. Leggett, T. K. Bierlein, and B. Mastel. Irradiation Behavior of High Purity Uranium, HW-79559. November 1963.

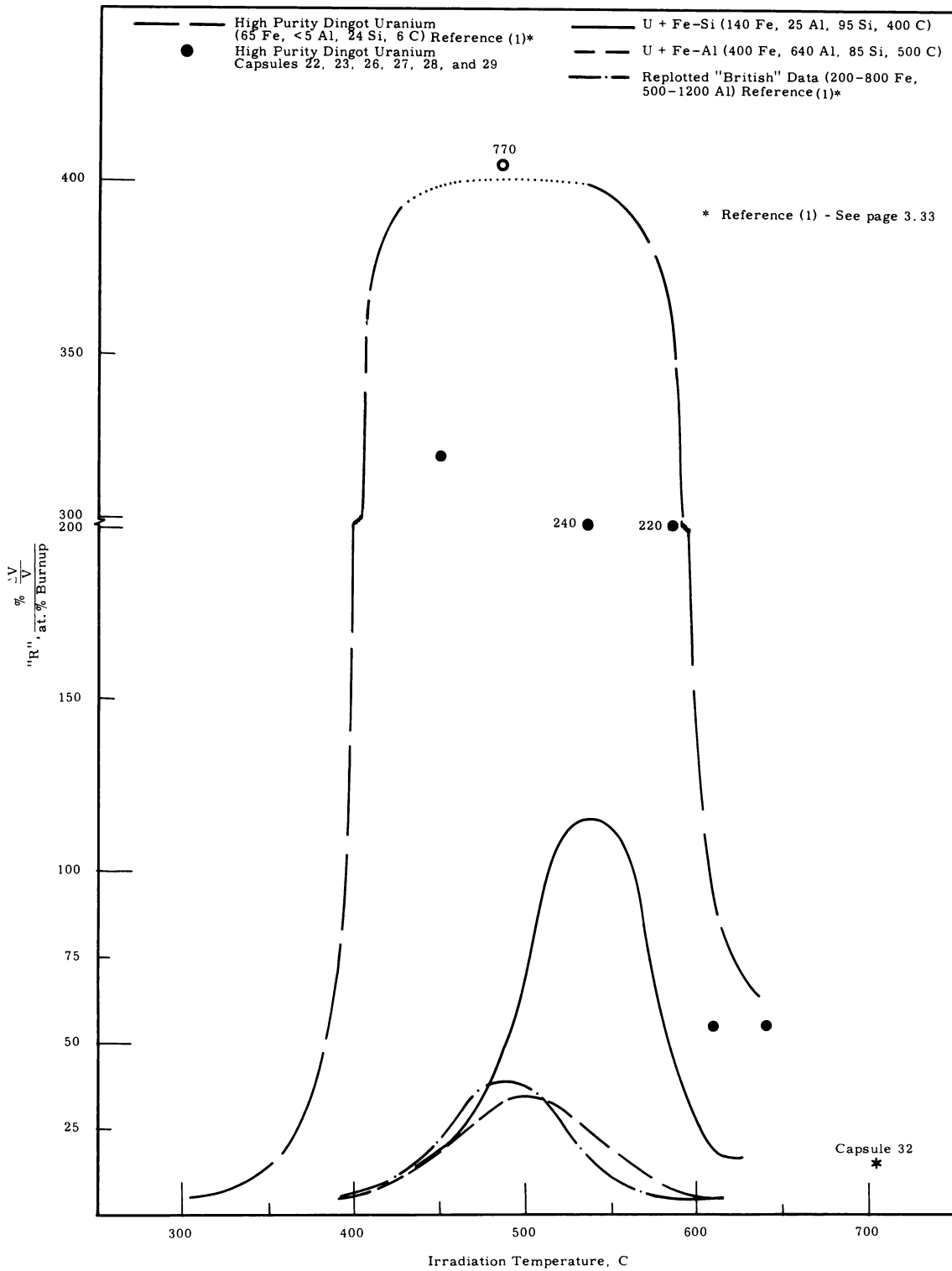


FIGURE 3.17

Influence of Minor Alloying Additions on the Irradiation Swelling of Uranium

TABLE 3.7

HISTORY AND SWELLING OF U + Fe-Si^(a) SPECIMENS IN CAPSULES 22, 23, 26, 27, 28 AND 29

Specimen Number	Heat Treatment	Irradiation Temperature, C		at. % BU	As-Irradiated Density, ρ g/cc	Swelling, % $\frac{\rho_i - \rho_f}{\rho_f} \times 100$	"R" % Swelling at. % BU
		Reactor Up	Reactor Down				
26-D-2	Beta Quenched in Bulk	535	535	0.11	16.8	13	120
27-D-2	Beta Quenched in Bulk	460	465	0.11	18.96	Questionable because of macro-appearance	
22-D-1	Beta Quenched in Bulk + 400 C - 3 days	485 ^(b)	200 ^(b)	0.087	18.67	1.5	41 ^(c)
23-D-1	Beta Quenched in Bulk + 400 C - 3 days	575	595	0.11	17.20	10	91
29-D-2	Beta Quenched in Bulk + 525 C - 24 hr	585	590	0.16	17.68	7.2	45
23-A-1	1000 C - 24 hr Water Quench + 400 C - 3 days	550	585	0.11	18.48	2.5	23
22-A-1	1000 C - 24 hr Water Quench + 400 C - 3 days	485 ^(b)	185 ^(b)	0.087	18.64	1.7	46
26-A-2	800 C - 2 hr Furnace Cooled + 730 C - 15 min Oil Quench	535	565	0.11	17.5	8	73
27-A-2	800 C - 2 hr Furnace Cooled + 730 C - 15 min Oil Quench	435	450	0.11	18.68	1.5	14
28-A-2	1000 C - 24 hr Water Quench + 525 C - 24 hr	450-500	Ambient	0.16	18.57	2.0	12
29-A-2	1000 C - 24 hr Water Quench + 525 C - 24 hr	605	615	0.16	18.30	3.5	22

(a) Composition: 140 Fe, 25 Al, 95 Si, 400 C

(b) First 0.037 at. % BU was at 485 C,

Last 0.05 at. % BU was at 185-200 C for a total of 0.087 at. % BU

(c) "R" was calculated on the basis of 0.037 at. % BU

 ρ_i - Initial Density = 18.95 g/cc

TABLE 3.8

HISTORY AND SWELLING OF U + Fe-Al^(a) SPECIMENS IN CAPSULES 22, 23, 26, 27, 28 AND 29

Specimen Number	Heat Treatment	Irradiation Temperature, C		at. % BU	As-Irradiated Density, ρ g/cc	Swelling, % $\frac{\rho_i - \rho_f}{\rho_f} \times 100$	"R" % Swelling at. % BU
		Reactor Up	Reactor Down				
26-D-1	Beta Quenched in Bulk	535	535	0.11	18.3	3	27
27-D-1	Beta Quenched in Bulk	460	465	0.11	18.58	1.7	15
22-D-2	Beta Quenched in Bulk + 400 C - 3 days	485 ^(b)	200 ^(b)	0.087	18.72	0.96	26 ^(c)
23-D-2	Beta Quenched in Bulk + 400 C - 3 days	575	595	0.11	18.60	1.6	14
29-D-1	Beta Quenched in Bulk + 525 C - 24 hr	585	590	0.16	18.70	1.1	7
28-D-1	Beta Quenched in Bulk + 525 C - 24 hr	400-450	Ambient	0.16	18.08	4.5	28
23-A-2	1000 C - 24 hr Water Quench + 400 C - 3 days	550	585	0.11	18.52	2.0	18
22-A-2	1000 C - 24 hr Water Quench + 400 C - 3 days	485 ^(b)	185 ^(b)	0.087	18.61	1.6	43 ^(c)
26-A-1	800 C - 2 hr Furnace Cooled + 730 C - 15 min Oil Quench	535	565	0.11	18.9	0	0
27-A-1	800 C - 2 hr Furnace Cooled + 730 C - 15 min Oil Quench	435	450	0.11	18.75	0.8	7
28-A-1	1000 C - 24 hr Water Quench + 525 C - 24 hr	450-500	Ambient	0.16	18.57	2.0	12
29-A-1	1000 C - 24 hr Water Quench + 525 C - 24 hr	605	615	0.16	18.74	0.9	6

(a) Composition: 400 Fe, 640 Al, 85 Si, 500 C

(b) First 0.037 at. % BU was at 485 C,

Last 0.05 at. % BU was at 185-200 C for a total of 0.087 at. % BU

(c) "R" was calculated on the basis of 0.037 at. % BU

ρ_i = Original Density = 18.9 g/cc

The first group received what amounts to a single treatment, being quenched from either the gamma phase or the beta phase. Part of these specimens received an additional treatment at 400 C for 3 days but this temperature was too low to produce discernable changes. The data from singly treated specimens are represented by the alloy curves in Figure 3.17. Interestingly enough in the temperature region where grain boundary tearing is the predominant mode of swelling (400-500 C) both alloys behaved quite similarly and both exhibited much improved behavior over high-purity uranium. In the 500 to 600 C temperature range where aligned microtearing predominates both alloys behaved much better than the high-purity uranium but the U + Fe-Al specimens were by far superior to the U + Fe-Si specimens. Published British data⁽¹⁾ for the same composition as the present U + Fe-Al specimens, when reinterpreted,^(2,3) is included in Figure 3.17 and indicates a behavior pattern very similar to the present U + Fe-Al data. The two curves in Figure 3.17 almost superimpose.

The second behavior group revealed by the data in Tables 3.7 and 3.8 received a dual heat treatment prior to irradiation. The first treatment was in the gamma and the second was either in the beta (730 C) or high alpha (525 C). Figure 3.18 compares the two groups of data for the two alloys. The U + Fe-Si alloy specimens probably received some benefit from the dual treatment but the number of data points is insufficient to establish that the effect is real. There is no question but that the U + Fe-Al alloy specimens derived a large benefit from the dual heat treatment. The swelling in

-
1. S. F. Pugh. "Swelling in Alpha Uranium Due to Irradiation," J. Nuc. Materials, vol. 4, pp. 177-199. 1961.
 2. S. Granata and F. Saraceno. "The Relationship Between Burnup, Temperature, and Swelling in Alpha Uranium," J. Nuc. Materials, vol. 9, no. 3, pp. 367-369. 1963.
 3. R. D. Leggett, T. K. Bierlein, and B. Mastel. Irradiation Behavior of High Purity Uranium, HW-79559. November 1963.

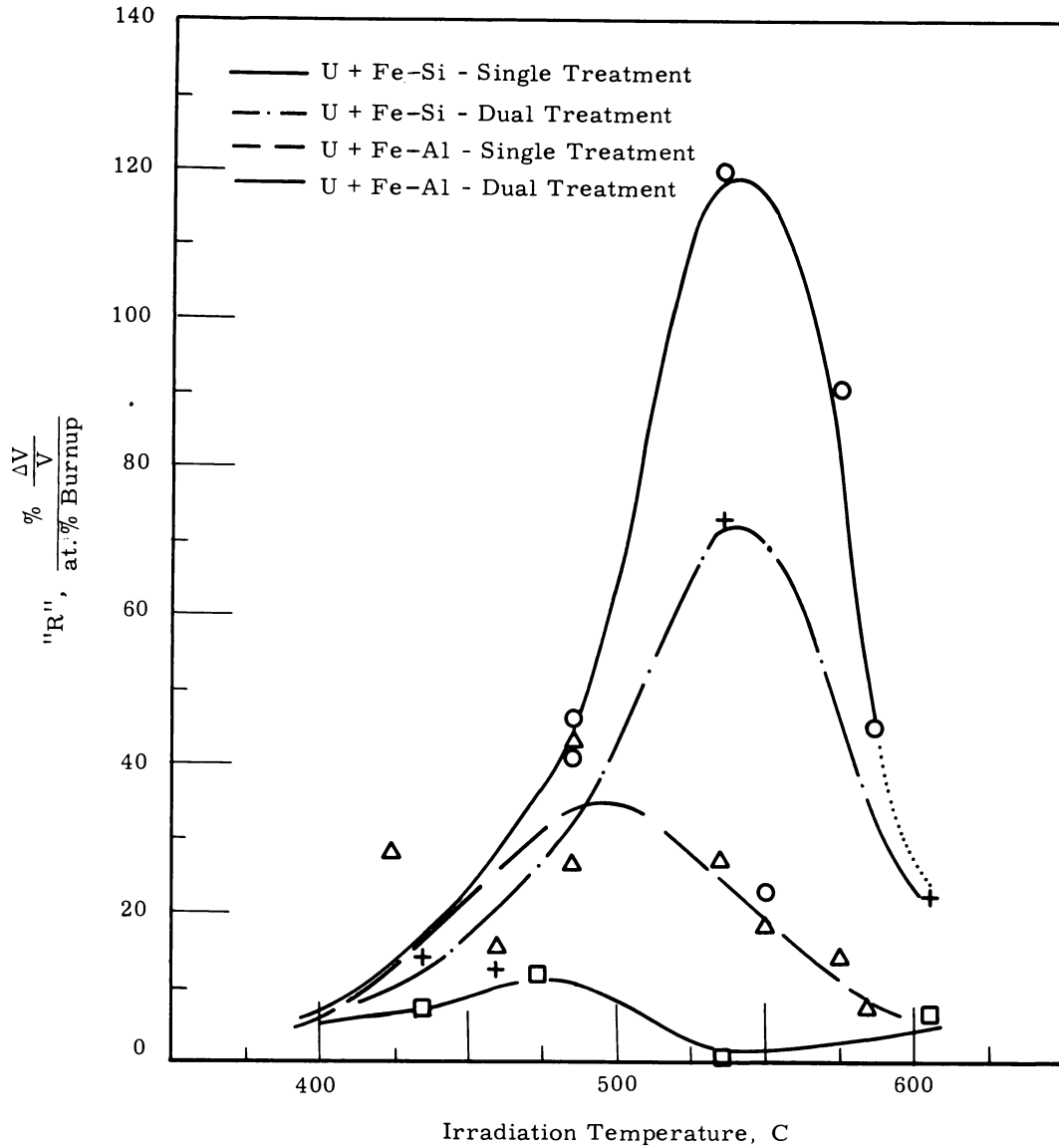


FIGURE 3.18

**The Influence of Preirradiation Heat Treatment
on the Irradiation Swelling of U + Fe-Si and U + Fe-Al Alloy Specimens**

these specimens is so small that the accuracy of the reported swelling values is poor. These U + Fe-Al alloy specimens exhibit little more than the theoretical swelling expected from consideration of the additional atoms that are produced from the fissioning process.

These data which are at best preliminary and cursory in nature strongly indicate that a well behaved metal fuel can be developed through a logical extension of the concepts evolved with the present study.

Another general swelling capsule (No. 32) controlled at 700 C (beta phase) was opened and the high-purity uranium specimens exposed to 0.05 at. % BU were recovered. Solid cylinders 1/8 in., 1/4 in., 3/8 in., and 1/2 in. in diameter and split tubes 1/2-in. diam. with 0.030-in., 0.060-in., and 0.120-in. -thick walls were included. The solid cylinders were initially in the as-extruded condition and one-half of each of the split tube specimens was as-extruded while the other half had been beta treated. All of the samples looked in excellent condition with little or no general warpage or surface bumping. Table 3.9 summarizes the estimated volume average irradiation temperature and the observed swelling for each specimen. The "R" values, obtained by dividing the percent swelling by the percent burnup, were 15-20 for the tubular samples and 30-40 for the rod specimens. This is due to the fact that the rods operated some 40 C hotter than did the tubes. There is no indication that geometry per se in any way influenced the behavior. It is significant that these "R" values are relatively low (see Figure 3.17 which plots the data point for Specimen 32C-1). This correlates quite nicely with previous conclusions that fission gas porosity only begins to be important to the irradiation swelling of uranium above 600 C.

TABLE 3.9
IRRADIATION SWELLING IN HIGH-PURITY URANIUM SPECIMENS
IRRADIATED TO 0.05 at. % BURNUP IN CAPSULE No. 32
CONTROLLED AT 700 C

Specimen Number	Specimen Geometry	Heat* Treatment	Estimated Average Volume Temperature, C	As-Irradiated Density ρ_f , g/cc	% Swelling $\frac{\rho_i - \rho_f}{\rho_f} \times 100$	"R" % Swelling % BU
A	1/2 in. rod	AE	745	18.73	1.5	30
B-1	0.060 in. tube	AE	685	18.84	0.9	18
B-2	0.060 in. tube	BQ	685	18.65	1.9	38
B-3	1/4 in. rod	AE	715	18.66	1.9	38
C-1	0.030 in. tube	AE	705	18.85	0.8	17
C-2	0.030 in. tube	BQ	705	18.87	0.7	15
C-3	3/8 in. rod	AE	740	18.63	2.0	41
D-1	0.120 in. tube	AE	705	18.83	1.0	20
D-2	0.120 in. tube	BQ	705	18.80	1.1	22
D-3	1/8 in. rod	AE	--- Specimen lost during capsule opening			

* AE = as-extruded

BQ = beta quenched, 730 C for 15 min, Oil Quenched

The bulk of the metallography is complete on specimens from Capsule 32. As it is consistent from one sample to another, only that of the 1/2-in. rod specimen will be described. Both a transverse and longitudinal section were prepared but it is sufficient to discuss only the longitudinal section. Figure 3.19, a photomosaic originally prepared at 75X under polarized light, shows the grain structure that presently exists in this specimen (the axis of the rod is horizontal in the figure). One corner of the sample has retained the original, small, equiaxed grain structure and operated only in the alpha phase. The bulk of the specimen consists of large columnar alpha grains which formed from the beta as the specimen cooled. This portion of the sample, of course, operated in the beta. Heat transfer calculations and difference in microstructure suggest that the core of the sample operated in the gamma temperature region. As can be seen in Figure 3.19 the columnar grain structure ends abruptly in this region and a large number of cracks are present which are believed to have formed as the sample cooled.

Figure 3.20 illustrates the appearance of the interface between the coarse and fine grain regions of the specimen. The area immediately adjacent to the fine grains now consists of large columnar alpha grains but a network exists which outlines the original alpha grains. The electron microscope examination of a negative replica of the fine grain region shows a mixture of particles and pores at the grain boundaries but no matrix porosity, Figure 3.21. The coarse grain region contains a similar network of particles and pores, and again, no "matrix" porosity, Figure 3.22. It is not certain that the pores in these networks are fission gas pores. It has occasionally been observed in the examination of nonirradiated uranium alloy specimens containing grain boundary precipitates that many pores are also present. This has been attributed to the fallout of second phase particles leaving a hole in the etched uranium surface. It is conceivable that the present observation of porosity in and adjacent to the fine grain region is also due to holes left behind as particles fall out during specimen preparation. To resolve this question it will be necessary to examine additional specimens irradiated under similar conditions of temperature but to higher burnup.

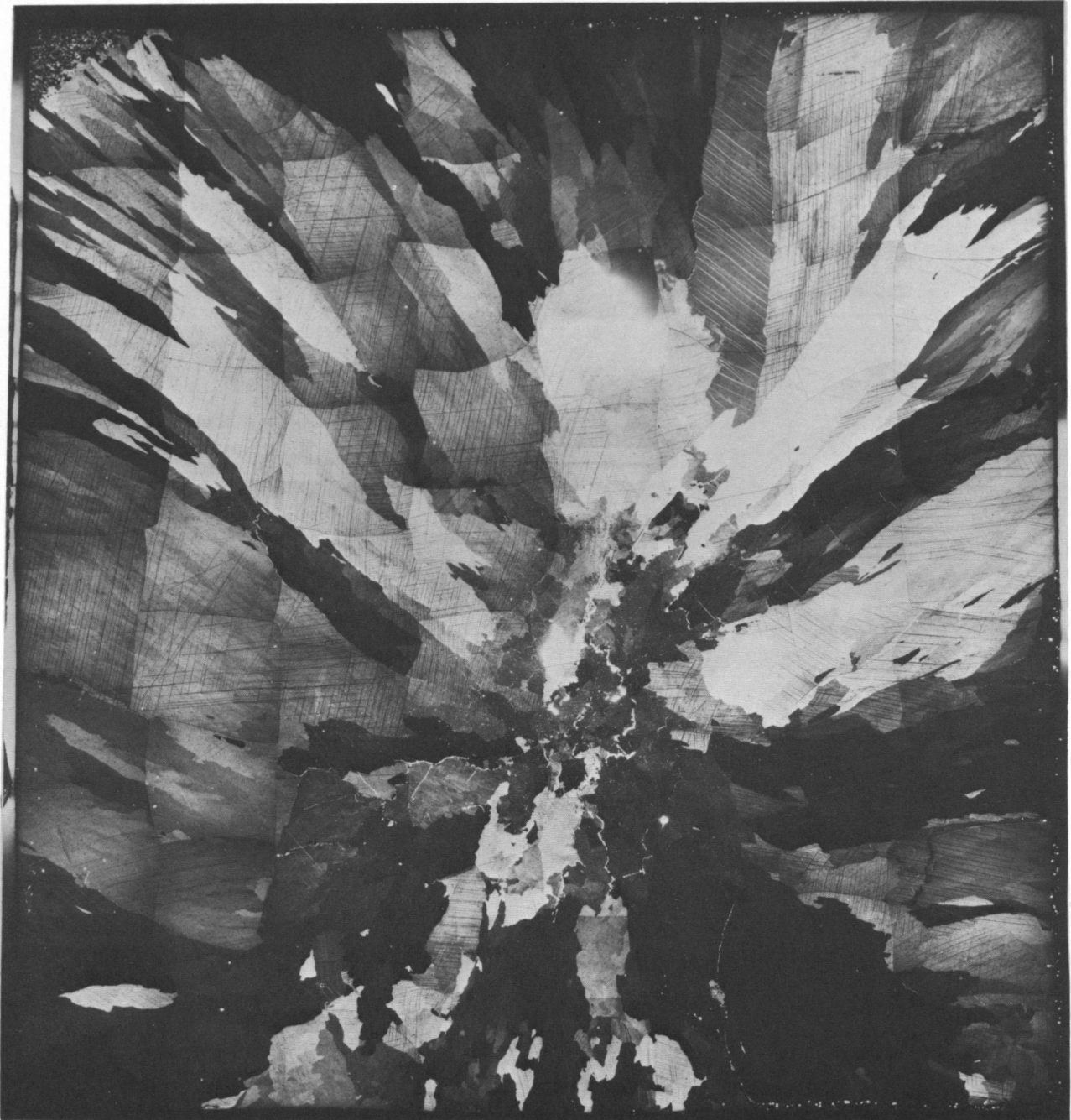
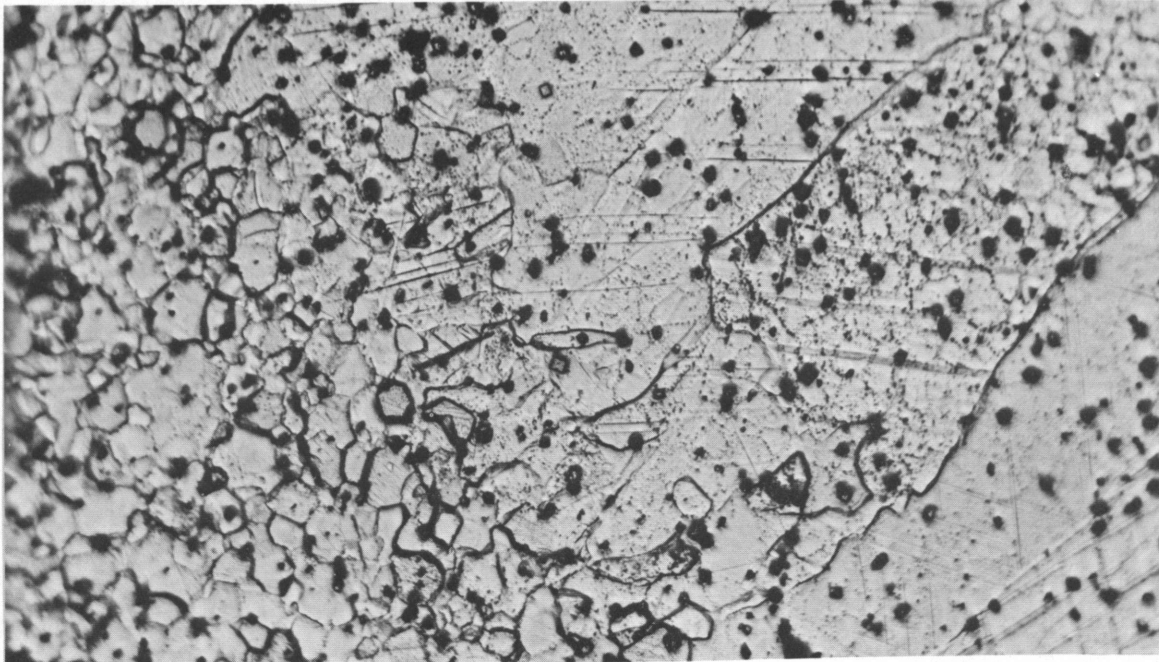
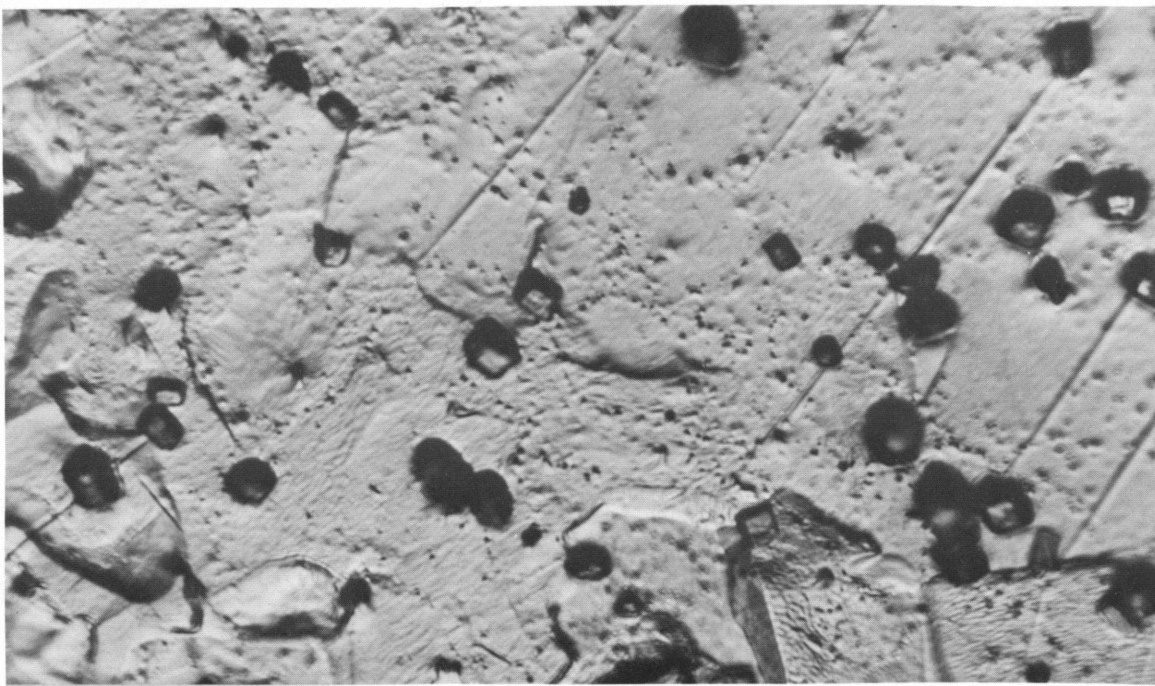


FIGURE 3.19

Longitudinal Section of 1/2 in. Rod Specimen 32A Irradiated to 0.05 at. % BU at a Volume Average Temperature of about 745 C (Note the fine grains in the upper left corner which operated in the alpha phase, the large columnar grains depicting beta phase operation and the core of smaller grains with cracks indicating gamma phase operation). (Magnification 15X as reduced from an original 75X photomosaic taken under polarized light) Neg. 0643464



(250X)



(1000X)

FIGURE 3. 20

As-Etched Microstructure of Specimen 32A in the Transition Region
Between Fine (alpha phase operation)
and Coarse (beta phase operation) Grains.

(Note outline of prior grain boundaries in the coarse grained region)

Neg. C-6957, C-6959



FIGURE 3. 21

Grain Boundary Precipitate and Porosity in Small Grain Region
of Specimen 32A Irradiated to 0.05 at. % BU.
This Region Operated at About 660 C
(Note the complete absence of matrix porosity)
(5500X)

Neg. 2923-C

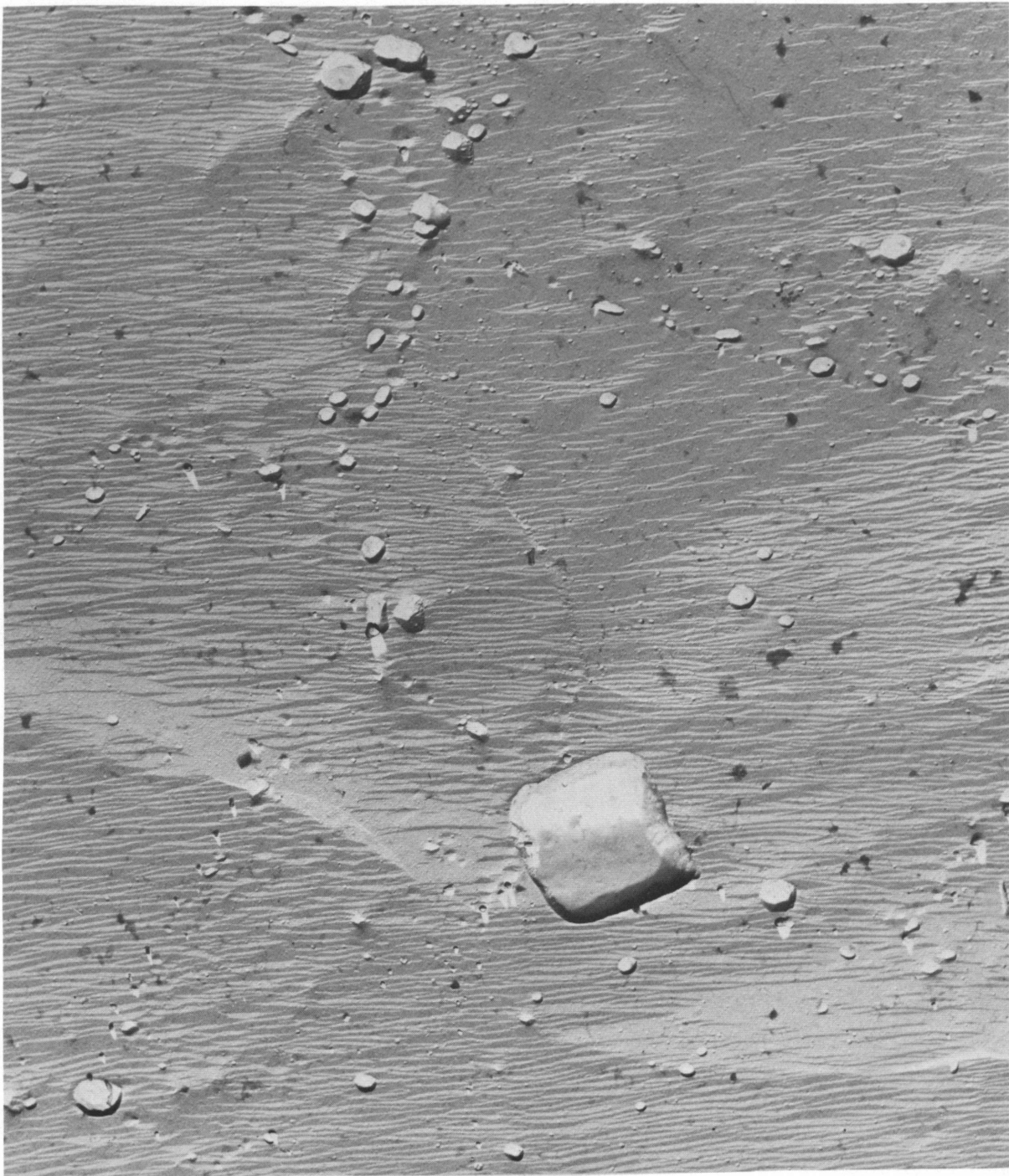


FIGURE 3.22

Rows of Precipitate and Porosity Along Original Alpha Grain Boundaries
in the Coarse Grain Region Adjacent to the Fine Grain Region in
Specimen 32A. This Area Operated Just into the Beta Phase
at About 670 C. (5500X)

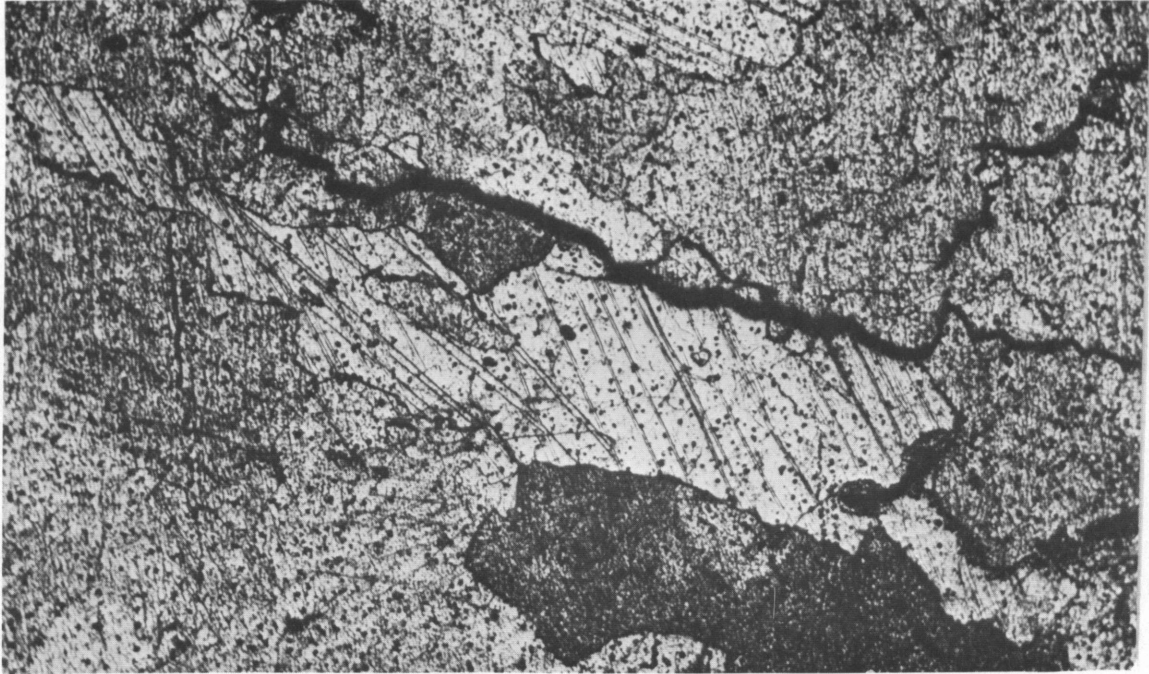
Neg. 2923-E

True fission gas porosity would be expected to increase with additional burnup whereas particle dropping would remain essentially constant.

In the core of Specimen 32A a prior set of boundaries is outlined, Figure 3.23, which probably locate prior gamma boundaries. The electron micrograph of Figure 3.24 reveals that this network consists of rows of fission gas pores. Appreciable matrix porosity is also present in the core which is believed to be due to the agglomeration of fission gases. Existing grain boundaries are free from both pores and particles. Matrix porosity continues up to the cracks that are present which suggests either that gas mobility is low despite the high operating temperature (approximately 780 C) or that the cracks were not present at temperature but formed on cooling. The fact that most of the cracks follow existing alpha boundaries is evidence for thinking that the cracks formed on cooling.

In an intermediate region of Specimen 32A which operated in the high beta (approximately 740 C) fission gas pores are dispersed uniformly throughout the existing alpha grains, Figure 3.25. In some cases pores also decorate segments of previous boundaries. As would be expected from the operating temperatures the amount of fission gas porosity is less in this intermediate region than was the case for the core which operated at about 780 C.

These data on specimens from Capsule 32 are highly significant to the study of the innate swelling characteristics of high-purity uranium exposed to neutron irradiation. As mentioned previously (Figure 3.17 on page 3.34), the density change for the split tubular specimen (32C-1) with a 0.030-in. wall thickness is less than the density change for similar specimens irradiated at lower temperatures. Specimen 32C-1 swelled about 0.8% and showed a few tiny pores in the electron microscope, Figure 3.26. This information, coupled with the observation that no matrix porosity existed in that region of Specimen 32A that operated in the very high alpha (Figure 3.21) or barely into the beta (Figure 3.22) and the data summarized by the high-purity uranium curve of Figure 3.17 corroborates the previously advanced concept that for this burnup level fission gases play but a very minor role in the swelling of uranium irradiated in the alpha phase. Mechanical processes



(75X)



(250X)

FIGURE 3.23

As-Etched Microstructure of Specimen 32A in the Core Region
(Note presence of network of prior boundaries)

Neg. C-6967, C-6968

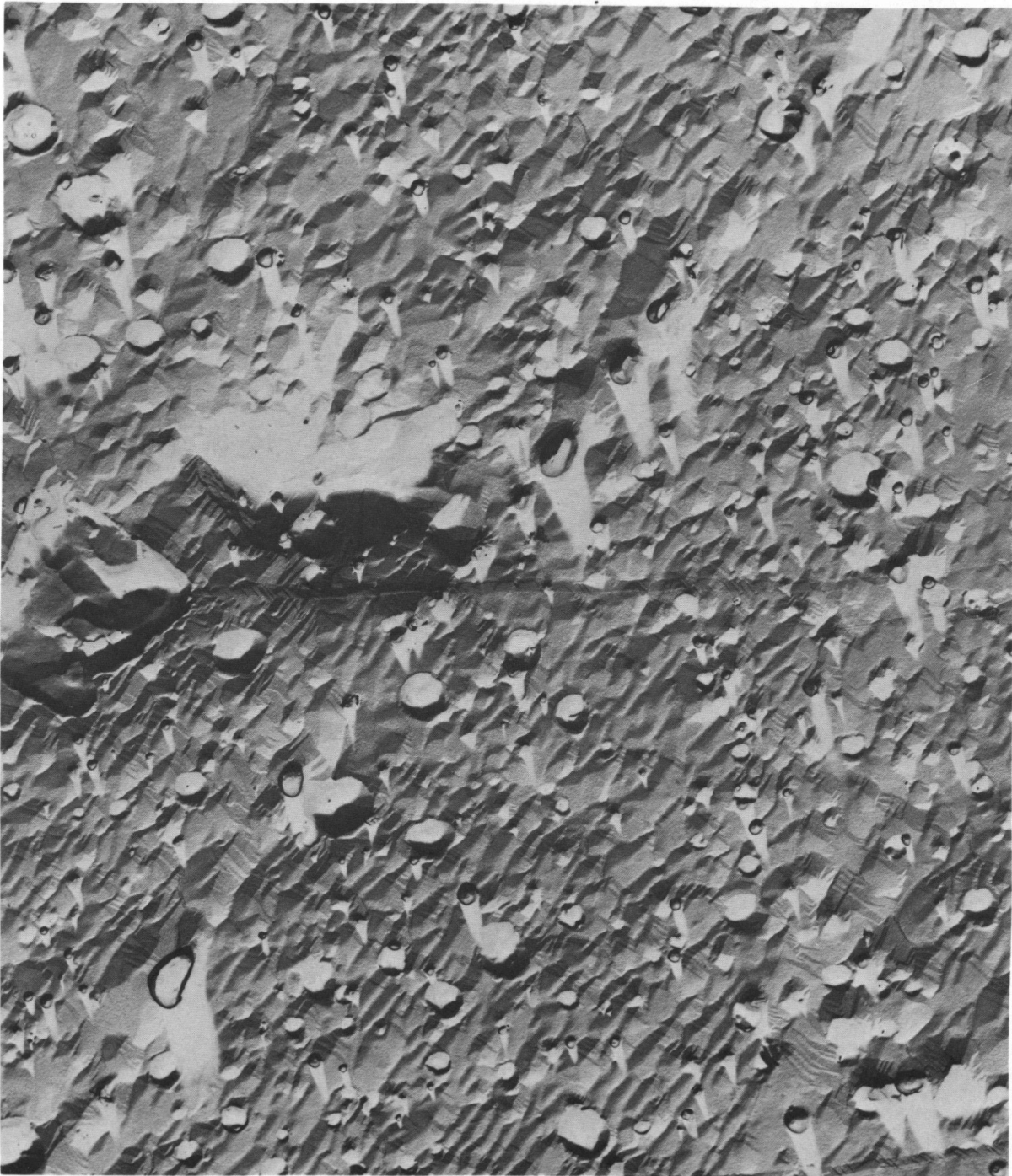


FIGURE 3.24

Matrix Porosity and Line-Up of Pores at a Prior Boundary in the Core Region of Specimen 32A. This Region Operated in the Gamma Phase at About 780 C. (5500 X)

Neg. 2955-B

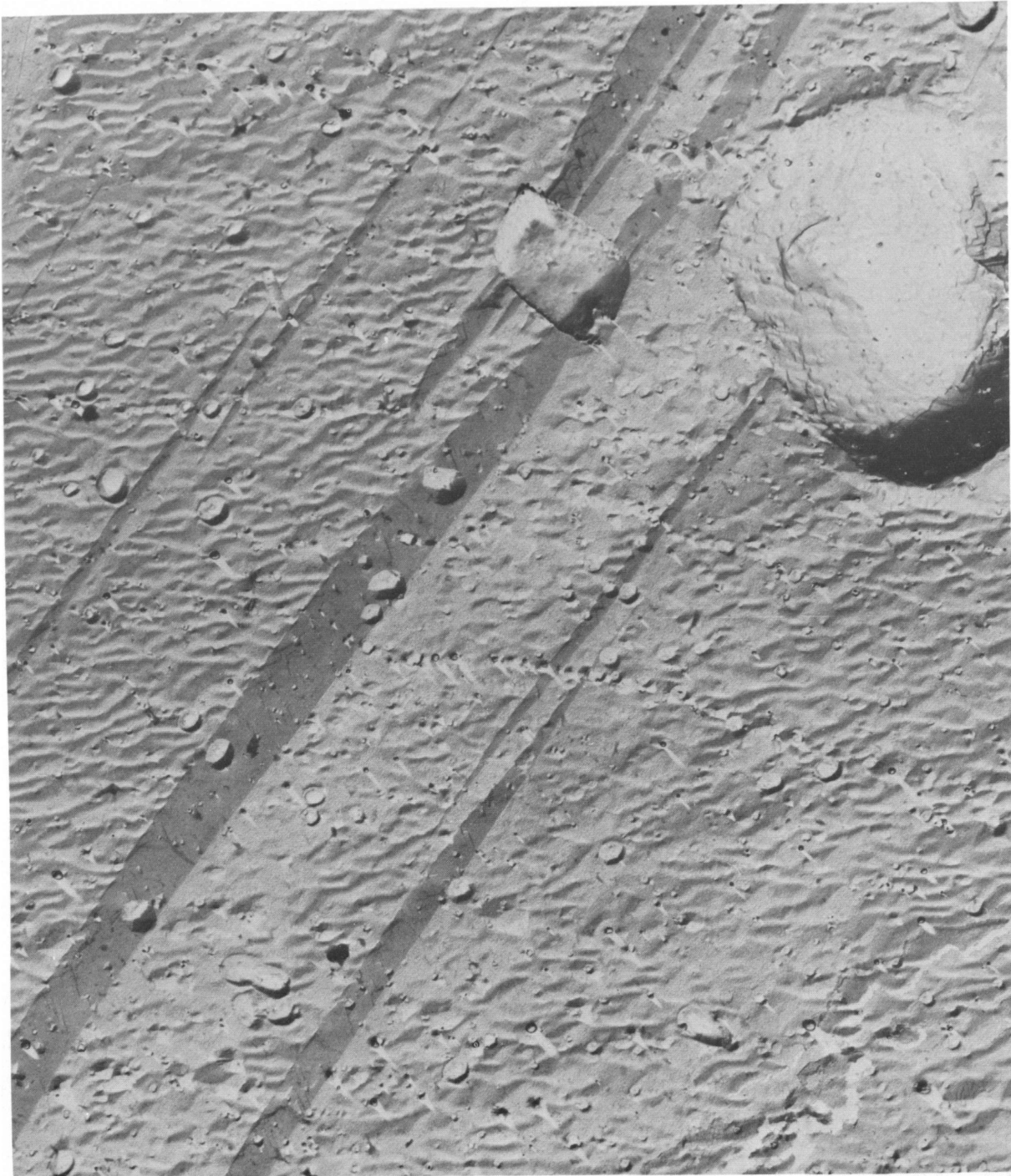


FIGURE 3.25

Matrix Porosity and Pore Line-Up at a Prior Boundary in That Region
of Specimen 32A Midway Between the Core and the Fine Grain Region.
This Region Operated at an Estimated 740 C
(5500X)

Neg. 2950-C

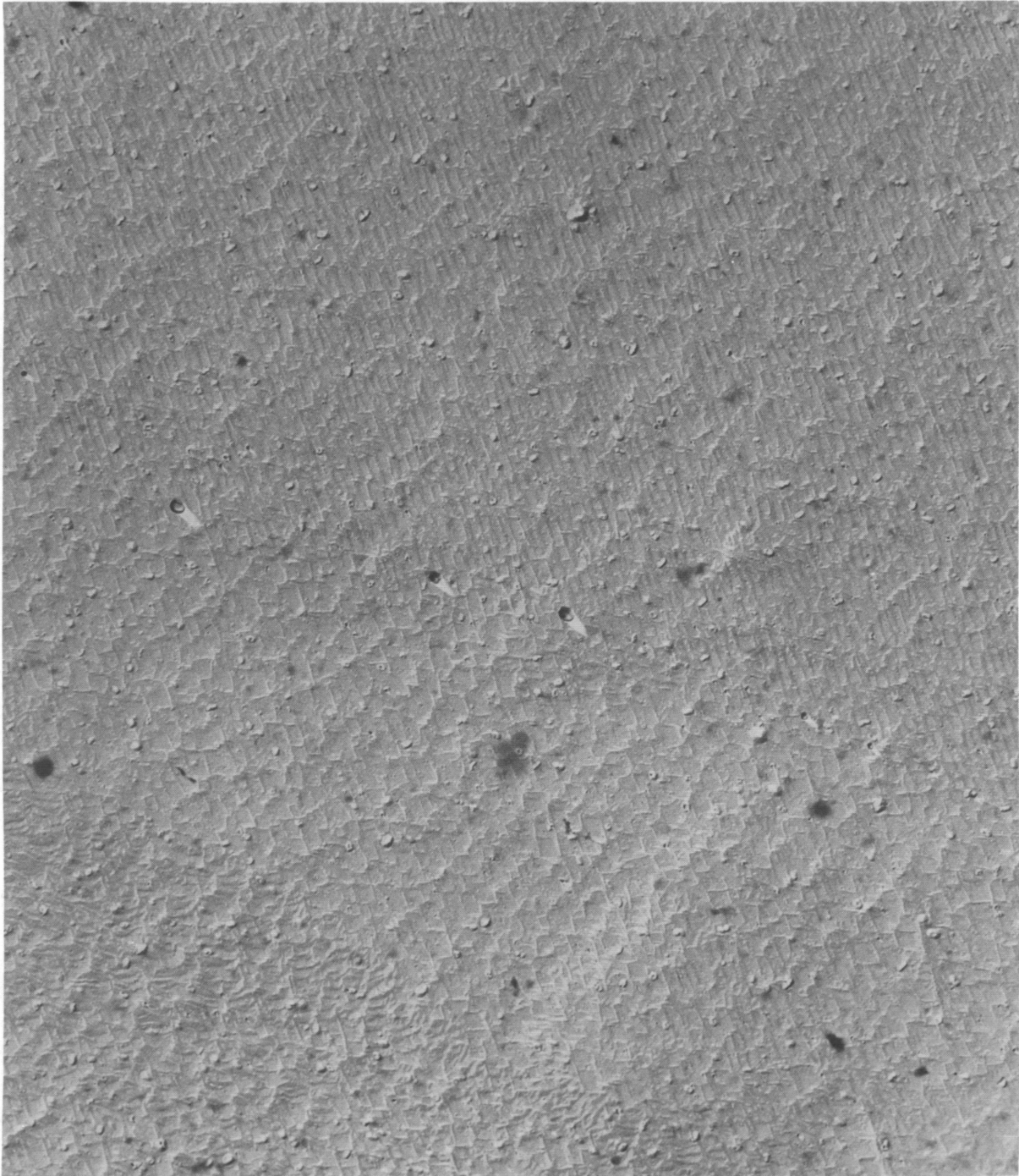


FIGURE 3.26

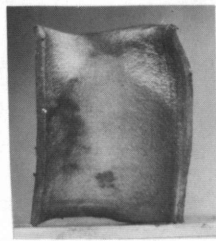
Limited Fission Gas Porosity in Specimen 32C-1 Irradiated at 705 C
to 0.05 at. % BU
(5500X)

Neg. 2925B

account for the swelling of alpha uranium. At very high alpha temperatures defect annihilation occurs before tearing can take place but the gas mobility is still too low to allow pore formation. The irradiation temperature has to be well into the beta before significant pore formation occurs. The data obtained with the specimens in Capsule 32 indicate that fission gas porosity becomes extensive above about 740 C and increases rapidly with increasing irradiation temperature. It is obvious that additional irradiations in the beta and gamma phase are in order so that true fission gas swelling can be evaluated. The other significant fact regarding these observations is that the approach to pursue in order to develop an irradiation resistant metallic fuel is now obvious. Rather than trying to overcome the effects of fission gas as has occupied the industry in the past, the mechanical processes responsible for tearing must be combated.

The first controlled pressure-temperature capsule which operated at 1000 psi and 450 C to 0.13 at. % BU was opened in Radiometallurgy and the specimens recovered. The capsule contained six high-purity uranium specimens, two U + Fe-Al and two U + Fe-Si specimens which had undergone several different heat treatments prior to irradiation. Postirradiation photomacrography and density measurements for the specimens are summarized in Figure 3.27 and Table 3.10, respectively. The density data shows very markedly the effectiveness with which pressure inhibited the swelling of the high-purity and alloy specimens in this capsule. For example, data from high-purity uranium specimens irradiated at about 450 C in general swelling capsules (controlled temperature only) reveal swelling of from 50 to 85% with corresponding "R" values from 320 to 770, respectively. The high-purity uranium specimens irradiated at 450 C in the pressurized capsule show swelling of only about 1% with corresponding "R" values of 8. This is but slightly more than the theoretical density decrease due to the birth of new atoms by the fission process.

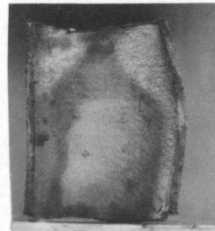
The macroappearance of the fine grained as-extruded specimens is very excellent. Some general warpage occurred but the surfaces have remained relatively smooth. A great deal of surface roughening occurred



A-1

High-Purity U
As-Extruded

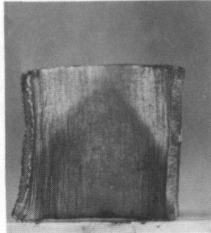
$$\frac{\Delta V}{V} = 0.85\%$$



A-2

High-Purity U
As-Extruded

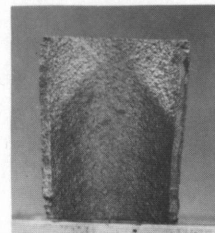
$$\frac{\Delta V}{V} = 1.1\%$$



B-1

U + Fe-Al
Beta Heat Treat

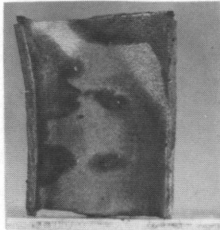
$$\frac{\Delta V}{V} = 0.26\%$$



B-2

U + Fe-Al
Beta Quench

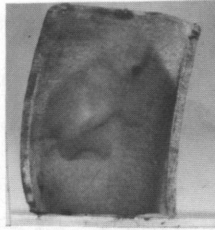
$$\frac{\Delta V}{V} = 0.53\%$$



C-1

High-Purity U
As-Extruded

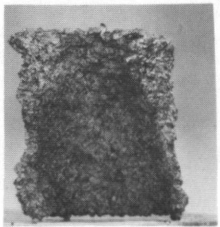
$$\frac{\Delta V}{V} = 1.1\%$$



C-2

High-Purity U
As-Extruded

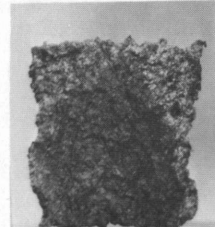
$$\frac{\Delta V}{V} = 2\%$$



D-1

High-Purity U
Beta Quench

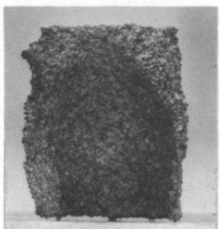
$$\frac{\Delta V}{V} = 1.7\%$$



D-2

High-Purity U
Beta Quench

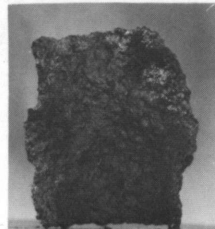
$$\frac{\Delta V}{V} = 2.7\%$$



E-1

U + Fe-Si
1000 C/24 hr
Water Quench

$$\frac{\Delta V}{V} = 0.64\%$$



E-2

U + Fe-Si
1000 C/24 hr +
Beta Quench

$$\frac{\Delta V}{V} = 0.8\%$$

FIGURE 3.27

Macroappearance of Specimens Irradiated in Capsule P-2
1000 psi, 450 C to 0.13 at.% BU
(1.5X)

Neg. C-6917, 6923, 6929, 6935, 6941. Neg. C-6920, 6929, 6932, 6938, 6944

TABLE 3.10

IRRADIATION HISTORY AND VOLUME CHANGE OF SPECIMENS IN CAPSULES P-2^(a)

Specimen Number	Material	Heat Treatment	Irradiation Temperature, C		As-Irradiated Density ρ , g/cc	% Swelling $\frac{\rho_i - \rho_f}{\rho_f} \times 100$	"R" % Swelling at.% BU
			Reactor Up	Reactor Down			
P-2 A-1	High-Purity U ^(b)	As-Extruded	375	380	18.85	0.8	6.5
A-2	High-Purity U	As-Extruded			18.80	1.1	8.5
P-2 B-1	U + Fe-Al ^(c)	Beta Heat Treat ^(d)	430	430	18.85	0.3	2.0
B-2	U + Fe-Al	730 C - 15 min Oil Quench			18.80	0.5	4.1
P-2 C-1	High-Purity U	As-Extruded	450	450	18.80	1.1	8.5
C-2	High-Purity U	As-Extruded			18.63	2.0	15
P-2 D-1	High-Purity U	730 C - 15 min Oil Quench	Not Recorded		18.70	1.7	13
D-2	High-Purity U	730 C - 15 min Oil Quench			18.50	2.7	21
P-2 E-1	U + Fe-Si ^(e)	1000 C - 24 hr Water Quench	415	425	18.83	0.6	4.8
E-2	U + Fe-Si	730 C - 15 min Oil Quench			18.80	0.8	6.2

(a) Capsule P-2 Irradiated at 1000 psi, 450 C to 0.13 at.% BU

(b) High-Purity Uranium - 65 Fe, < 5 Al, 24 Si, 6 C

(c) U + Fe-Al - 400 Fe, 640 Al, 85 Si, 500 C

(d) Beta Heat Treat - Large specimen heat treated in the bulk prior to specimen machining.

(e) U + Fe-Si - 140 Fe, 25 Al, 95 Si, 400 C

with the very large grained beta quenched specimens and also some general warpage. These large grain specimens (D-1 and D-2) exhibited very slightly more swelling than did the fine grain specimens but part of this may be due to a slightly low density measurement because of the very rough surface of the large grain specimens.

Preliminary metallographic examination of these specimens corroborates the macroappearance and the density changes. Figure 3.28 depicts the structure of the high-purity uranium, as-extruded Specimen P-2 C-1. The worked nature of the microstructure is obvious and typical for uranium irradiated at this temperature. It is significant that no tears are present in this sample. This is to be compared with the large amount of tearing depicted in Figure 3.8(a) which illustrates the microstructure of similar material irradiated at the same temperature to about the same burnup but at about 1 atm pressure.

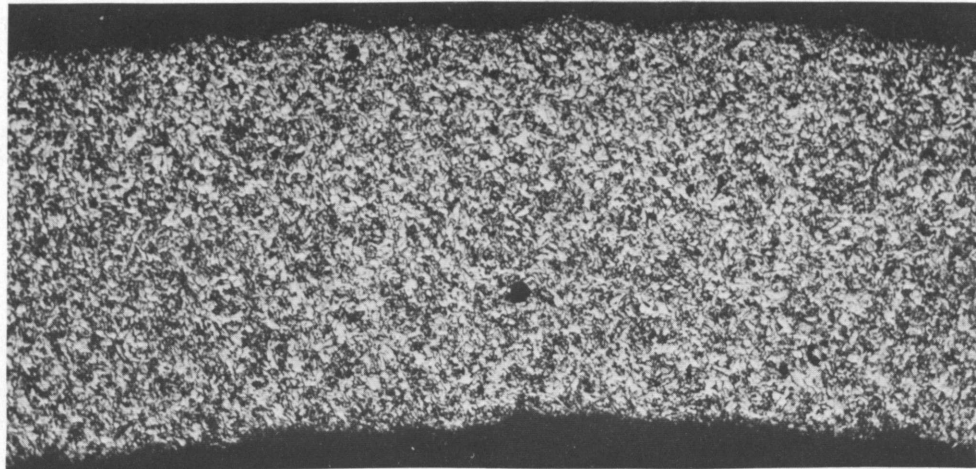
Metallographic examination of the Capsule P-2 specimens is continuing and the results will be available shortly.

Supplemental Studies

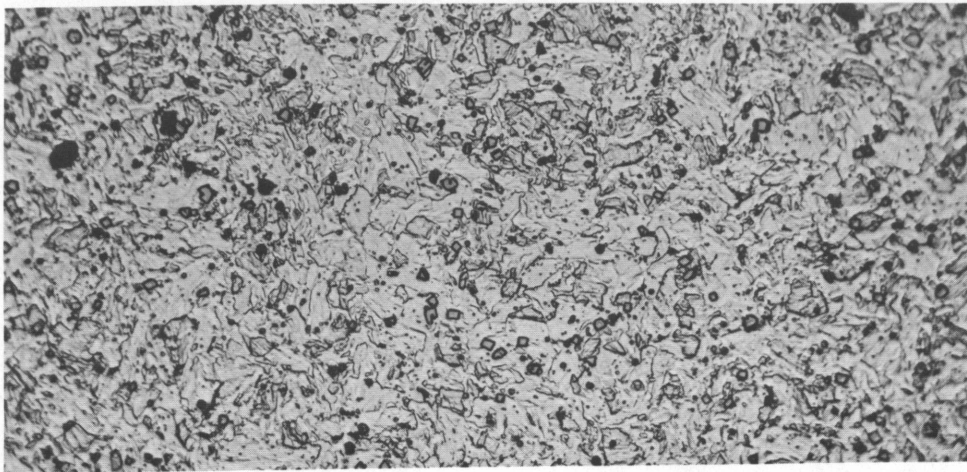
Thin Foils

Previous Quarterly Progress Reports have described techniques utilized to thin dilute uranium alloys for viewing by transmission electron microscopy.⁽¹⁾ It was found that the size of the particles observed by transmission techniques agreed well with those obtained from surface replicas. A semiquantitative method has been developed to determine the number of particles per unit volume for these alloys from transmission micrographs. Based on the assumption that the particles are spherical, the particles do not change in size during electropolishing, and a thickness can be assigned

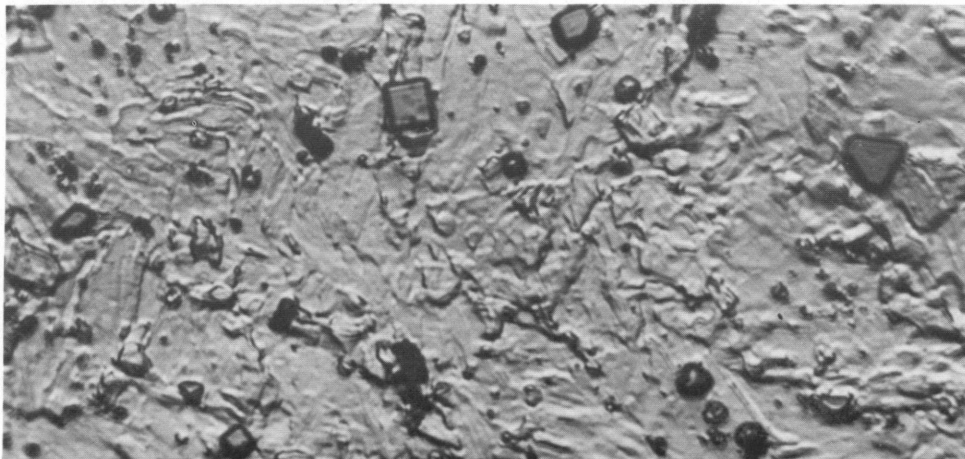
1. Quarterly Progress Report, Metallurgy Research Operation, July, August, September, 1964, edited by J. J. Cadwell, HW-84281, p. 3.56. September 15, 1964.



(75X)



(250X)



(1000X)

FIGURE 3.28

Microappearance of High Purity Uranium Specimen P-2 C-1
(1000 psi, 450 C, 0.13 at.% BU). Lightly Etched by Ion Bombardment
Neg. C-7418, C-7419, C-7420

to the thinned foil, then the number of particles per unit volume, PD, may be derived from the observed diameters from the relationship:

$$PD = \sum_i \frac{N_i}{(2 \hat{D}_i + t) \times A} \dots$$

where PD = the total number of particles per unit volume

N_i = the number of particles with diameters which fall in size range i revealed in the micrograph

\hat{D}_i = the average diameter of particles in an arbitrary but specific size range i

t = the foil thickness

A = the area of the micrograph

A relationship similar to the above has been developed on a theoretical basis by Hilliard⁽¹⁾ and yields comparable results when applied to the data discussed below.

The particle density for a uranium alloy containing 185 ppm Fe and 95 ppm Si rolled in the alpha phase was determined and compared with results derived from replicas. For a foil thickness of 250 Å, a particle density of 4.4×10^{11} particles/cc was calculated from transmission micrographs of this alloy. This agrees well with the value 5.1×10^{11} particles/cc which was determined by replica techniques by Woods, et al.⁽²⁾ Transmission micrographs were also prepared from an alloy whose composition was identical to that above but was beta-quenched and aged 1 hr at 590 C. Quantitative metallography, based on replica techniques, predicted the presence

-
1. J. E. Hilliard. The Counting and Sizing of Particles in Transmission Microscopy, 61RL-2885 M, General Electric Company, Research Laboratory, Schenectady, N. Y. December 1961.
 2. K. N. Woods, R. D. Leggett, and Y. E. Smith. Precipitate Particles in Dilutely Alloyed Uranium - Quantitative Metallography, HW-SA-3579, June 11, 1964.

of many particles having diameters less than 800 \AA , the lower limit of resolution of the technique. The diameter of the particles observed by transmission microscopy ranged from 100 to 3000 \AA . Indeed most diameters were less than 1000 \AA , in agreement with predictions based on replica techniques. Unfortunately, many of the small particles are the same size as dislocations and loops, and differentiation of particles is difficult. Several micrographs of a given area of the specimen at various orientations were obtained and analyzed. Only those spots or particles were measured which were not tilt sensitive. The particle density of this specimen had been estimated at 4.2×10^{11} particles/cc by replica techniques. The density of particles greater than 800 \AA was derived from transmission micrographs by the relationship given above; the value was 3.2×10^{11} particles/cc, again in good agreement with the value derived from replicas. In a similar fashion the density of particles with diameters smaller than 800 \AA was estimated from transmission micrographs and a value of 4.3×10^{14} particles/cc was obtained. This latter density is three orders of magnitude greater than the density ascribable to particles with diameters greater than 800 \AA . This difference most certainly emphasizes the value of high resolution transmission electron microscopy in the determination of particle density.

Line Broadening

Study of the X-ray line broadening of irradiated uranium subjected to postirradiation annealing has continued using the method developed by Warren.⁽¹⁾

The breadth of the (111) and (112) X-ray diffraction peaks has been determined in irradiated uranium as a function of postirradiation annealing. Figure 3.29(a) and (b) show the change in peak breadth as a function of

1. B. E. Warren. "X-Ray Studies of Deformed Metals," Prog. Met. Phys., vol. 8, p. 147, Pergamon Press, New York. 1959.

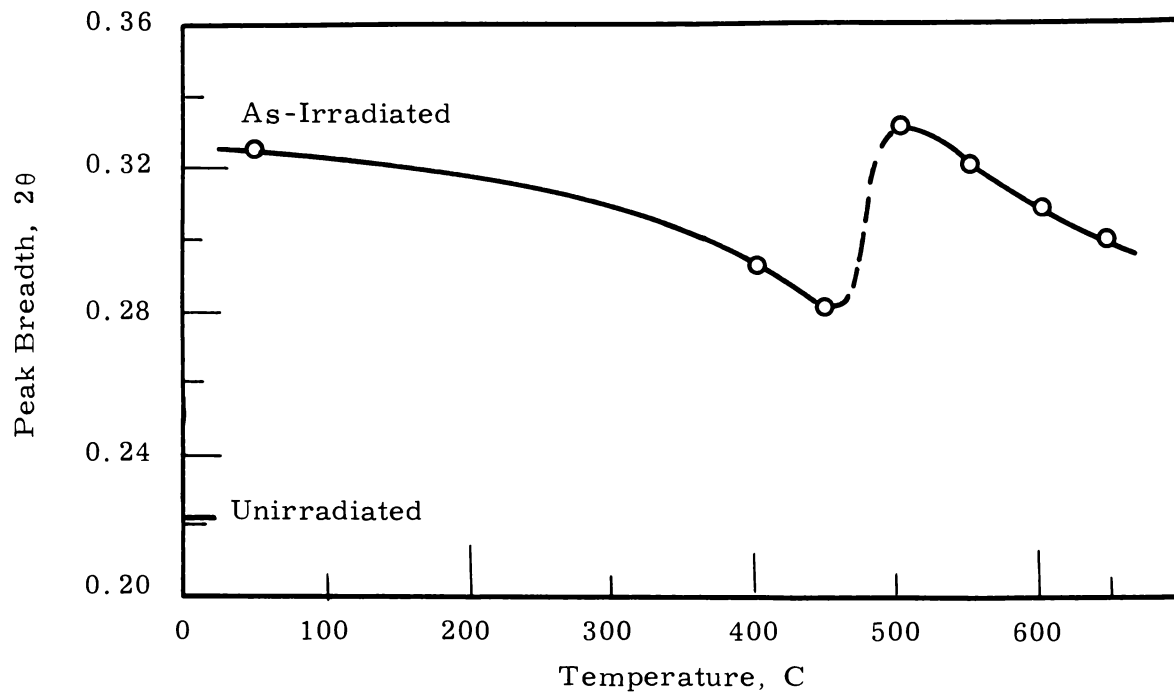
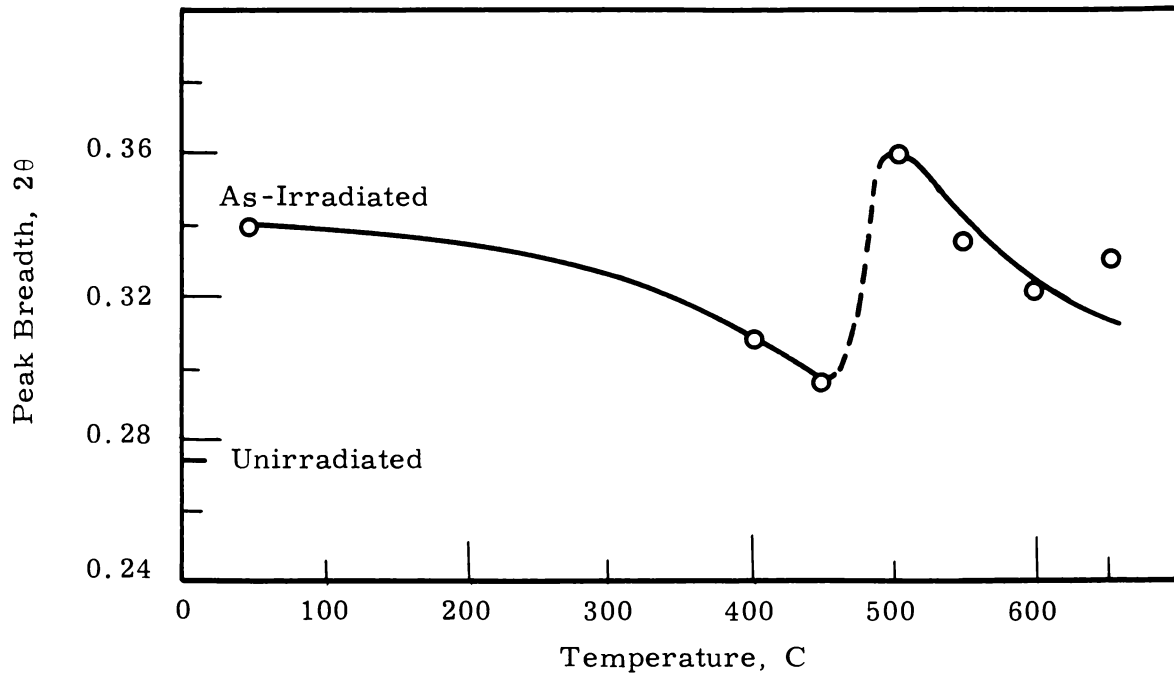


FIGURE 3.29

Peak Breadth vs. Annealing Temperature of Uranium
Irradiated to 0.37 at. % BU

annealing temperature for holding times of 30 min. Anomalous behavior is noted in the range 450 to 500 C where the breadth increases significantly after initially decreasing up to 450 C. Upon annealing at temperatures greater than 500 C, the breadth decreases again.

These observations suggest that some process associated with post-irradiation annealing is inducing an additional strain in the lattice. The strain may arise from submicroscopic pores in the lattice since pore formation due to gas accumulation is known to occur in the higher temperature ranges. Replica electron microscopy is currently being done on the samples to determine their structural state and degree of pore formation.

PLUTONIUM PHYSICAL METALLURGY - R. D. Nelson, F. E. Bowman,
H. E. Kissinger, and B. Mastel

The objective of this program is to conduct basic studies on the properties of high-purity unalloyed and alloyed plutonium. Studies will include investigation of phase transformation, phase stabilization, deformation, fracture, texturing, internal stresses, microcracking, grain growth, recovery and recrystallization, and measurement of mechanical and physical properties. The unique structure of several of the plutonium allotropes and their narrow temperature span of stability leads to characteristics and anomalies which, if explained, will contribute to the general area of solid state science.

Phase Transformation Studies

Research studies have been performed on the effect of concurrent applied compressive stress and prior plastic deformation on the $\beta \rightarrow \alpha$, $\alpha \rightarrow \beta$, $\beta \rightarrow \gamma$, and $\gamma \rightarrow \beta$ transformations. The primary objective of this activity was to obtain indirect information on the mechanisms of these transformations; a secondary objective was to study phase transformations in a metal that is unique because: (1) changes in volume of 9 and 3% are associated with the $\beta \rightarrow \alpha$ and $\gamma \rightarrow \beta$ transformations, respectively, (2) the transformations are between complex crystal structures, (3) the creep of the beta phase at a given stress and temperature can be varied between two and three orders of magnitude, (4) the ductility and the creep rate of the beta phase can be much greater than the ductility and creep rate of the alpha phase, and (5) the ductility and creep rate of the beta phase can either be less than or greater than the corresponding properties of the gamma phase.

The study of the $\alpha \rightarrow \beta$ transformation under applied compressive stress was reported previously.⁽¹⁾

1. Quarterly Progress Report, Metallurgy Research Operation, July, August, September, 1963, edited by J. J. Cadwell, HW-78962. October 15, 1963.

The strain during the $\beta \rightarrow \alpha$ transformation was studied as a function of applied compressive stress from 200 to 20,000 psi. The beta phase was formed by two methods, by transformation from the alpha and from the gamma phases. The beta phase was significantly strengthened by first transforming the metal to gamma and then transforming back to beta. This procedure for strengthening the beta phase was advantageous because the much lower creep rate of beta formed from gamma permitted tests at stresses up to 15,000 psi. When the beta was formed from alpha, tests could be performed at stresses no higher than 5000 psi without appreciable creep of the beta phase.

Specimens were heated to 260 C and held at temperature for 30 min to transform the metal to gamma. They were then cooled to 120 C to transform the gamma phase to the beta phase. The $\gamma \rightarrow \beta$ transformation was presumed complete after 1 hr at 120 C. Specimens in which the beta was formed directly from alpha were heated to 180 C and kept there for 1 hr to ensure complete $\alpha \rightarrow \beta$ transformation. All specimens were cooled to 110 C for testing.

Representative unit length changes associated with $\beta \rightarrow \alpha$ transformation with no applied stress as well as creep curves of the single phase alpha and beta phases are shown in Figure 3.30.

The unit length change during $\beta \rightarrow \alpha$ transformation was investigated as a function of the transformation rate. The unit length changes of plutonium under an applied compressive stress of 5000 psi are shown in Figure 3.31 as a function of time for three cooling rates. These curves clearly show the total unit length change during transformation to be only slightly dependent on the $\beta \rightarrow \alpha$ transformation rate. The unit length change was correlated with the approximated maximum transformation rate, because this was believed to be the best parameter describing transformation rate. A decrease in the maximum transformation rate from 50%/min to 0.15%/min caused only a 20% increase in the total unit length change associated with the $\beta \rightarrow \alpha$ transformation, Figure 3.32. The transformation temperature was raised approximately 15 C to decrease the maximum transformation rate

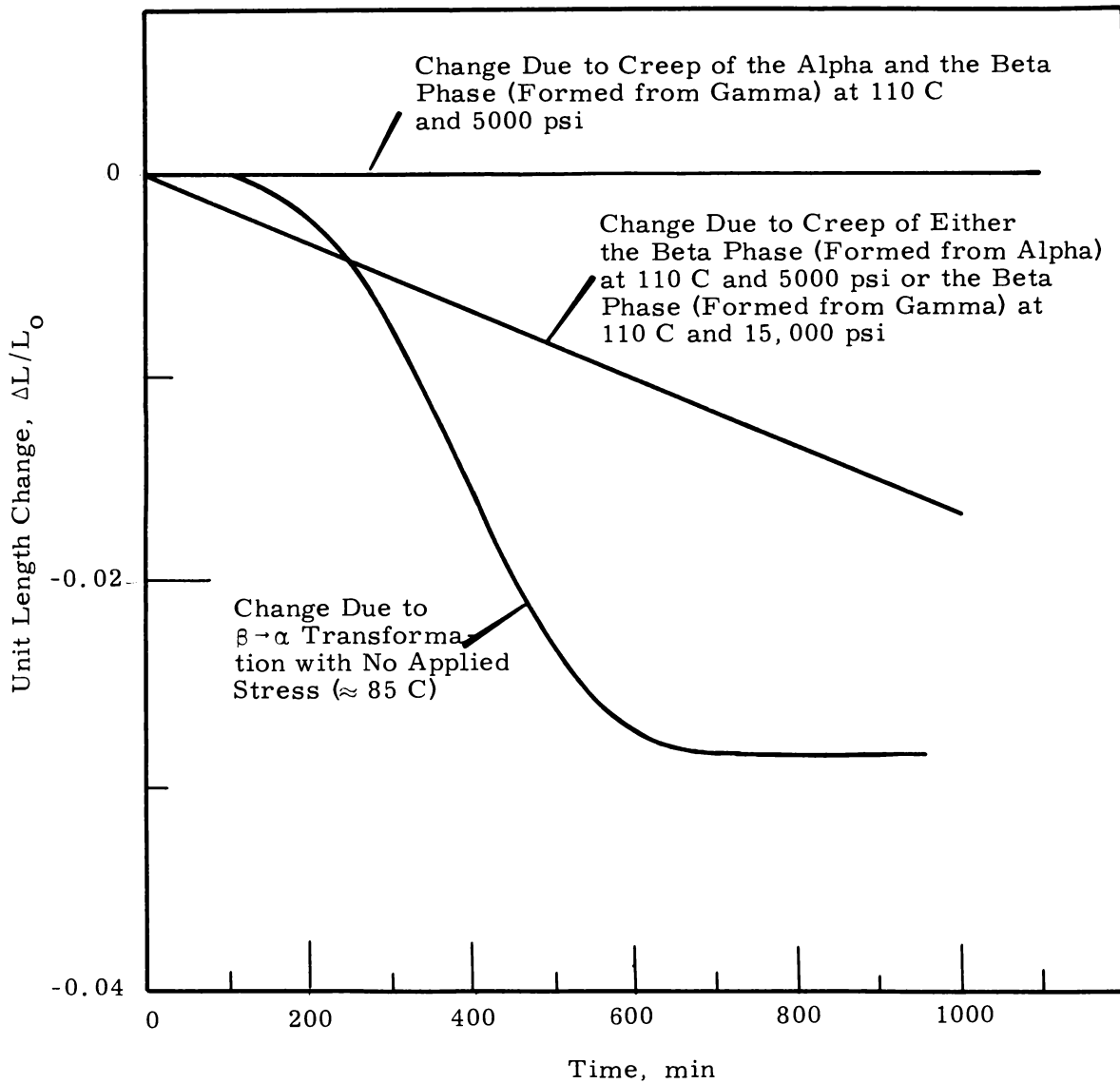


FIGURE 3.30

Representative Unit Length Change of Plutonium During Transformation from Beta to Alpha, and of Single Phase Alpha and Beta Plutonium at 110 C Under Applied Compressive Stresses

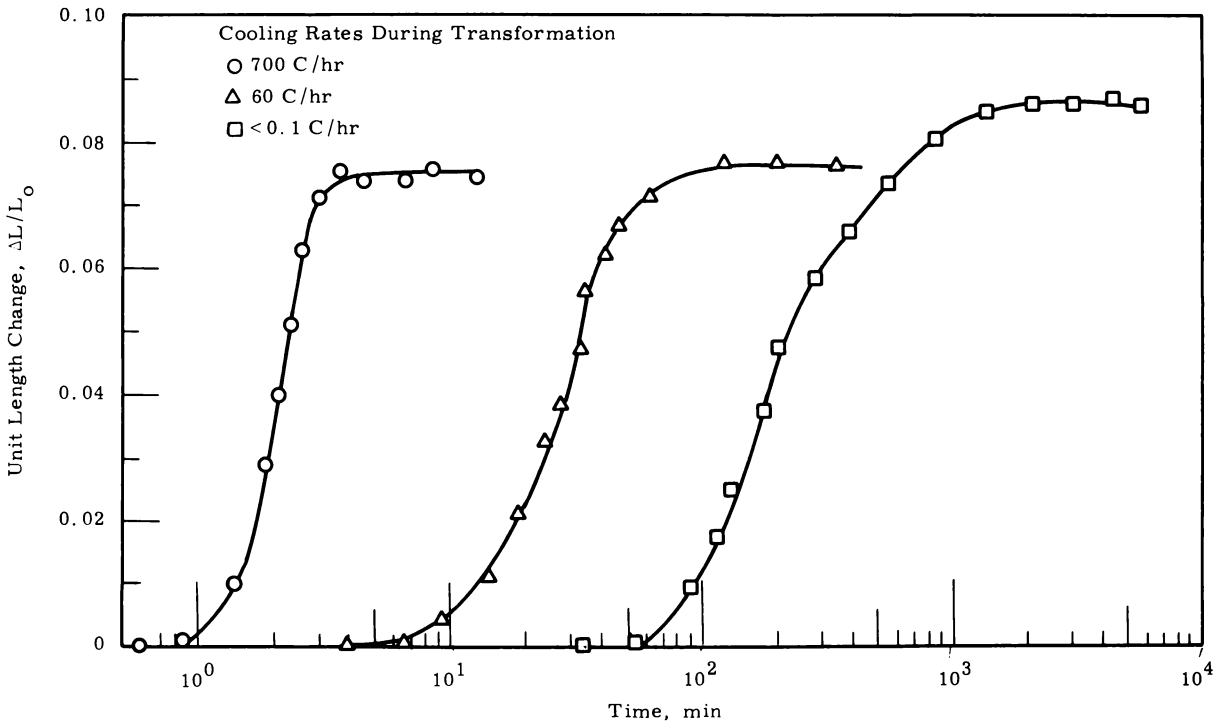


FIGURE 3.31

Unit Length Changes of Plutonium During the $\beta \rightarrow \alpha$ Transformation at 5000 psi. The Beta was Formed from Gamma.

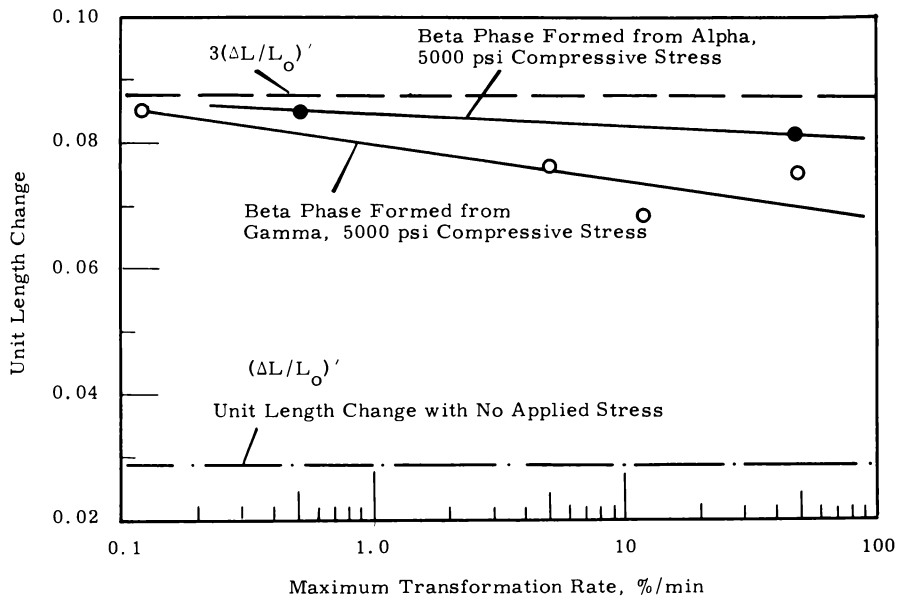


FIGURE 3.32

Effect of Transformation on the $\beta \rightarrow \alpha$ Transformation Strain

from 50%/min to 0.15%/min. Note that the unit length change is nearly the same regardless of whether beta was formed from alpha or gamma.

The unit length change during transformation rapidly increases with applied stress and reaches a constant value at about 9000 psi, Figure 3.33. This constant value of 0.09 is equal to $\Delta V/V_0$ and is approximately three times the isotropic unit length change, 0.03, expected for the change when transformation occurs with no applied stress. Thus the data might lead to the conclusion that the effect of applied stress is to cause all of the dimensional change during the $\beta \rightarrow \alpha$ transformation to occur in one direction only. If this is the case, then little or no creep deformation should occur.

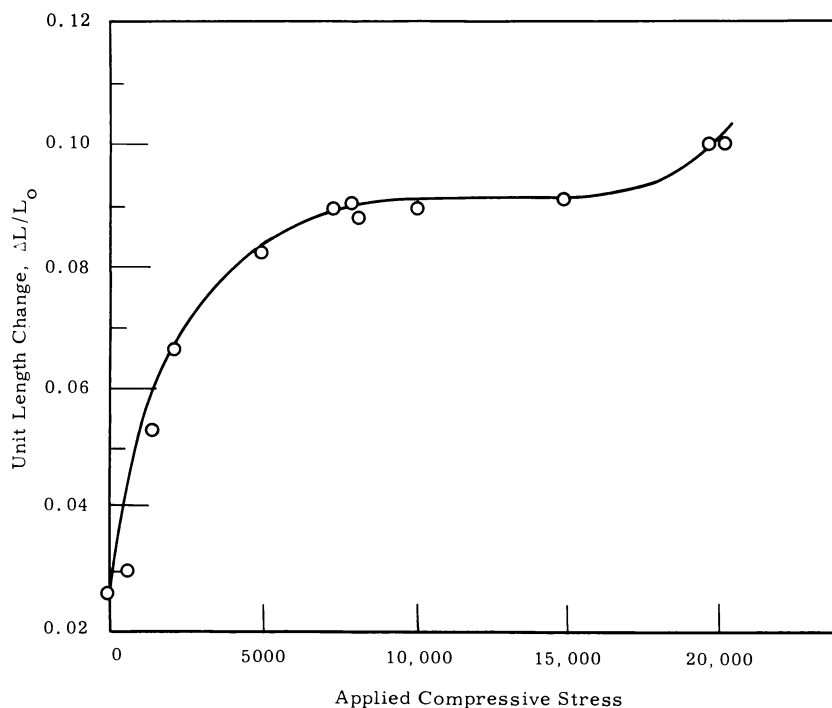


FIGURE 3.33

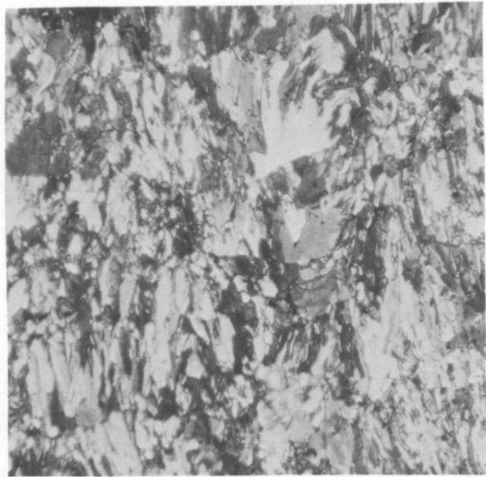
Effect of Applied Compressive Stress on the Unit Length Change During the $\beta \rightarrow \alpha$ Transformation at a Cooling Rate of 0.5-1.0 C/hr

If the $\beta \rightarrow \alpha$ transformation produces an abundance of excess vacancies which are trapped during the formation of the more dense phase, then creep of the specimen undergoing such transformation might very well be high if creep occurs by a vacancy diffusion mechanism. If transformation of the beta into alpha proceeds by a diffusion process involving vacancy migration, then the creep characteristics of the specimen undergoing transformation might well be altered. Because this is not the case, it might be inferred that diffusion during the $\beta \rightarrow \alpha$ transformation is not significant, and that diffusion does not play a major role in this transformation. This implies that the $\beta \rightarrow \alpha$ transformation is a diffusionless transformation.

Previously it was reported that alpha grains form in bands at transformation temperatures high in the alpha phase region.⁽¹⁾ These bands are randomly oriented in the absence of applied stress or thermal gradients. It was also reported that if a compressive stress of 15,000 psi is applied to the metal, the bands form at right angles to the compressive stress, while the grains within the bands are parallel with the applied stress. The banding is also evident in specimens transformed at only 2000 psi, Figure 3.34.

A specimen was also cycled 10 times through the $\alpha \rightarrow \beta$ and $\beta \rightarrow \alpha$ transformations. A compressive stress of 60,000 psi was applied to the specimen during the $\beta \rightarrow \alpha$ transformations. No stress was applied during the $\alpha \rightarrow \beta$ transformations. This procedure can produce large alpha grains, as revealed in the transverse section of the specimen shown in Figure 3.35.

1. Quarterly Progress Report, Metallurgy Research Operation, January, February, March, 1963, edited by J. J. Cadwell, HW-77052. April 15, 1963.



(a)

Neg. N-107

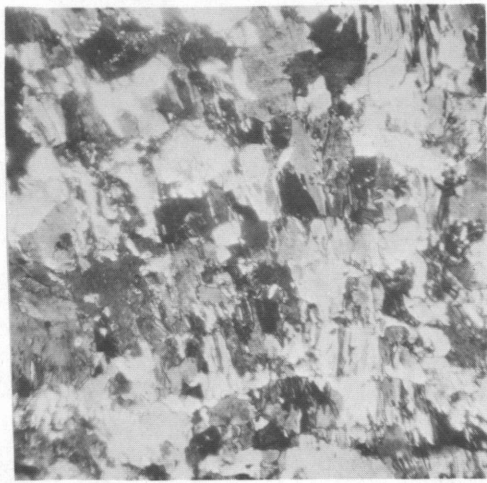
(100X)



(b)

Neg. N-96

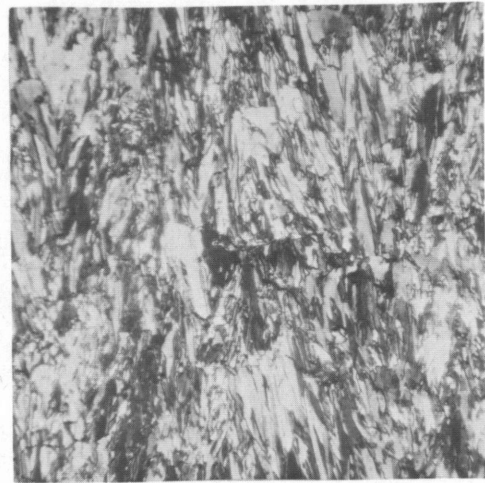
(100X)



(c)

Neg. N-103

(100X)



(d)

Neg. N-98

(100X)

FIGURE 3. 34

Photomicrographs Showing the Texturing That Occurs During the Transformation Under an Applied Compressive Stress. The Direction of the Applied Stress was Vertical.

	(a)	(b)	(c)	(d)
Applied Stress, psi	2000	7200	5000	5000
Cooling Rate, °C/min	0.005	0.005	0.005	0.5-1
Maximum Transformation Rate, %/min	0.5	0.5	0.5	10

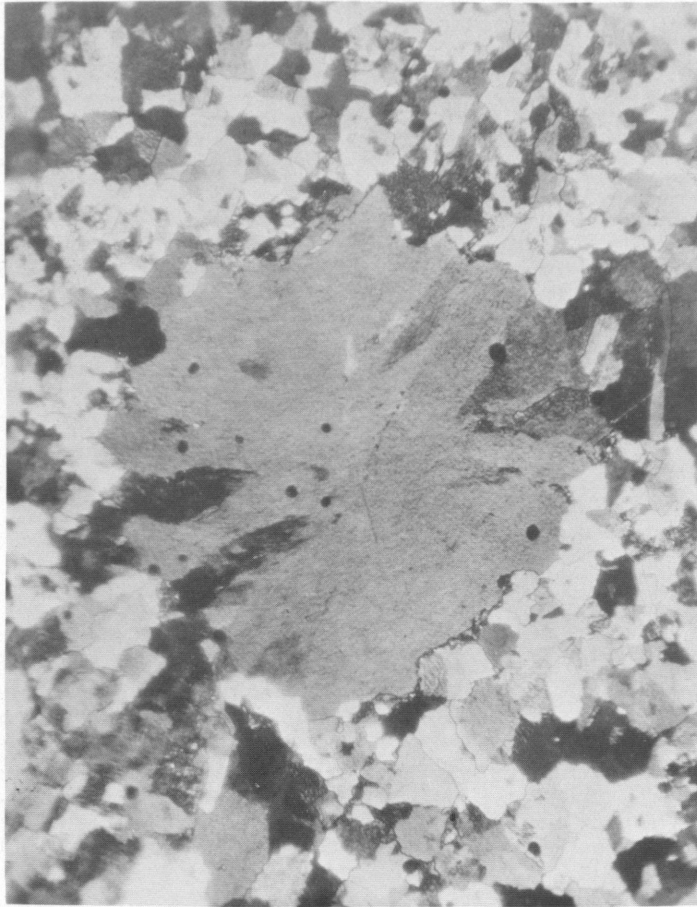


FIGURE 3.35

Large Alpha Grain Formed in a Specimen Cycled Through Ten Transformations During Which a Compressive Stress of 60,000 psi was Applied to the $\beta \rightarrow \alpha$ Transformations Only (200X)

Neg. N-117

A highly textured rod specimen with the 010 plane parallel to the cross sectional area was cycled once each through the $\alpha \rightarrow \beta$ and $\beta \rightarrow \alpha$ transformations. The length increased 7.9% and the diameter increased 0.8% during the $\alpha \rightarrow \beta$ transformation. This indicates that nearly all of the volume change during transformation occurred in a direction parallel to the length of the specimen. The length and the diameter decreased 1.2 and 4.3%, respectively, during the $\beta \rightarrow \alpha$ transformation. The sample after transformation cycling had increased in length by 6.5%. The diameter after transformation cycling had decreased by 3.4%. It is quite evident that both the $\alpha \rightarrow \beta$ and $\beta \rightarrow \alpha$ transformations result in anisotropic volume changes.

The unit length change during the $\gamma \rightarrow \beta$ transformation was evaluated as a function of applied compressive stress from 100 to 3000 psi. Representative data of the unit length changes associated with the $\gamma \rightarrow \beta$ and $\beta \rightarrow \gamma$ transformations with no applied stress and creep curves of the single phase beta and gamma phases are shown in Figure 3.36. Creep of the gamma phase at 190 C at stresses above 3000 psi is so great that it obscures the unit length change associated with the $\gamma \rightarrow \beta$ transformation.

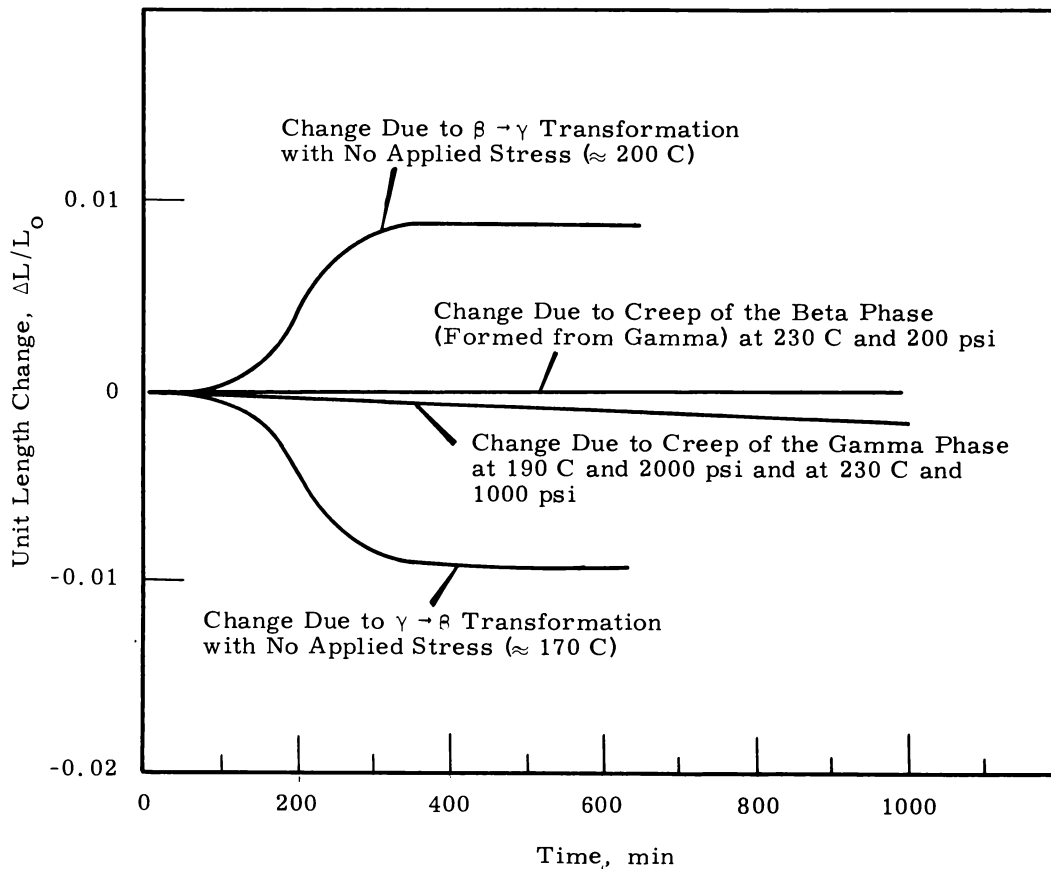


FIGURE 3.36

Representative Unit Length Changes of Plutonium During Transformation from $\gamma \rightarrow \beta$ and $\beta \rightarrow \gamma$ and of the Beta and Gamma Phases Under Applied Compressive Stresses

In the $\gamma \rightarrow \beta$ transformation investigations specimens 0.30-in. in diameter and 0.45 in. in length were heated to 260 C for 30 min to transform the metal to gamma and then cooled to 195 C at which temperature the tests

were started. Prior to performing the $\beta \rightarrow \gamma$ transformation creep experiments, the specimens were subjected to a $\gamma \rightarrow \beta$ pretreatment. The gamma pretreatment ensures that stresses up to 2000 psi at 230 C can be applied to the specimen with negligible creep of the beta phase. Ordinarily stresses of only 1000 psi would cause extensive creep at 230 C of beta formed from alpha.

The unit length change was investigated as a function of the transformation rate, Figures 3.37 and 3.38, and as a function of the applied stress, Figure 3.39. These curves clearly show that the $\gamma \rightarrow \beta$ transformation is strongly dependent upon the transformation rate; certainly more than in the $\beta \rightarrow \alpha$ transformation.

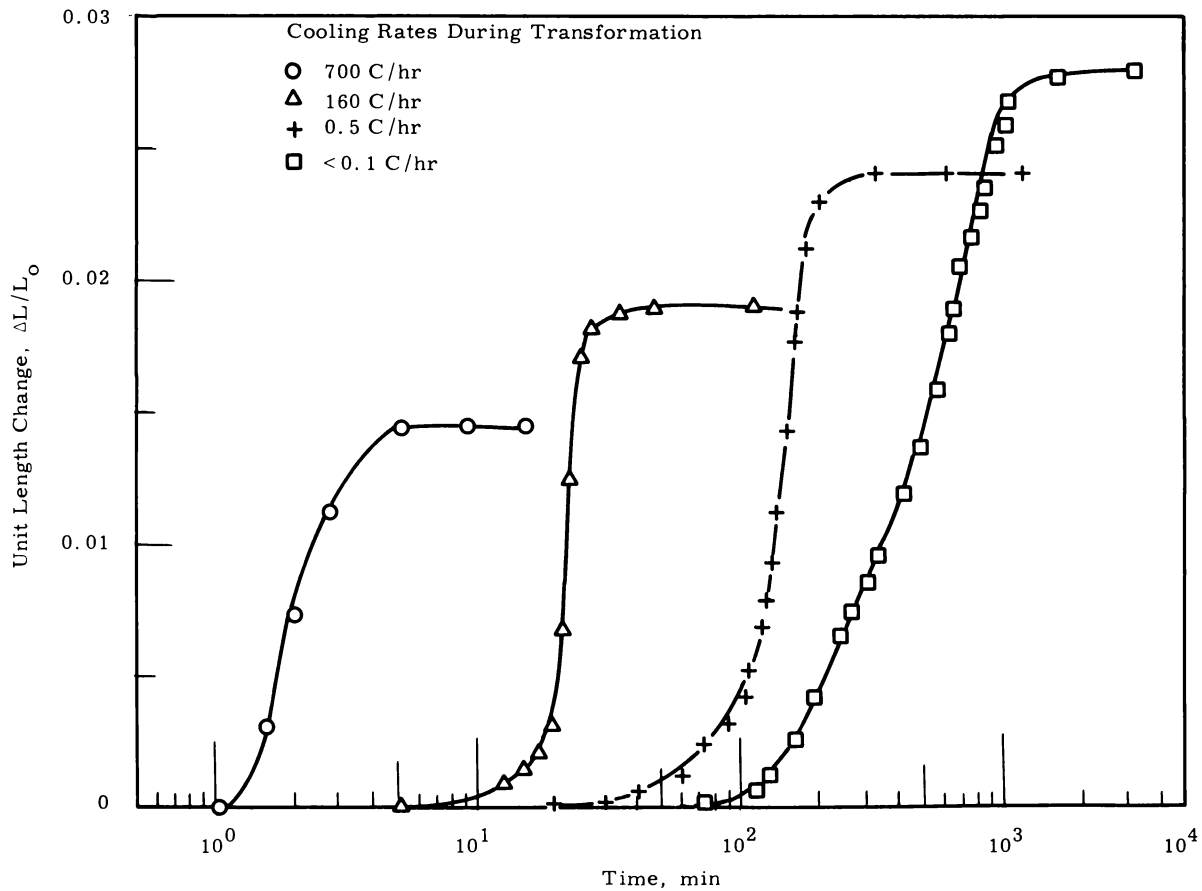


FIGURE 3.37

Unit Length Changes of Plutonium
During the $\gamma \rightarrow \beta$ Transformation at 2000 psi

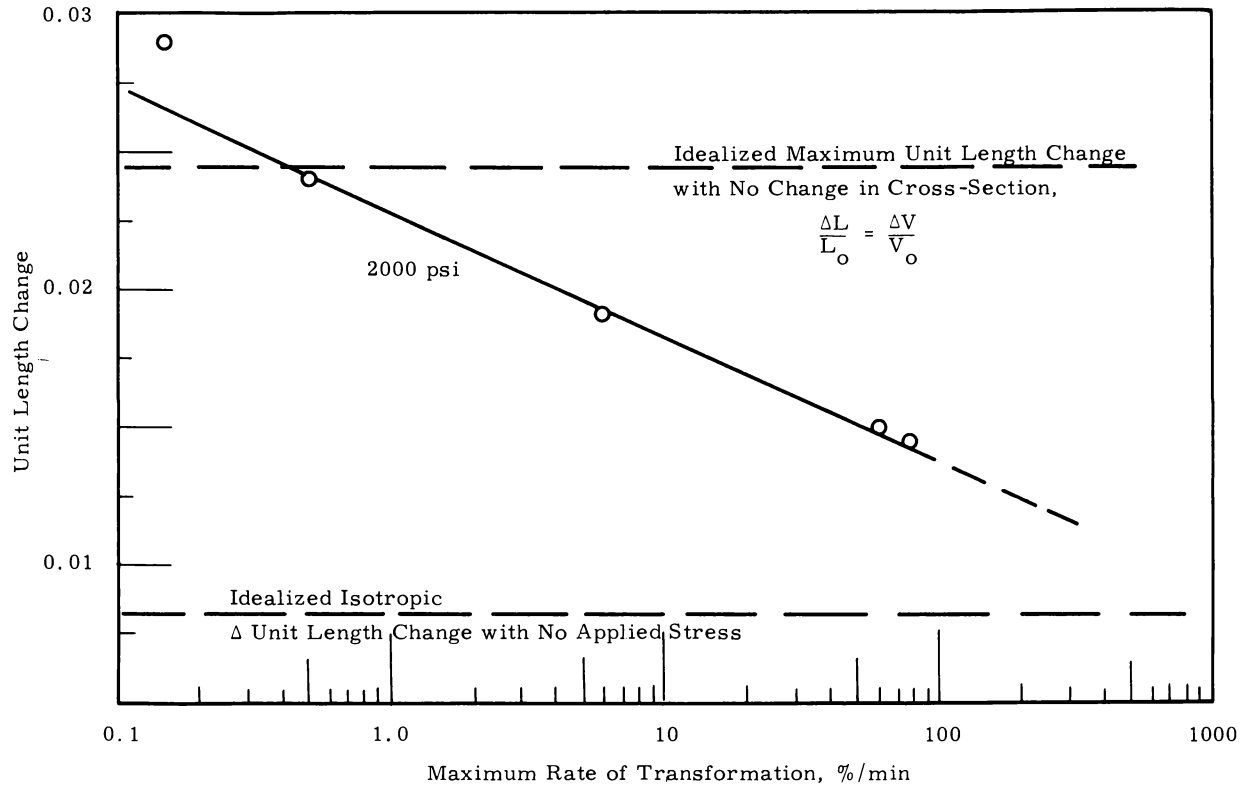


FIGURE 3.38

Effect of Transformation Rate on the $\gamma \rightarrow \beta$ Transformation Strain

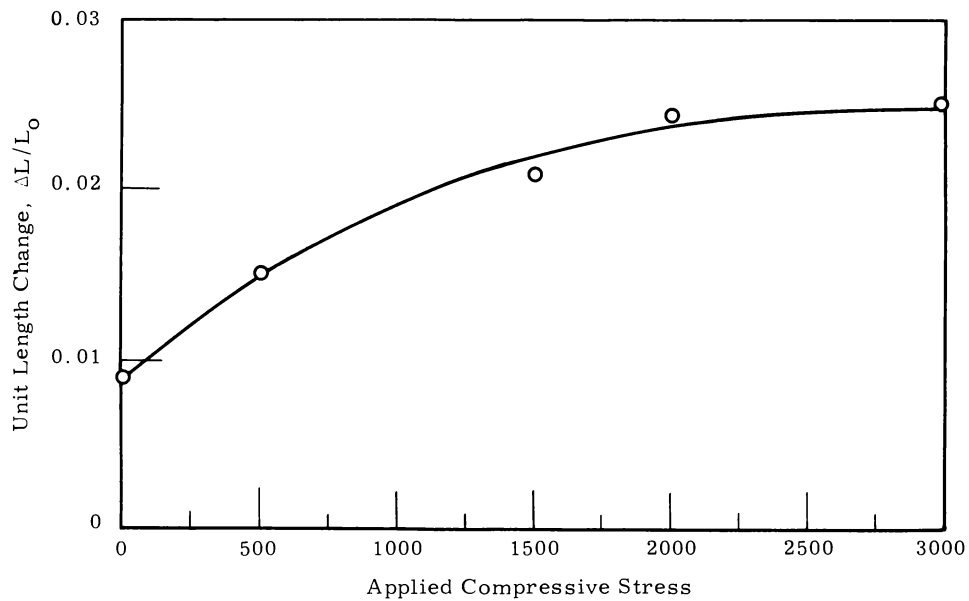


FIGURE 3.39

Effect of Applied Compressive Stress on the Unit Length Change During the $\gamma \rightarrow \beta$ Transformation at a Cooling Rate of 0.5 C/hr

The study of the influence of plastic deformation of beta plutonium on subsequent transformation to the alpha phase was completed. A series of specimens from the same melt were compressed from 0 to 95% reduction in thickness in the beta phase. The beta phase material, originally formed from both alpha and from gamma, was allowed to transform to the alpha phase at different temperatures. Also, the effect of plastic deformation by compression was compared to the effect of plastic deformation by tension in an analogous set of specimens. It was previously shown that beta plastic deformation by compression increases the $\beta \rightarrow \alpha$ incubation time and decreases the $\beta \rightarrow \alpha$ transformation rate, regardless of whether beta was formed from alpha or gamma. Plastic deformation by tension also decreases the transformation rate. The decrease in transformation rate is not as great for beta deformed by tension as it is for beta deformed by compression.

The study of the effect of deformation temperature on the $\beta \rightarrow \alpha$ transformation showed that the higher deformation temperature caused a slower rate of transformation, Figure 3.40. The $\beta \rightarrow \alpha$ transformation rates after 75 to 85% reduction in thickness showed very little difference between beta formed from alpha or beta formed from gamma. Increasing the extent of deformation to amounts greater than 20% reduction in thickness has little effect on the $\beta \rightarrow \alpha$ transformation rate of beta formed from alpha; however, increasing the extent of deformation decreases the transformation rate of beta formed from gamma, Figure 3.41.

The influence of gamma plastic deformation and its relationship to the mechanism of the $\gamma \rightarrow \beta$ transformation was also investigated. One specimen was compressed to 80% reduction in thickness at 220 C after a $\beta \rightarrow \gamma$ transformation at 250 C for 30 min. This was followed by a $\gamma \rightarrow \beta$ transformation at 155 C, which permitted a reasonable time for transformation.

The reaction rate of the gamma deformed metal was compared to the reaction rate of undeformed metal. It is evident from Figure 3.42 that gamma deformation accelerates the $\gamma \rightarrow \beta$ transformation. This is the opposite effect of beta deformation on the $\beta \rightarrow \alpha$ transformation and is more characteristic of nucleation and growth reactions.

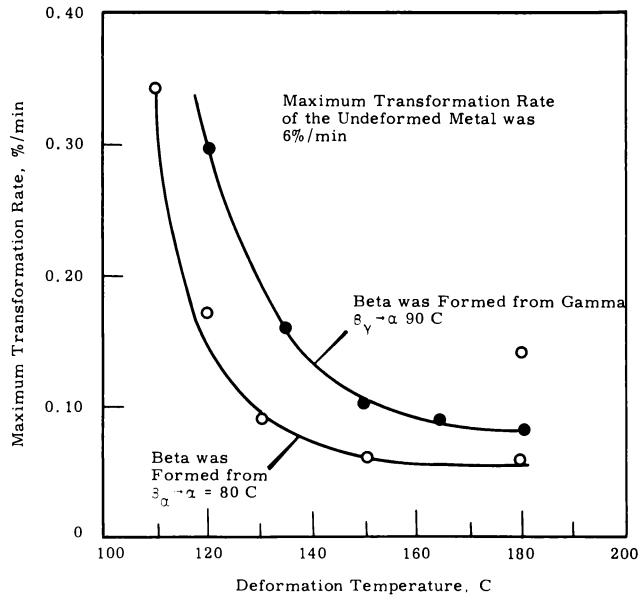


FIGURE 3.40

Effect of Beta Deformation Temperature on the $\beta \rightarrow \alpha$ Transformation

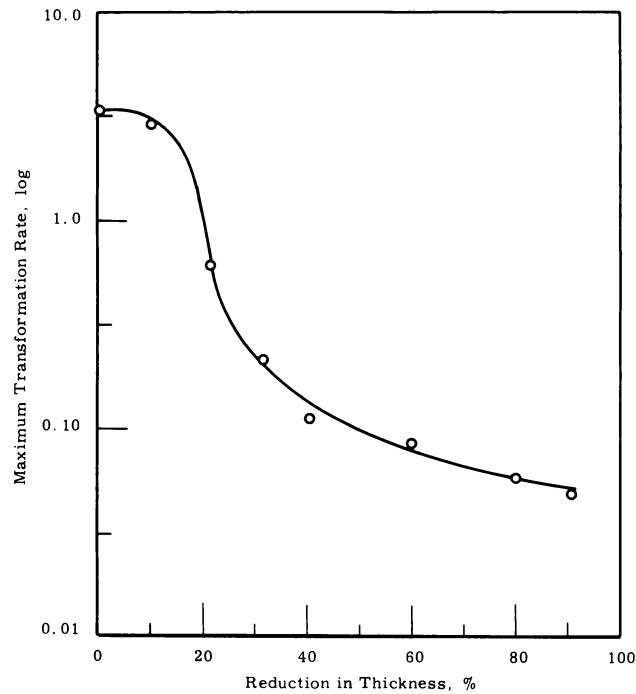


FIGURE 3.41

Effect of Beta Plastic Deformation by Compression on the $\beta_{\gamma} \rightarrow \alpha$ Maximum Transformation Rate

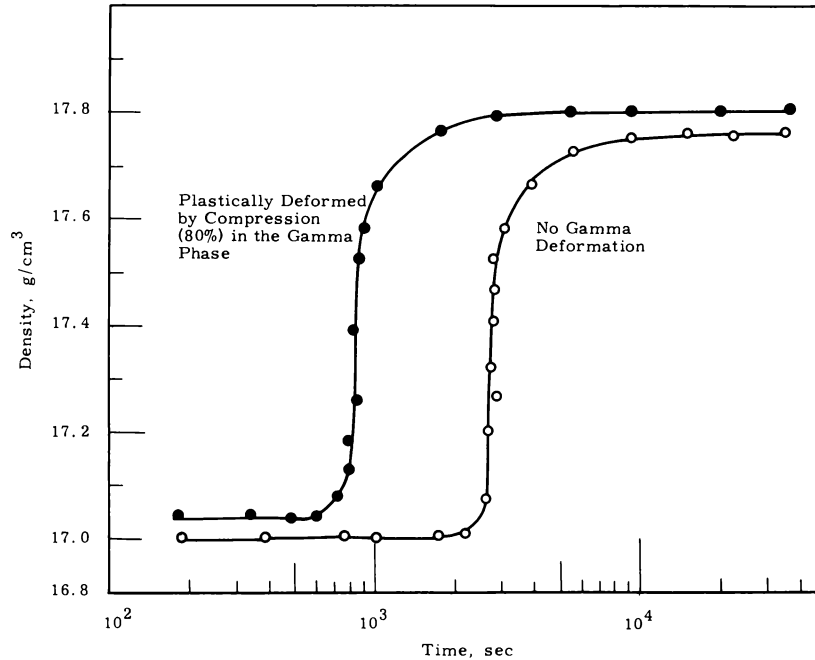


FIGURE 3.42

Effect of Plastic Deformation on the $\gamma \rightarrow \beta$ Transformation

Crystallographic Studies

The installation of an elevated temperature holder on the X-ray diffractometer has permitted the initiation of a study of the crystallographic phenomena involved in the transformations of plutonium. Initially, work was undertaken to calibrate the new equipment and determine its capabilities. The results, however, have been of such interest and show sufficient promise of leading to an understanding of the mechanisms involved in the various lower temperature phase transformations that these studies have been pursued to a much greater extent than originally planned.

The new equipment is an evacuable high temperature specimen holder built by Electronics and Alloys and designed for use with the General Electric XRD-5 X-ray diffractometer. The difference in the maximum design temperature and the range of interest in connection with plutonium made possible some radical changes in the method of heating the sample. As now in use the sample—a relatively thin section about 1/2 in. in diameter—

is heated from the rear by a cigar lighter type of resistance heater. The temperature is measured by two thermocouples in contact with the sample surface. Tests have indicated that at 250 C a temperature gradient of no more than 2 degrees exists across the sample face. The attainable vacuum is such that plutonium samples can be held in the gamma phase for as long as 24 hr before serious oxide interference is encountered.

To date two types of samples have been included in the investigation. Although both are of high purity, one type is a random structure produced by quenching from the gamma phase to -80 C and the other has the fiber texture produced by transforming from beta to alpha under a compressive load. As has been reported previously, this produces a texture in which the 020 plane lies perpendicular to the direction of applied stress. In the case of this latter type specimen both the transverse and the longitudinal section surfaces have been included in the investigation.

Briefly the investigation has consisted of following the changes induced in the alpha, the beta and the gamma patterns after repeated phase transformations. An opportunity is also afforded to follow the actual transformation as it affects the intensity of one line in the parent phase pattern. Although only one, essentially uncontrollable, cooling rate is available it is reproducible and permits a direct comparison of the transformation rates under slow cooling conditions.

At the present time it is not possible to investigate the texture of the specimens in the beta and gamma phases by means of a goniometer. The relative line intensities in the respective 2θ patterns gives some indication of the formation of a texture in each phase as a result of repeated cycling through the transformations. Obviously this must be looked at in several samples and after many cycles in each before it can be assumed that there is real consistency in the results. The detailed analysis of these data directed toward a determination of crystallographic relationships existing between the various phases is underway. It is apparent, however, that the task is a major one.

A few general observations can be made with some certainty. In the case of the initially textured, pressed samples it has become apparent that repeated $\alpha \rightarrow \beta$ cycles do not significantly alter the alpha texture. It has not been possible as yet to establish with any degree of certainty a related beta texture. It would appear reasonable to expect the existence of such a texture, however. The initially randomly oriented specimens have given evidence of developing a texture as a consequence of the $\alpha \rightarrow \beta$ cycling. The degree and rapidity with which this texture assumes importance appears to be associated with the thickness of the sample—the thinner the specimen the more readily it develops an orientation. This may be related to the heating and cooling process or it may be the result of the stress patterns set up during the transformation process.

In connection with the actual transformation process as observed on the diffractometer several phenomena have been observed. There appears to be, for example, a significant difference in the $\beta \rightarrow \alpha$ transformation rate for the beta formed from alpha and that from gamma, the latter being the most rapid. There also appears to be approximately 10 C difference in the temperature at which this transformation begins under the existing cooling conditions. The beta formed from gamma seems to start the transformation to alpha at about 90 to 95 C as compared to 80 to 85 C for the beta formed from alpha. There are indications that the $\beta \rightarrow \alpha$ transformation rate is related in some manner to the resulting alpha texture which must in turn be related to that in the beta phase.

The investigations have not as yet reached the stage at which crystallographic details can be discussed with certainty. There is an increasing amount of evidence that the increased beta strength, noted when that phase results from a $\gamma \rightarrow \beta$ transformation as compared with beta formed by an $\alpha \rightarrow \beta$ transformation, is related to the different crystallographic orientations established in the beta material by the transformations.

REACTOR METALS RESEARCH

ALLOY SELECTION - T. T. Claudson

Mechanical Property Testing

Several nickel-base alloys are being irradiated and tested to determine the effects of irradiation and environment upon their mechanical properties. These materials are being irradiated at 50, 280, 580, and 740 C and tested in tension at room temperature and 650 C. Exposures achieved to date vary between 5×10^{19} and 8.3×10^{20} nvt fast.

Specimens of Hastelloy X-280 irradiated at 280 C to exposures of 8.3×10^{20} nvt fast have been tested at 650 C. Preliminary results of these tests are shown in Table 4.1 together with data previously reported for room temperature tests. Data from this table indicates that a marked reduction in ductility occurs at the 650 C test temperature. Specimens irradiated at 280 C and tested at 650 C have a uniform elongation of about 5% after an exposure of 8.3×10^{20} nvt fast compared to values of about 30% when tested at room temperature at nearly the same exposure. Similar comparisons can be made for total elongation and percent reduction in area.

TABLE 4.1
TENSILE DATA FOR HASTELLOY X-280 IRRADIATED AT 50, 280, AND 740 C

Specimen Number	Exposure, nvt E > 1 Mev	0.2% Yield Strength, psi	Ultimate Strength, psi	Reduction in Area, %	Total Elongation, %	Uniform Elongation, %	Temperatures, C	
							Irradiation	Test
137-2	1.03×10^{20}	25,700	48,600	16.6	4.8	4.8	280	650
138-2	1.57×10^{20}	26,800	52,500	27.0	7.3	6.8	280	650
104-5	8.3×10^{20}	39,800	59,400	25.8	4.5	4.5	280	650
99-4	4.96×10^{19}	73,270	120,090	48.6	--	40.6	280	RT*
99-5	4.96×10^{19}	70,930	116,980	41.01	--	46.9	280	RT
100-4	7.41×10^{19}	73,970	118,720	46.03	--	46.03	280	RT
100-5	7.41×10^{19}	77,340	126,110	46.31	--	46.31	280	RT
434-3	9.8×10^{19}	94,920	124,870	59.30	42.34	34.21	50	RT
434-4	9.8×10^{19}	95,480	125,380	57.29	37.33	34.81	50	RT
435-5	7.64×10^{20}	103,830	128,830	53.57	32.29	27.51	50	RT
435-6	7.64×10^{20}	106,440	131,440	55.15	37.32	29.88	50	RT
436-7	4.61×10^{20}	97,960	118,670	53.57	37.82	32.07	50	RT
436-8	4.61×10^{20}	98,740	125,170	53.77	37.08	30.90	50	RT
A-55	9.0×10^{19}	56,060	125,050	16.67	--	26.56	740	RT

* RT = Room Temperature

Specimens of Inconel 625 have now been irradiated at average temperatures of 740, 280, and 50 C and tested at room temperature. Data for these tests are shown in Table 4.2. From these data it is evident that the higher irradiation temperature has a definite effect upon the ductility of the material. The percent reduction in area for the 740 C irradiation was found to be about 10% as compared to about 43% and 60% for the 280 C and 50 C irradiations, respectively, at fairly comparable exposures.

TABLE 4.2
TENSILE DATA FOR IRRADIATED INCONEL 625 ALLOY

Specimen Number	Temperature, C		Exposure nvt E > 1 Mev	0.2% Yield Strength, psi	Ultimate Tensile Strength, psi	Reduction in Area %	Uniform Elongation, %	Total Elongation, %
	Irradiation	Test						
A-43	740	RT*	9.02×10^{19}	113,260	155,360	9.94	12.72	13.01
A-44	740	RT	9.02×10^{19}	114,410	158,190	10.17	11.45	11.85
92-D2	280	RT	5.8×10^{19}	125,830	187,720	39.07	39.08	--
92-D3	280	RT	5.8×10^{19}	111,140	152,300	47.56	37.34	--
434-5	50	RT	9.8×10^{19}	124,580	149,720	60.34	29.29	33.59

* RT = Room Temperature

An even greater effect of test temperature is shown in Table 4.3. This table shows the tensile data for Inconel 625 specimens irradiated at 280 C to an exposure of 1.03×10^{20} nvt (E > 1 Mev) and tested at room temperature, 300 C, and 650 C. The effects of test temperature was to decrease the yield and ultimate strength of this alloy by 48%. A marked decrease in ductility was also found, the percent uniform elongation decreasing from 39% at room temperature to 5% at a test temperature of 650 C.

TABLE 4.3
TENSILE DATA FOR INCONEL 625 IRRADIATED
AT 280 C TO AN EXPOSURE OF 1.03×10^{20} nvt (E > 1 Mev)

Specimen Number	0.2% Yield Strength, psi	Ultimate Strength, psi	Reduction in Area, %	Total Elongation, %	Uniform Elongation, %	Test Temperature, C
137-13	110,950	153,730	49.75	41.99	38.87	RT*
137-15	94,300	139,500	17.2	27.0	26.7	300
137-14	75,000	103,000	13.5	5.0	5.0	650

* RT = Room Temperature

IN-REACTOR MEASUREMENTS OF MECHANICAL PROPERTIES -

J. A. Williams, D. H. Nyman, and J. W. Carter

The objective of the in-reactor measurements program is to define the effects of fast neutron irradiation on the mechanical properties of structural materials. The program is presently involved with the studies of the in-reactor creep properties of annealed AISI 304 SS.

In-Reactor Measurements

During the past quarter in-reactor creep tests on annealed AISI 304 SS at 650 C, 20,000 psi and 550 C, 30,000 psi were started. The 550 C, 30,000 psi in-reactor tests exhibited a creep rate of 2.8×10^{-5} /hr after 300 hr, which is very close to the out-of-reactor rate of 2.7×10^{-5} /hr at the same experimental conditions. The 650 C, 20,000 psi test showed a rate of 5.7×10^{-4} /hr at 60 hr, at which time the reactor shut down. During the outage the rate decreased to a minimum of 3.6×10^{-4} /hr at 120 hr. Due to the reactor outage a minimum strain rate during neutron irradiation was not obtained. The out-of-reactor test at 650 C, 20,000 psi exhibited creep rates of 7.8×10^{-4} /hr at 60 hr and 3.9×10^{-4} /hr at 380 hr. A marked effect of neutron irradiation on the ductility and rupture life of annealed AISI 304 SS was observed with the 650 C, 20,000 psi creep tests. The in-reactor creep test failed at ~8 to 9% total elongation after 145 hr of test time, while the out-of-reactor test exhibited a 29% elongation on failure after after 480 hr of testing.

The data to date, with the exception of the preceding two in-reactor tests, is shown on Arrhenius plot in Figure 4.1. The data compares favorably with that found in the literature.^(1, 2) The activation energy, as determined from the plot, for out-of-reactor creep of annealed AISI 304 SS is 95,000 cal/mole for the Hanford data and 100,000 cal/mole for the referenced data.

-
1. G. V. Smith, E. J. Dulis, and E. G. Houston. "Creep and Rupture of Several Chromium-Nickel Austenitic Stainless Steels," ASM Transactions, vol. 42, pp. 935-978. 1950.
 2. E. J. Dulis, G. V. Smith, and E. G. Houston. "Creep and Rupture of Chromium-Nickel Austenitic Stainless Steels," ASM Transactions, vol. 45, pp. 42-76. 1953.

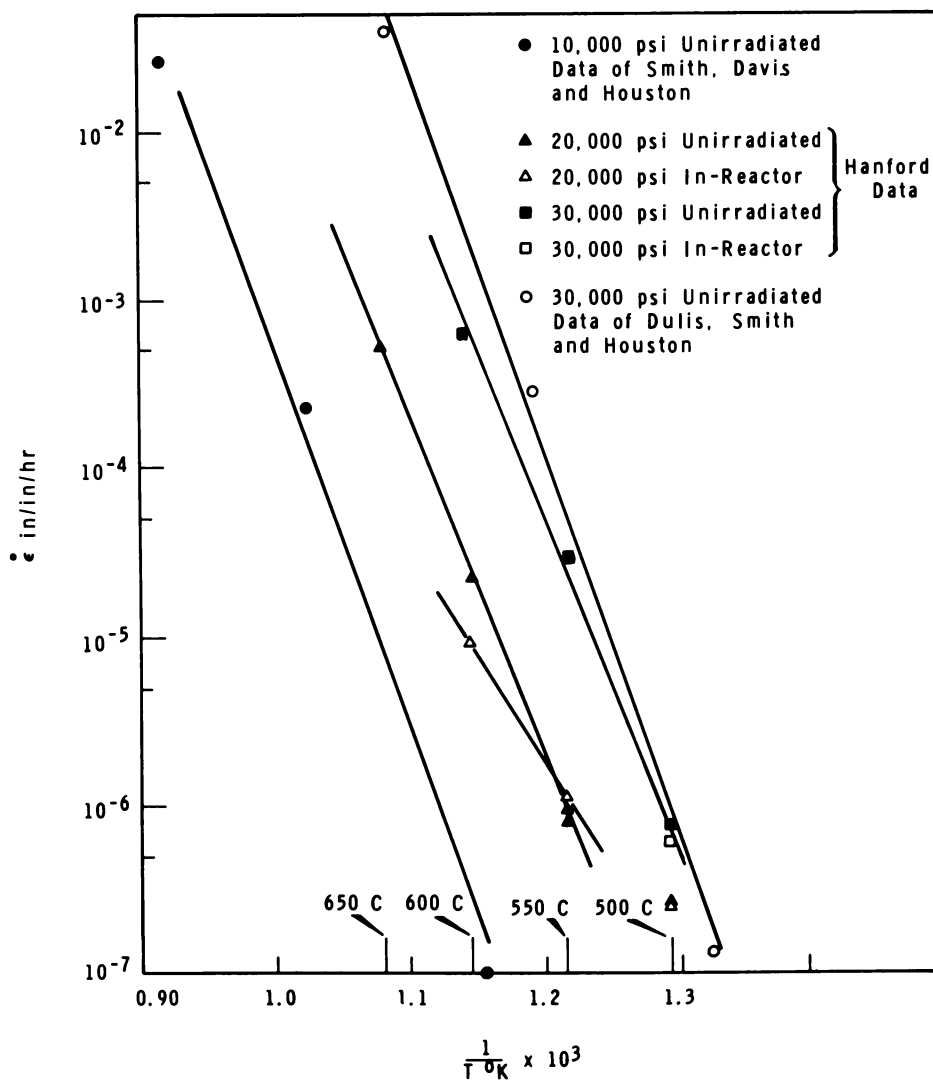


FIGURE 4.1

Arrhenius Plot of Creep of Annealed AISI 304 SS

Neg. 0643586

Activation energy measurements for in-reactor creep of annealed AISI 304 SS were reported to have been made in the last quarterly report. ⁽¹⁾

-
1. J. A. Williams, D. H. Nyman, and J. W. Carter. "In-Reactor Measurements of Mechanical Properties," Quarterly Progress Report - Metallurgy Research Operation - July, August, September, 1964, edited by J. J. Cadwell, HW-84281, pp. 4.6-4.7. September 15, 1964.

The results of these measurements are shown in Figure 4.2. Unlike the out-of-reactor creep, activation energies for in-reactor creep exhibit a temperature and stress dependency. Activation energies range from a low of 60 to 70 Kcal/mole to a high of 145 Kcal/mole.

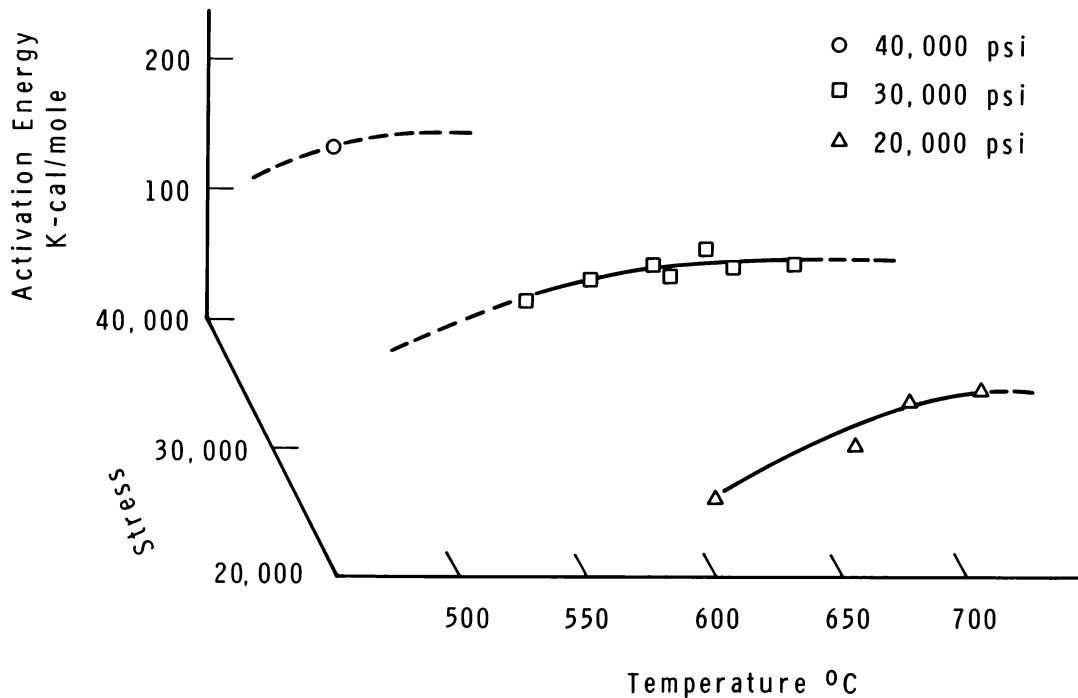


FIGURE 4.2

Activations for In-Reactor Creep of Annealed AISI 304 SS

Neg. 0643104

An in-reactor test capsule was discharged from the reactor and sent to the Radiometallurgy facility. This is the first time it has been possible to save a capsule for postirradiation examination. The capsule, with a section of the outer shell removed, is shown in Figure 4.3. The overall appearance of the capsule was very good. Elongation on breaking, as measured on the annealed AISI 304 SS specimen after the test, was 11%. The last in-reactor measurement just prior to breaking indicated an elongation

of approximately 9%. This is a great deal less than is expected from out-of-reactor tests. Metallography studies of the broken specimen are planned.

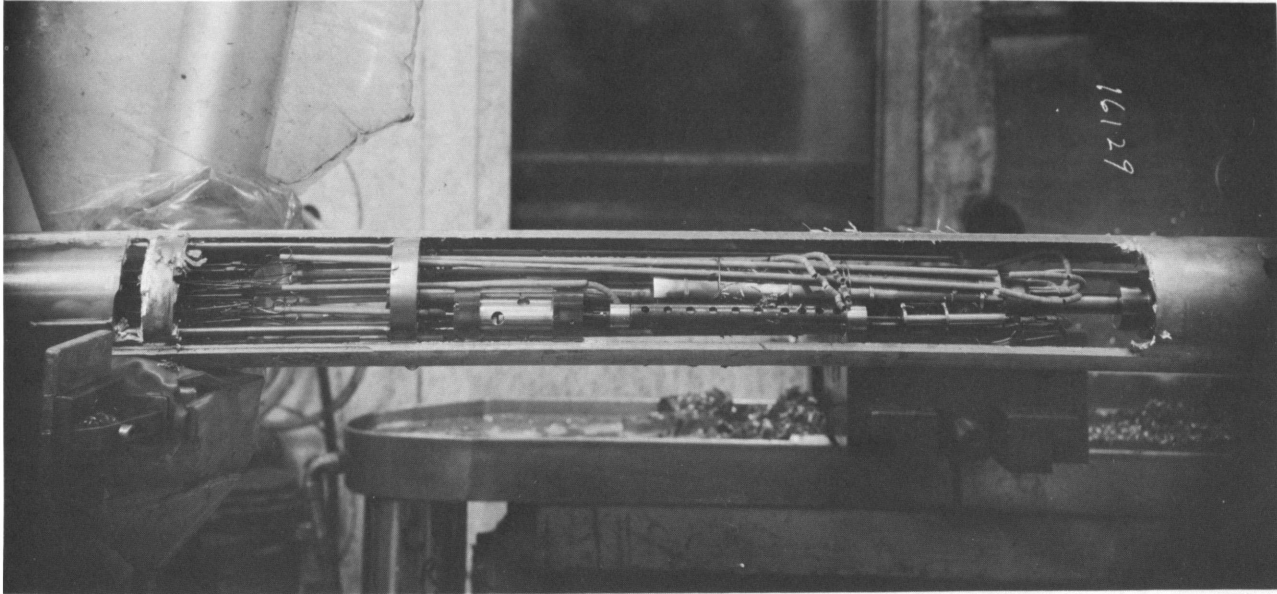


FIGURE 4.3

In-Reactor Creep Capsule after Irradiation
with Section of Outer Shell Removed for Postirradiation Examination

Neg. 16129

Capsule Development

To meet the demands for high temperature mechanical properties data of structural materials during and after neutron irradiation, considerable equipment development has been completed during the past quarter.

The prototype design of a high temperature in-reactor creep capsule has been completed and parts are being made. This capsule utilizes self-supporting tungsten or molybdenum heaters. It will operate at temperatures of up to 1900 C. The specimen and heaters are surrounded by an alumina tube and reflector shields to minimize heat loss to the outer walls. Capsule pressure is kept low at 1 atm of helium in order to prevent heat transfer from the hot zone to the rest of the capsule. Loading of the specimen is accomplished through internal pressurization of a yoked bellows. The specimen and pull rods are machined as an integral part to eliminate high temperature

grip problems. The extensometry system consists of a micropositioner reading off one end of the specimen pull rod and a temperature compensated yoke that is attached to the pull rod just beyond the specimen section. Creep tests of high temperature alloys and refractory metals will be possible with this apparatus.

A high temperature creep-rupture apparatus has been developed. The apparatus is capable of being operated remotely for use in postirradiation testing. Figure 4.4 shows a schematic diagram of the apparatus.

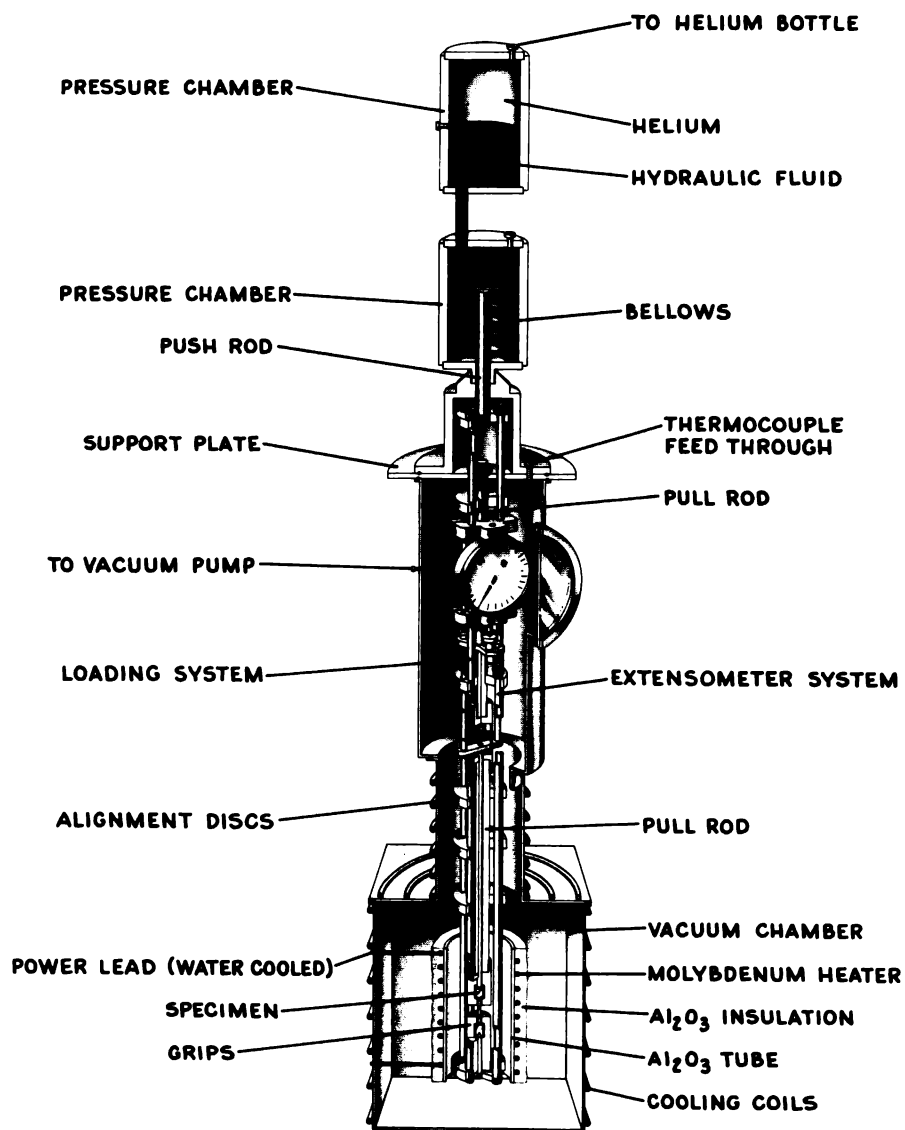


FIGURE 4.4

High Temperature Creep-Rupture Apparatus

The unit is basically constructed from molybdenum. A high current, low voltage heating element made from molybdenum rod and coiled on a high purity alumina tube produces a temperature capability of 1300 C. A 40 volt, 300 amp motor-generator set is used as a power supply. The extensometer system measures specimen end-to-end separation and strain is read from a dial gage with an accuracy of 10^{-4} in. For remote operation the dial gage is replaced with a transducer arrangement. The load is applied by controlling differential pressure across the bellows. The bellows, calibrated with respect to pressure vs. the force, transmits the load to the push rod which in turn applies the stress to the specimen. Stresses up to 40,000 psi may be obtained with the present specimen design. The entire system is enclosed in a cold wall vacuum chamber which can be back-filled with an inert gas if desired.

Creep-Rupture Tests

To date, Haynes 25 and Hastelloy X have been tested in vacuum at 2100 F. The results are shown in Table 4.4 and Figures 4.5, 4.6, and 4.7.

TABLE 4.4
HAYNES 25 AND HASTELLOY X CREEP-RUPTURE RESULTS

<u>Material</u>	<u>Temperature, F</u>	<u>Stress, psi</u>	<u>Minimum Creep Rate, hr</u>	<u>Elongation, %</u>	<u>Time to Rupture, hr</u>
Haynes 25	2100	4000	1.9×10^{-1}	15.9	0.63
		4000	1.9×10^{-1}	13.9	0.53
		3000	7.2×10^{-2}	9.5	1.06
		3000	6.7×10^{-2}	10.1	1.30
		2000	9.6×10^{-3}	10.3	6.50
		1500	7.0×10^{-3}	11.7	12.00
		1000	1.5×10^{-3}	8.4	33.25
Hastelloy X	2100	4000	5.6×10^{-1}	24.3	0.24
		3000	4.0×10^{-1}	21.9	0.46
		2200	1.4×10^{-1}	18.5	1.07
		1800	1.0×10^{-1}	21.3	1.85

Figures 4.5 and 4.6 show percent elongation vs. time for Haynes 25 and Hastelloy X at various stresses. Figure 4.7 is a stress-to-rupture

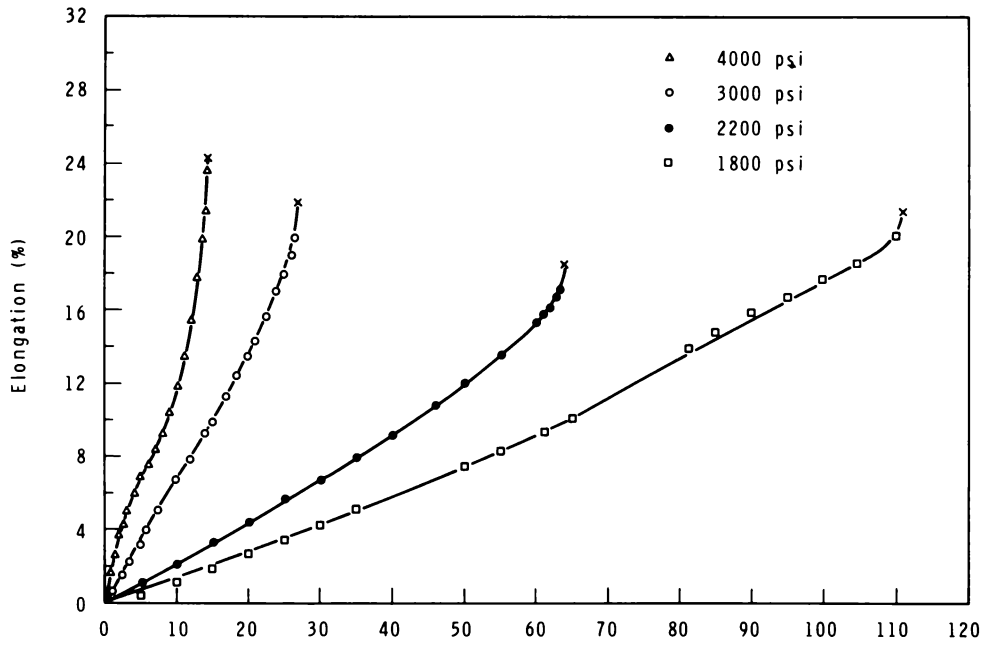


FIGURE 4.5
Creep-Rupture Tests of Haynes 25 at 2100 F

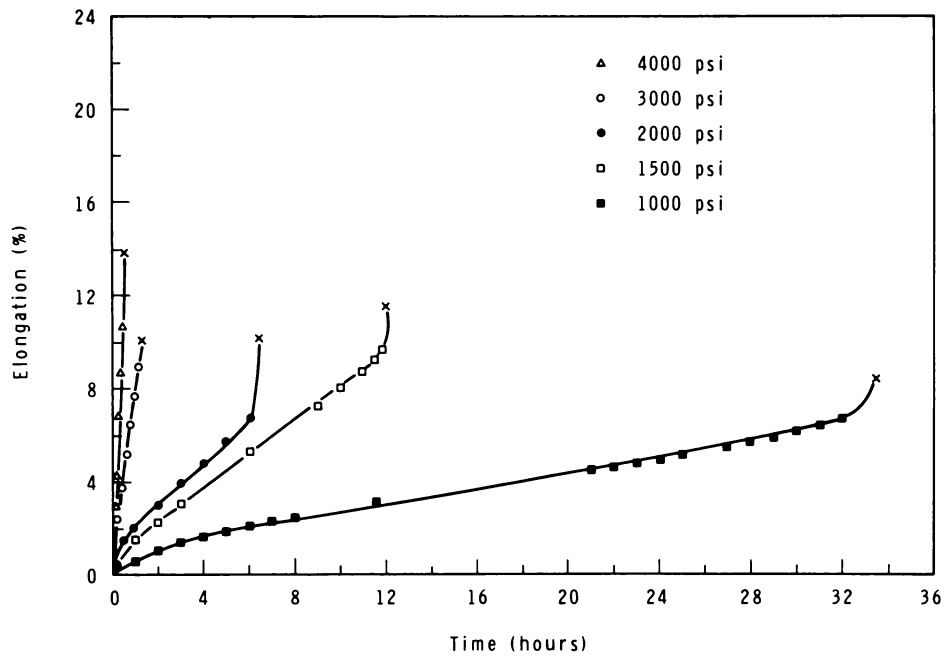


FIGURE 4.6
Creep-Rupture Tests of Hastelloy X at 2100 F
Neg. 0643381-2, 0643381-3

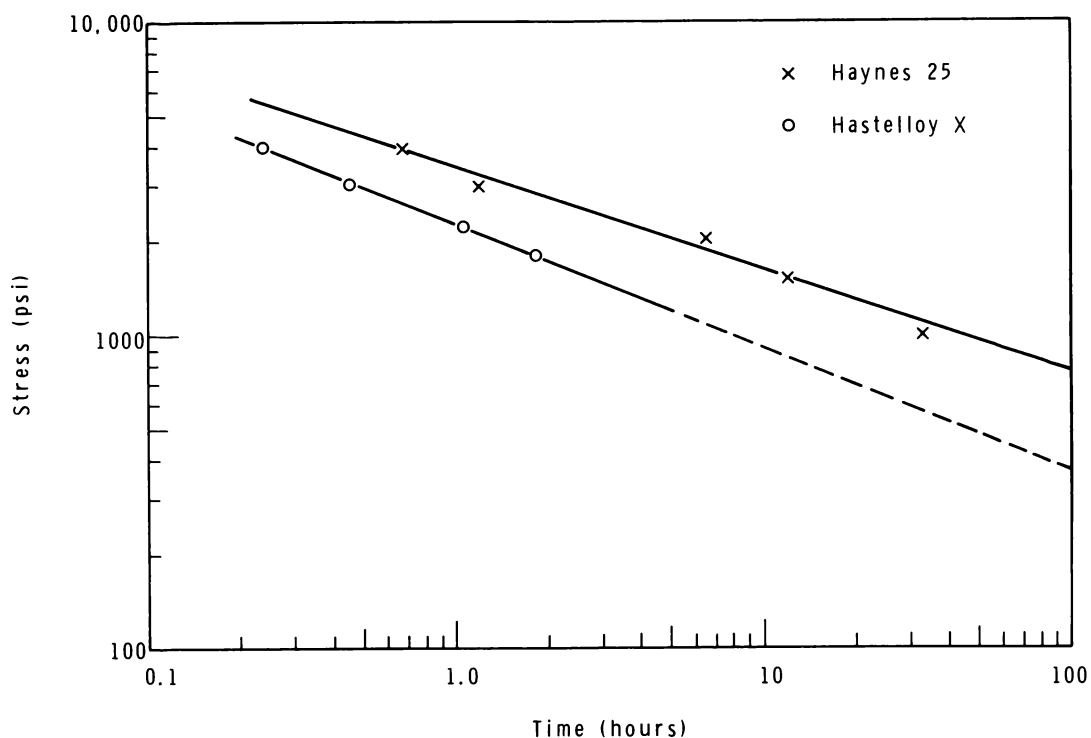


FIGURE 4.7

Stress-Rupture Properties at 2100 F

Neg. 0643381-1

plot. The Haynes 25 results indicate a more pessimistic rupture time with lower stress than was found in an earlier study. ⁽¹⁾

A literature search showed that Hastelloy X has not been extensively tested above 1800 F. Figure 4.4 shows the results of four tests on Hastelloy X at 2100 F. A complete study of Hastelloy X from 1800 to 2200 F is planned.

1. K. R. Wheeler and D. H. Nyman. Stress-Rupture Tests of Haynes 25 Alloy at High Temperatures, HW-79810. November 1963.

IRRADIATION FACILITIES OPERATION - J. E. Irvin

The purpose of this phase of the program is to provide for the timely accomplishment of irradiating, testing, and subsequent processing of the data obtained from a number of different structural materials. Irradiations will be performed in aqueous, gaseous, and molten metal environments. Elevated temperature irradiations and tests will be emphasized. Special tests applicable to both irradiated and unirradiated specimens will be developed.

Facilities Operation

The experiments discharged from the various ETR core positions at the conclusion of Cycles 66, 67, and 68 are given in Table 4.5 along with the estimated neutron fluxes and exposures (> 1 Mev). No discharges were made from the G-7 Hot Water Loop at the end of Cycle 66. The deposition of an organic contaminant prevented the irradiation of specimens in the loop during this cycle. None of the ambient temperature capsules in either the G-6 or M-7 core positions were discharged at the end of ETR Cycle 68. The operating histories of the ETR and the G-7 Hot Water Loop are given in Table 4.6. There were no control tests conducted in the out-of-reactor loop during Cycles 65 and 66. Exposures duplicating the history of ETR Cycle 67 are currently in progress.

Two of the four special quadrants⁽¹⁾ containing Inconel 600-Zircaloy-2 transition tensile specimens have been irradiated and discharged from the G-7 Hot Water Loop after exposures between 1.0 and 1.2×10^{20} nvt (> 1 Mev). Two quadrants containing 12 control specimens were loaded into the out-of-reactor loop to receive exposures similar to that obtained in the G-7 Loop.

1. J. E. Irvin. "Irradiation Facilities Operation," Quarterly Progress Report - Metallurgy Research Operation - July, August, September, 1964, edited by J. J. Cadwell, HW-84281, pp. 4.21-4.23. October 15, 1964.

TABLE 4.5
SUMMARY OF EXPERIMENTS DISCHARGED
FOLLOWING ETR CYCLES 66, 67, AND 68

<u>Quadrant Number</u>	<u>Number and Type of Specimen</u>	<u>Estimated Flux, nv*</u>	<u>Estimated Exposure, nvt*</u>
<u>Quadrant Discharges - ETR Cycle 67</u>			
111	18 Nickel-Base Tensiles	(a)	1.0×10^{21}
114	18 Nickel-Base Tensiles	2.0×10^{13}	3.9×10^{20}
121	18 AISI 406 SS Tensiles	6.8×10^{13}	1.0×10^{21}
177	6 Inconel 600-Zircaloy-2 Tensiles	$5.5 \times 10^{13(b)}$	1.0×10^{20}
<u>Quadrant Discharges - ETR Cycle 68</u>			
130	18 AISI 348 SS Tensiles	3.7×10^{13}	3.3×10^{20}
131	18 AISI 348 and 304 SS Tensiles	6.0×10^{13}	3.3×10^{20}
176	6 Inconel 600-Zircaloy-2 Tensiles	$4.2 \times 10^{13(b)}$	1.0×10^{20}
<u>Capsules Discharges - ETR Cycle 66</u>			
GEH-14-320	11 Zircaloy Tensiles	1.9×10^{14}	5.0×10^{21}
GEH-14-477	8 Nickel-Base Tensiles	2.0×10^{14}	1.0×10^{21}
GEH-14-483	7 Refractory Tensiles	3.7×10^{14}	3.2×10^{20}
GEH-14-484	7 Refractory Tensiles	3.9×10^{14}	3.4×10^{20}
GEH-14-652	7 Refractory Tensiles	3.7×10^{14}	3.2×10^{20}
<u>Capsule Discharges - ETR Cycle 67</u>			
GEH-14-479	4 Nickel-Base Tensiles	2.3×10^{14}	1.0×10^{21}

* Neutrons with energies greater than 1 Mev

(a) This quadrant was irradiated in two positions during different cycles. The flux was not the same for each position.

(b) This quadrant was twice the normal quadrant length and therefore occupied two positions during the same cycle. The average flux seen by the gage length of the specimen is given.

Total number of specimens discharged, Cycles 66, 67, and 68 = 146.

Total number of specimens discharged from G-7 Hot Water Loop, Cycles 67 and 68 = 102

Total number of specimens discharged from G-7 Loop to date = 2216.

TABLE 4.6
OPERATING HISTORY OF ETR AND G-7 LOOP FACILITY

<u>Operating History</u>	<u>Cycle Number</u>		
	<u>65</u>	<u>66</u>	<u>67</u>
1. <u>Reactor History</u>			
Startup ^(a)	7-19-64	8-27-64	10-9-64
End of Cycle	8-16-64	9-27-64	11-15-64
Megawatt Days	3263	4510	5154
Effective Days at 175 Mw	18.7	25.8	29.5
Number of Scrams ^(b)	8	6	6
Number of Shutdowns	3	3	3
2. <u>G-7 Loop History</u>			
Maximum Temperature, F	535	(c)	535
Effective Days above 200 F	19.6	--	30.2
Effective Days at Operating Temperature	16.4		27.3
Operating Efficiency ^(d)	100.4%		100.1%
Temperature Efficiency ^(e)	84.0%		90.5%

(a) Includes flux run

(b) Power drops below half-full power with immediate recovery

(c) There was no assembly in the loop this cycle

(d) Effective days of loop operation above 200 F with respect to effective days of reactor operation at 175 Mw.

(e) Effective days of operation between 500 and 550 F with respect to days of operation above 200 F

Special testing fixtures are being fabricated to test both the irradiated and unirradiated specimens at room temperature and at 550 F. This study is being performed in support of the "Advanced BONUS Core Development Program"⁽¹⁾ being conducted by Combustion Engineering, Inc.

-
1. J. F. Gibbons, R. L. Lyerly, W. A. Maxwell, and K. E. Roach. "Advanced BONUS Core Development Program," Quarterly Progress Report No. 3 - May, June, July, 1964, GNEC-361. General Nuclear Engineering Corporation. August 15, 1964.

IRRADIATION DAMAGE TO ZIRCALOY-2 - J. E. Irvin

The purpose of this phase of the program is to investigate the combined effects of irradiation and environment on the mechanical properties of Zircaloy-2. Special attention will be given to the determination of mechanical property changes produced by irradiation at elevated temperatures. The change in mechanical properties as a function of fabrication history will be determined for sheet, rod, and tube materials.

Surveillance of NPR Tubing

Tensile specimens fabricated from tubing supplied for the N-Reactor at Hanford are being used in a surveillance program to determine effects of long term irradiations at elevated temperatures on the mechanical properties of Zircaloy-2. These same specimens also provide data on weight gain and hydrogen pickup as a function of time, temperature, and integrated neutron exposure.

Approximately 350 specimens were fabricated from three different tubes. All of the specimens were made to the same specification by one vendor. Spot checks were made on random specimens to verify that the dimensional tolerances had been met. A maximum and minimum surface area was calculated using the greatest and least dimensions specified. The maximum and minimum areas for tensile specimens with 7/16 in. tab lengths are 1.902 in.² (0.1227 dm²) and 1.876 in.² (0.1210 dm²), respectively.

All of the tensile specimens were weighed before and after autoclaving treatments and are reweighed after exposures in either an in-reactor or out-of-reactor test. Weight gains per unit area are listed in Table 4.7 for several test conditions. The maximum area was used to determine a minimum weight gain. The number of specimens averaged for each condition is also listed in the table. A composite of the data in Table 4.7 is given in Table 4.8 in the order of increasing exposure time, or increasing integrated flux for the irradiated specimens. The data from Table 4.7 is plotted in Figure 4.8.

TABLE 4.7

WEIGHT GAIN FOR N-REACTOR ZIRCALOY-2 TUBES

Experiment Designation	Tube Designation	Average Weight Gain After Autoclaving ^(a)	mg/dm ² After Autoclaving	Average Weight Gain After Exposure	mg/dm ² After Exposure	Total mg/dm ²	Comments
116-A ^(b)	AT-50	0.0015	12.2 (4) ^(c)	0.0003	2.5 (4)	14.7	668.6 hr (26.9 days) > 200 C
	HT-37	0.0012	9.8 (4)	0.0007	5.7 (4)	15.5	508.5 hr (21.2 days) > 282 C
	CT-19	0.0012	9.8 (4)	0.0006	4.9 (4)	14.7	
116 ^(d)	AT-50	0.0012	9.8 (6)	0.0020	16.3 (6)	26.1	nvt > 1 Mev = 6.93 x 10 ¹⁹
	HT-37	0.0012	9.8 (6)	0.0024	19.6 (6)	29.4	nvt > 1 Mev ≈ 3.7 x 10 ¹³ (A-4)
	CT-19	0.0012	9.8 (6)	0.0023	18.7 (6)	28.5	508.5 hr (21.2 days) > 282 C
118 ^(d)	AT-50	0.0014	11.4 (6)	0.0041	33.4 (6)	44.8	nvt > 1 Mev = 1.11 x 10 ²⁰
	HT-37	0.0013	10.6 (6)	0.0040	32.6 (6)	43.2	nvt > 1 Mev ≈ 5.5 x 10 ¹³ (B-3)
	CT-19	0.0013	10.6 (6)	0.0034	27.7 (6)	38.3	508.5 hr (21.2 days) > 282 C
119-A ^(e)	AT-50	0.0014	11.4 (4)	0.0016	13.0 (4)	24.4	5022.4 hr (210 days) > 200 C
	HT-37	0.0014	11.4 (4)	0.0013	10.6 (4)	22.0	4211.3 hr (175.8 days) > 282 C
	CT-19	0.0015	12.2 (4)	0.0015	12.2 (4)	24.4	
119 ^(f)	AT-50	0.0014	11.4 (6)	(g)			nvt > 1 Mev = 1.33 x 10 ²¹
	HT-37	0.0012	9.8 (6)				nvt > 1 Mev ≈ 8.0 x 10 ¹³ (C-3)
	CT-19	0.0010	8.2 (6)				4211.3 hr (175.8 days) > 282 C

(a) All specimens were autoclaved at 300 C and 1500 psi for 72 hr.

(b) Exposed in out-of-reactor loop for Cycle 56 only.

(c) Number of specimens averaged to determine weight gain.

(d) Exposed in G-7 Hot Water Loop for ETR Cycle 56 only.

(e) Exposed in out-of-reactor loop during Cycles 56 through 64 (excluding Cycle 61).

(f) Exposed in G-7 Hot Water Loop during ETR Cycles 56 through 64 (excluding Cycle 61).

(g) Data not available at this time.

TABLE 4.7 (contd)

WEIGHT GAIN FOR N-REACTOR ZIRCALOY-2 TUBES

Experiment Designation	Tube Designation	Average Weight Gain After Autoclaving ^(a)	mg/dm ² After Autoclaving	Average Weight Gain After Exposure	mg/dm ² After Exposure	Total mg/dm ²	Comments
124 ^(b)	AT-50	0.0014	11.4 (6) ^(c)	0.0063	51.2 (4)	62.6	nvt > 1 Mev = 1.63 x 10 ²⁰
	HT-37	0.0013	10.6 (6)	0.0061	49.6 (4)	60.2	nv > 1 Mev ≈ 6.0 x 10 ¹³ (B-1)
	CT-19	0.0012	9.8 (6)	0.0071	57.8 (4)	67.6	859.0 hr (35.7 days) > 282 C
126-A ^(d)	AT-50	0.0016	13.0 (4)	0.0005	4.1 (4)	17.1	1629.4 hr (67.9 days) > 200 C
	HT-37	0.0015	12.2 (4)	0.0005	4.1 (4)	16.3	1385.0 hr (57.7 days) > 282 C
	CT-19	0.0015	12.2 (4)	0.0005	4.1 (4)	16.3	
126 ^(e)	AT-50	0.0013	10.6 (6)	0.0154	125.5 (4)	136.1	nvt > 1 Mev = 5.64 x 10 ²⁰
	HT-37	0.0012	9.8 (6)	0.0133	108.0 (4)	117.8	nv > 1 Mev ≈ 1.0 x 10 ¹⁴ (G-1)
	CT-19	0.0011	9.0 (6)	0.0176	143.5 (4)	152.5	1385.0 hr (57.7 days) > 282 C
120-A ^(f)	AT-50	0.0015	12.2 (4)	(g)			
	HT-37	0.0014	11.4 (4)				
	CT-19	0.0012	9.8 (4)				
120 ^(h)	AT-50	0.0013	10.6 (6)	(g)			
	HT-37	0.0010	8.2 (6)				
	CT-19	0.0011	9.0 (6)				

(a) All specimens were autoclaved at 300 C and 1500 psi for 72 hr.

(b) Exposed in G-7 Hot Water Loop for ETR Cycles 57 and 58.

(c) Number of specimens averaged to determine weight gain.

(d) Exposed in out-of-reactor loop during Cycles 57 through 59.

(e) Exposed in G-7 Hot Water Loop during Cycles 57 through 59.

(f) Experiment currently being exposed in out-of-reactor loop.

(g) Data not available at this time.

(h) Experiment currently being exposed in G-7 Hot Water Loop.

TABLE 4.7 (contd)

WEIGHT GAIN FOR N-REACTOR ZIRCALOY-2 TUBES

Experiment Designation	Tube Designation	Average Weight Gain After Autoclaving ^(a)	mg/dm ² After Autoclaving	Average Weight Gain After Exposure	mg/dm ² After Exposure	Total mg/dm ²	Comments
122-A ^(b)	AT-50	0.0014	11.4 (4) ^(c)	0.0018	14.6 (4)	26.0	4353.8 hr (181.5 days) > 200 C
	HT-37	0.0014	11.4 (4)	0.0015	12.2 (4)	23.6	3702.4 hr (154.2 days) > 282 C
	CT-19	0.0016	13.0 (4)	0.0016	13.0 (4)	26.0	
122 ^(d)	AT-50	0.0013	10.6 (6)	(e)			nvt > 1 Mev = 3.50 x 10 ²⁰
	HT-37	0.0013	10.6 (6)				nv > 1 Mev ≈ 3.0 x 10 ¹³ (A-3)
	CT-19	0.0012	9.8 (6)				3702.4 hr (154.2 days) > 282 C
140-A ^(f)	AT-50	0.0016	13.0 (4)	(e)			
	HT-37	0.0014	11.4 (4)				
	CT-19	0.0016	13.0 (4)				
140 ^(g)	AT-50	0.0013	10.6 (6)	(e)			
	HT-37	0.0011	9.0 (6)				
	CT-19	0.0012	9.8 (6)				
141-A ^(h)	AT-50	0.0014	11.4 (4)	0.0019	15.5 (4)	26.9	3342.7 hr (139.0 days) > 200 C
	HT-37	0.0014	11.4 (4)	0.0012	9.8 (4)	21.2	2843.4 hr (118.0 days) > 282 C
	CT-19	0.0016	13.0 (4)	0.0018	14.6 (4)	27.6	
141 ⁽ⁱ⁾	AT-50	0.0017	13.8 (6)	(e)			nvt > 1 Mev = 9.49 x 10 ²⁰
	HT-37	0.0017	13.8 (6)				nv > 1 Mev ≈ 8.0 x 10 ¹³ (E-2)
	CT-19	0.0013	10.6 (6)				2843.4 hr (118.0 days) > 282 C

(a) All specimens were autoclaved at 300 C and 1500 psi for 72 hr.

(b) Exposed in out-of-reactor loop during Cycles 57 through 64 (excluding Cycle 61).

(c) Number of specimens averaged to determine weight gain.

(d) Exposed in G-7 Hot Water Loop during ETR Cycles 57 through 64 (excluding Cycle 61).

(e) Data not available at this time.

(f) Experiment currently being exposed in out-of-reactor loop.

(g) Experiment currently being exposed in G-7 Hot Water Loop.

(h) Exposed in out-of-reactor loop during Cycles 59 through 64 (excluding Cycle 61).

(i) Exposed in G-7 Hot Water Loop during ETR Cycles 59 through 64 (excluding Cycle 61).

TABLE 4.8
WEIGHT GAIN FOR N-REACTOR ZIRCALOY-2 TUBES

Experiment Number	Tube Designation	Autoclave Weight Gain mg/dm ²	Exposure Weight Gain mg/dm ²	Total mg/dm ²	Comments
116-A	AT-50	12.2	2.5	14.7	21.2 days > 282 C
	HT-37	9.8	5.7	15.5	
	CT-19	9.8	4.9	14.7	
126-A	AT-50	13.0	4.1	17.1	57.7 days > 282 C
	HT-37	12.2	4.1	16.3	
	CT-19	12.2	4.1	16.3	
141-A	AT-50	11.4	15.5	26.9	118.0 days > 282 C
	HT-37	11.4	9.8	21.2	
	CT-19	13.0	14.6	27.6	
122-A	AT-50	11.4	14.6	26.0	154.2 days > 282 C
	HT-37	11.4	12.2	23.6	
	CT-19	13.0	13.0	26.0	
119-A	AT-50	11.4	13.0	24.4	175.8 days > 282 C
	HT-37	11.4	10.6	22.0	
	CT-19	12.2	12.2	24.4	
116	AT-50	9.8	16.3	26.1	6.93 x 10 ¹⁹
	HT-37	9.8	19.6	29.4	21.2 days > 282 C
	CT-19	9.8	18.7	28.5	~ 3.7 x 10 ¹³
118	AT-50	11.4	33.4	44.8	1.11 x 10 ²⁰
	HT-37	10.6	32.6	43.2	21.2 days > 282 C
	CT-19	10.6	27.7	38.3	~ 5.5 x 10 ¹³
124	AT-50	11.4	51.2	62.6	1.63 x 10 ²⁰
	HT-37	10.6	49.6	60.2	35.7 days > 282 C
	CT-19	9.8	57.8	67.6	~ 6.0 x 10 ¹³
126	AT-50	10.6	125.5	136.1	5.64 x 10 ²⁰
	HT-37	9.8	108.0	117.8	57.7 days > 282 C
	CT-19	9.0	143.5	152.5	~ 1.0 x 10 ¹⁴

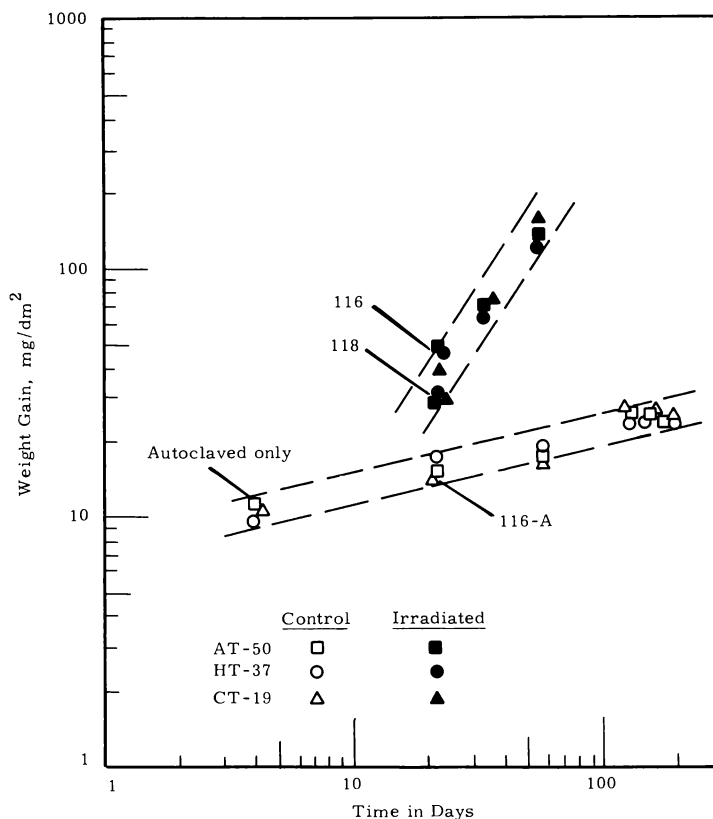


FIGURE 4.8

Corrosion Characteristics of N-Reactor Zircaloy-2 Tubing

The corrosion rate of the irradiated tube material is a factor of 10 greater than that exposed for a similar length of time in the out-of-reactor loop. In one instance it was possible to compare two experiments which were irradiated for the same length of time at different flux rates. The specimens in the higher flux zone exhibited a weight gain which was 50% greater than specimens exposed at the same time in a lower flux. Quadrants 116 and 118 were both exposed in the ETR G-7 loop during Cycle 56 only. The history of these two quadrants was duplicated in the out-of-reactor loop by quadrant 116-A.

Corrosion rates of N-Reactor tube material was compared with data obtained from rolled plate material. Preliminary results of this comparison indicate that corrosion characteristics of the tube material and the plate

stock are the same. Weight gain data will be obtained for long term exposures in both the in-reactor and out-of-reactor loops on both plate and tube material.

Tensile tests have been conducted on specimens irradiated to exposures greater than 1.0×10^{21} nvt (> 1 Mev). These tests were performed at room temperature and at 300 C. Additional tests are being performed on control specimens exposed in the out-of-reactor loop for greater than 5000 hr. The results of these tests are being processed on the REM computer program. Selected pieces of the broken irradiated specimens are being analyzed to determine the hydrogen pickup. Preliminary results of these analyses indicate a theoretical corrosion hydrogen pickup of 50% or greater for each of the tubes exposed in either quadrant 116 or 118. Additional results from other quadrants will be available soon.

FRACTURE STUDIES - R. G. Hoagland

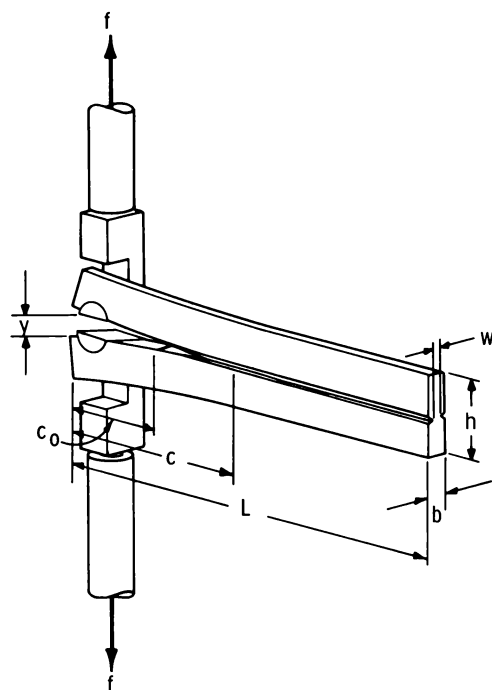
Efforts are being devoted to the development of a technique for the acquisition of a large amount of relevant fracture data from a limited number of relatively small specimens. The determination of ductile-to-brittle transition temperatures and plane strain fracture toughness data on irradiated materials using conventional specimens, e. g., notch bend, round notch tensile, singly and doubly notch plate, etc., requires an irradiation volume not readily available in the ETR or in other test reactors. This is particularly true when one wants to irradiate a number of large size specimens in the hot water environment of the ETR G-7 loop.

Gilman⁽¹⁾ and Berry⁽²⁾ have described the use of a double cantilever beam (DCB) specimen for the determination of surface energies of single ionic crystals and plastics. Berry⁽³⁾ has shown that if the material possesses an effective surface energy independent of crack velocity, catastrophic crack propagation in the DCB specimen is impossible. It is this crack stability feature of the DCB specimen which is particularly important, and studies have been underway to determine the feasibility of using the DCB specimen for the evaluation of the effects of in-reactor environments on the fracture properties of candidate reactor materials.

Figure 4.9 is a schematic showing a DCB specimen and a method of loading. Although the method of loading is not important, it is important that the length direction of the specimen is perpendicular to the direction of loading. The specimen dimensions that are presently being used are shown in Figure 4.9. The purpose of the initial slot, C_0 , is to facilitate easier

-
1. J. J. Gilman. "Cleavage, Ductility, and Tenacity in Crystals," Fracture, edited by B. L. Averbach, D. K. Felbeck, G. T. Haln, and D. A. Thomas. Published jointly by the Technology Press, Massachusetts Institute of Technology, and John Wiley & Sons, Inc., New York, pp. 193-224. 1959.
 2. J. P. Berry. "Determination of Fracture Surface Energies by the Cleavage Technique," J. Appl. Phys., vol. 34, No. 1, pp. 62-68. 1964.
 3. J. P. Berry. "Some Kinetic Considerations of the Griffith Criterion of Fracture I & II," J. Mech. Phys. Solids, vol. 8, pp. 194-216. 1960.

starting of the crack. The grooves running at mid-width along the length of the specimen prevent the crack from breaking off one of the arms. In additions, these grooves provide important restraints along the side of the crack preventing the formation of shear lips. A number of trials with specimens of different groove depths showed that if the groove is too much shallower than 0.060 in. premature failure by breaking off one of the arms results, while too much deeper causes crack propagation along the groove tip.



Specimen Dimensions
inches

L	h	b	w	c_0
7	1	0.250	0.130	1-1/2

FIGURE 4.9
DCB Specimen
and Loading Arrangement

An example of the behavior exhibited by a DCB specimen made of material which exhibits a crack velocity dependent fracture toughness is shown schematically in Figure 4.10. Catastrophic crack propagation occurs due to a decrease in the toughness with increasing velocity resulting in a short (usually 0.020 to 0.200 in.) and rapid increase in crack length. This is shown as a distinct drop in load. Measurement of both crack initiation and arrest toughness values can be made from data in this form. As

many as 30 to 35 toughness values may be obtained in this manner from a single specimen.

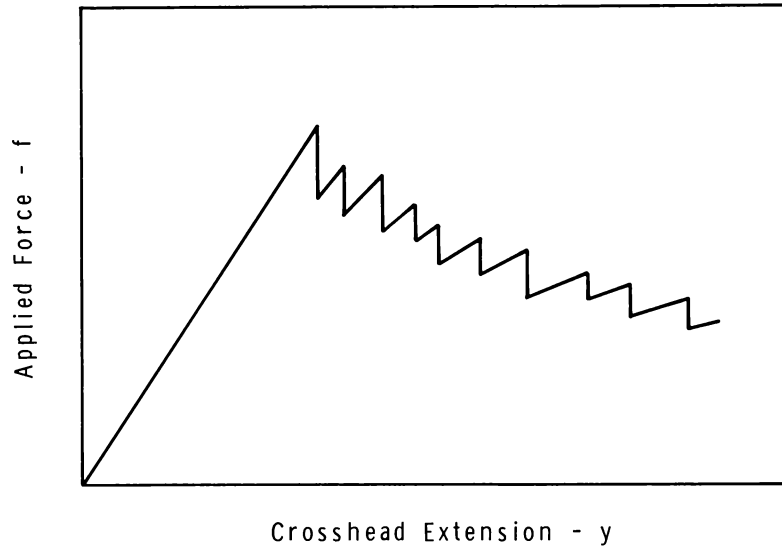


FIGURE 4.10

Typical DCB Specimen Fracture Behavior
at Constant Crosshead Speed

The calculation of the strain energy release rate or fracture toughness from the DCB specimen may be made once the relationship has been ascertained between the applied load, f , the resultant extension of the arms, y , for a given crack length, c . Although one arm of the specimen behaves in a manner similar to a cantilever beam, the simple beam formula neglects the strain in the unbroken part of the specimen. To obtain the exact relationship the following function is used:

$$y = \frac{f}{cE} \Phi \quad (1)$$

where E is the modulus and Φ is a function of the crack length and the moment of inertia. The function Φ is determined experimentally from the compliance or spring constant of the specimen for a given crack length. For the determination of the function, Φ , for the Figure 4.9 specimen geometry, DCB specimens of 7075-T6 Al were used. Measurements of compliance were taken from the slope of Instron recordings and crack lengths were measured using a traveling microscope. The results of one of the Φ vs. c determinations

is shown in Figure 4.11 which indicates that over most of the length of the specimen the relationship between $\bar{\phi}$ and c is

$$\bar{\phi} = Bc^n. \quad (2)$$

Substituting into Equation (1) we obtain

$$y = \frac{Bf}{E} c^{n-1}. \quad (3)$$

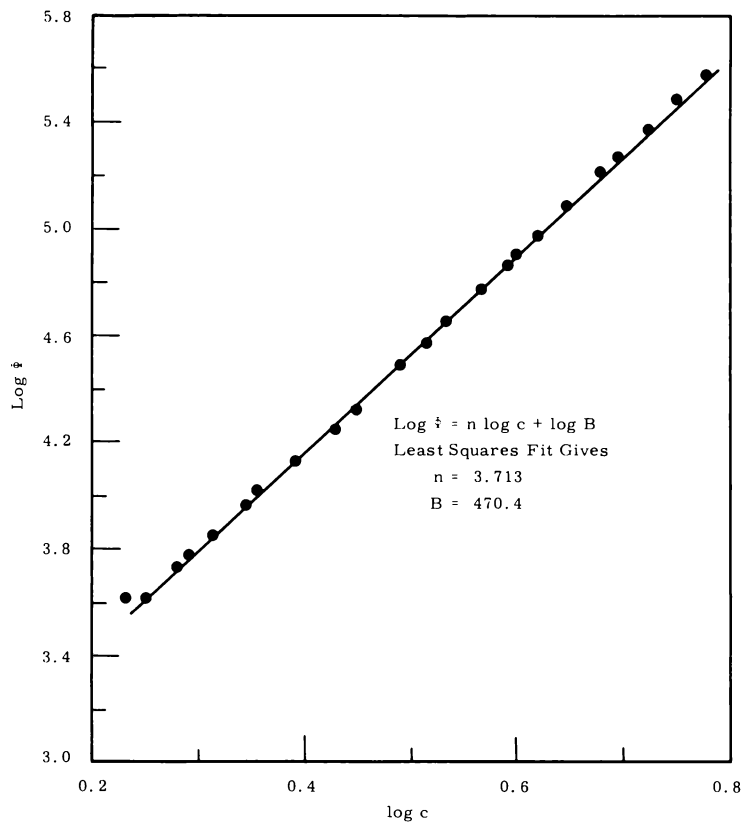


FIGURE 4.11
Results of DCB Specimen
Calibration on 7075-T6 Al

The strain energy release rate is now easily derived in the following manner:

$$\text{strain energy in one arm} = U = \frac{1}{4} fy \quad (4)$$

strain energy release per

$$\text{unit crack area increase} = G = - \frac{1}{W} \left(\frac{\partial U}{\partial c} \right)_y. \quad (5)$$

Combining Equations (3) and (4) into Equation (5) one obtains

$$G = \frac{E(n-1)y^2}{4 B W} \left(\frac{Bf}{E_y} \right)^{\frac{n}{n-1}} \quad (6)$$

Some preliminary data using the DCB technique on A-302B and Zircaloy-2 has been obtained. These results are shown in Figures 4.12 and 4.13. The data from the A-302B specimen in Figure 4.12 shows the typical increase in crack initiation toughness values with increasing temperatures. The crack arrest values, however, remain constant up to the highest temperature reached. It will be interesting to see, with further testing, the behavior above -120 C. The Zircaloy-2 behavior (Figure 4.13) differs from that of A-302B in that both the initiation and arrest toughness values increase together with increasing temperature. It is important to note that both the fracture initiation and arrest conditions are made available by the DCB specimen. It is also important to note that the data shown here is in good agreement with the plane strain fracture data obtained from much larger conventional specimens.^(1, 2, 3) Finally, data obtained from a DCB specimen possesses less scatter than is normally found in the literature, since all data comes from one specimen.

One difficulty encountered in conducting tests on DCB specimens at temperatures other than room temperature is that of measuring the temperature at the crack tip, since the tip continues to move down the length of the specimen as the testing progresses. It is anticipated that this problem will be solved by a special cryostat now under development.

-
1. D. F. Mowbray. Fracture Toughness Determinations of A302-B and Ni-Mo-V Rotor Steel with Various-Sized Specimens, KAPL-3031, Knolls Atomic Power Laboratory. March 13, 1964.
 2. M. J. Manjoine. Biaxial Brittle Fracture Tests, Westinghouse Research Report 62-107-543-R1. September 10, 1962.
 3. R. G. Hoagland and A. L. Bement, Jr. Fracture Studies of Zircaloy-2, HW-82631. June 4, 1964.

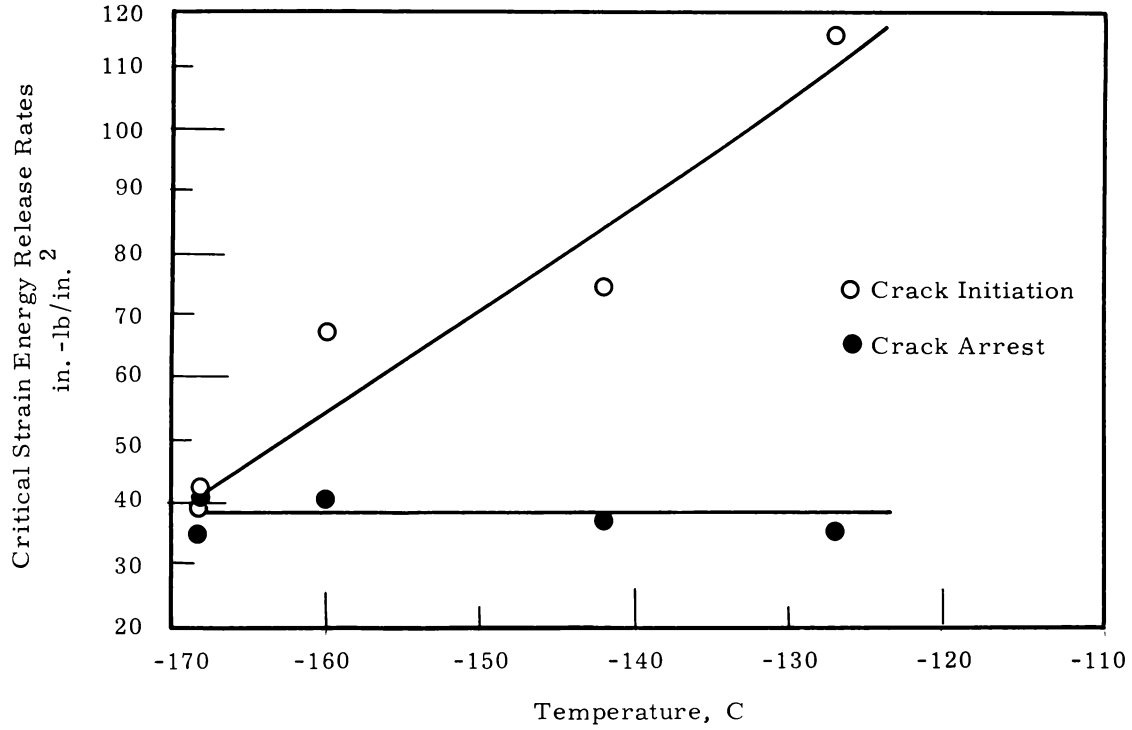


FIGURE 4. 12

DCB Test Results on A-302B

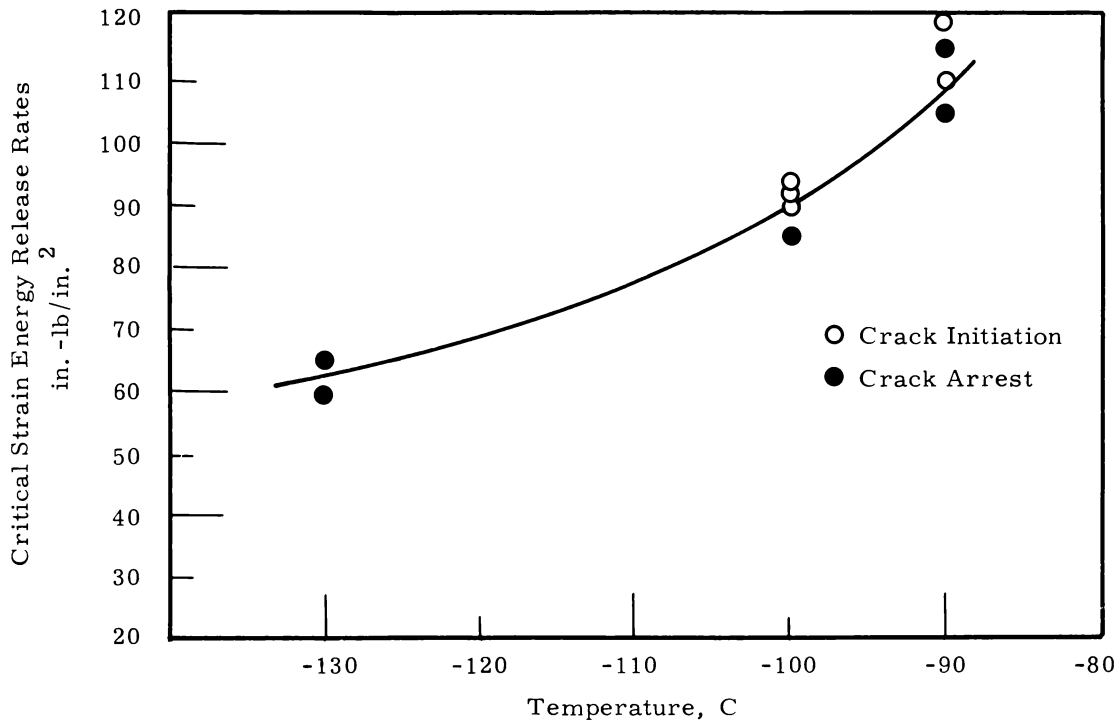


FIGURE 4. 13

DCB Test Results on Zircaloy-2

DAMAGE MECHANISMS - F. A. Smidt

The objective of this program is to determine the mechanism by which defects produced by neutron bombardment interact with dislocations to modify the plastic deformation characteristics of the metal.

It has become apparent during the course of this investigation that rate effects are present in the deformation of both irradiated and unirradiated iron. The flow stress in this temperature range should be described in terms of a rate sensitive component and a rate insensitive component. In addition, it is known that temperature has a large effect on the magnitude of the rate sensitive component, but has a very small effect on the rate insensitive component. Experimentally it is difficult to separate the flow stress into these two parts although changes in the rate and temperature sensitive one during variations in strain rate or temperature are easy to measure. It would be most desirable to find an analytical expression to relate absolute values of τ^* (the rate sensitive component) to absolute values of temperature and strain rate. Basically this is a problem of finding a function of τ^* which has the same relation to the temperature and strain rate as does the activation energy, namely

$$U = kT \ln \dot{\epsilon}_0 / \dot{\epsilon} = cf(\tau^*) . \quad (1)$$

For changes in strain rate at constant temperature this reduces to

$$U = \text{constant} \ln \dot{\epsilon}_0 / \dot{\epsilon} = cf(\tau^*) \quad (2)$$

with the boundary conditions that $U \rightarrow 0$ as $\dot{\epsilon} \rightarrow \dot{\epsilon}_0$ and $U \rightarrow -\infty$ as $\dot{\epsilon} \rightarrow 0$, unless the process ceases to be thermally activated at low strain rates. A variation in $\dot{\epsilon}_0$ will also cause changes in U and τ^* as can be seen from Equation (1) although it is commonly treated as a constant.

For changes in temperature at constant strain rate the equations will reduce to

$$U = \text{constant} T = f(\tau^*) \quad (3)$$

with boundary conditions $U \rightarrow 0$ as $T \rightarrow 0$ and $U \rightarrow$ a finite value as $T \rightarrow$ temperature at which thermal activation ceases. Several theoretical relations have

been suggested to satisfy these equations and since some applicable data have been obtained during the course of this investigation it seems profitable to compare the experimental data with several of these relations to test their applicability.

Conrad and Seeger have proposed relations of the form $U = A - B \ln(\tau^*/\tau_p)$, where τ_p is the Peierls' stress, while Dorn has derived a nonanalytical expression from the saddle-point activation energy for nucleation of a pair of kinks. This latter relation is fairly close to a logarithmic function from $\tau^* = \tau_p$ to about $0.4 \tau_p$ if $A = 0$ in the log equation, but deviates markedly in the lower boundary condition. Dorn's expression gives $U/\text{constant} = -1.0$ at $\tau^*/\tau_p = \dot{0}$, while the log relation gives $U/\text{constant} = -1.0$ at $\tau^*/\tau_p = 0.1$.

As shown in past quarterly reports, the log equation can be developed from the empirical relation between strain rate and stress originally proposed by Gilman and Johnston. When this is modified to make it compatible with thermally activated flow theory it gives an expression

$$\ln \dot{\epsilon}/\dot{\epsilon}_0 = n \ln (\tau^*/\tau_p) . \quad (4)$$

Comparing this with Equation (2) shows

$$U/kT = -c/kT f(\tau^*) = \ln \dot{\epsilon}/\dot{\epsilon}_0 \quad (5)$$

where $f(\tau^*)$ is $\ln (\tau^*/\tau_p)$ and n is c/kT or $U = -c \ln (\tau^*/\tau_p)$. This also leads to $V^* = c/\tau^*$.

Values of n obtained from double strain rate change experiments on Ferrovac E iron give n 's = 3.3 at 295 K, 7.9 at 241 K, and 31 at 201 K. These lead to values of c at these temperatures of 0.086 at 295 K, 0.164 at 241 K, and 0.54 at 201 K, i. e., a constant that is not constant. In addition, values of τ^* calculated from the double strain rate change tests are much too large at 201 K and slightly high at 241 K. In short, $\dot{\epsilon}/\dot{\epsilon}_0 = (\tau^*/\tau_p)^{c/kT}$ appears to be a fair approximation for the variation of τ^* with $\dot{\epsilon}$ at a constant temperature but fails to fit the data at all temperatures with a unique value of c .

In a previous quarterly report, it was shown that the variation of τ^* with temperature could be represented by the empirical equation

$$\tau^* = AT^2 - BT + \tau_{\max} . \quad (6)$$

Several attempts were made to fit this equation to a relation of the form

$$\tau^*/\tau_p = (\dot{\epsilon}_0/\dot{\epsilon})^{-kT/c} \approx \left[1 - \ln \dot{\epsilon}_0/\dot{\epsilon} \cdot kT/c + 1/2! (\ln \dot{\epsilon}_0/\dot{\epsilon} \cdot kT/c)^2 \right] \quad (7)$$

which would be compatible with Equation (3). These attempts were unsuccessful.

Instead the best fit is obtained for a parabolic temperature dependence with

$$\tau^*/\tau_p = (1 - T/\alpha T_0)^2 \quad (8)$$

which can be rearranged to give

$$T = \alpha T_0 (1 - \sqrt{\tau^*/\tau_p}). \quad (9)$$

Comparing this result with Equation (1) we see that

$$U = (k \ln \dot{\epsilon}_0/\dot{\epsilon}) T = (k \ln \dot{\epsilon}_0/\dot{\epsilon}) \alpha T_0 (1 - \sqrt{\tau^*/\tau_p}) = c f(\tau^*) \quad (10)$$

where $f(\tau^*) = (1 - \sqrt{\tau^*/\tau_p})$ and $\alpha T_0 = \frac{c}{k \ln \dot{\epsilon}_0/\dot{\epsilon}}$. This relation satisfies

Dorn's boundary conditions at $\tau^*/\tau_p > 0$ and 1 and yields a value of $c = 0.9$ ev for experimental values of αT_0 and $k \ln \dot{\epsilon}_0/\dot{\epsilon}$ measured at strain rates of 0.02 min^{-1} and 0.002 min^{-1} . At constant temperature this would lead to the equation

$$\ln \dot{\epsilon}_0/\dot{\epsilon} = c/kT (1 - \sqrt{\tau^*/\tau_p}) \quad (11)$$

and an activation volume of the $V^* = K/\tau^{*2}$.

When the double strain rate change experiments are analyzed with

this equation it can be shown that τ^* is given by
$$\frac{\Delta\tau}{\left[\left(\frac{\Delta\tau}{\tau} \right)^2 - 1 \right]}$$

where $\Delta\tau$ is the change in effective stress for a change in strain rate from 0.002 to 0.02 min^{-1} and $\Delta\tau'$ is the stress change for a strain rate change from 0.02 to 0.2 min^{-1} .

These calculations give τ^* at a strain rate of 0.002 min^{-1} as 0.11 kg/mm^2 at 295 K, 1.58 kg/mm^2 at 241 K and 13.1 kg/mm^2 at 201 K which are fairly close to the measured values.

Although no theoretical significance is immediately apparent in Equation (11), the fact remains that it gives a good representation of the experimental data both in the original form and in the relations derived from it by differentiation, a fact which is not true of the logarithmic expressions.

CHEMICAL METALLURGYENVIRONMENTAL EFFECTSWater Environment with Hydrogen Addition - W. A. Burns

Analyses of zirconium alloy specimens exposed to hydrogen-bearing water in the ETR G-7 loop during Cycle 65 and discharged in mid-August were continued during the quarter. The preliminary data which were previously reported⁽¹⁾ have been refined and supplemented by flux wire information, out-of-reactor exposure results, hydrogen analyses and hardness test data to permit more accurate comparison with in- and out-of-reactor behaviour results previously obtained at this laboratory and elsewhere. Data available to date are summarized in Tables 5.1 and 5.2. Compositions and heat treatments pertaining to specimens other than Irradiation Effects Program Zircaloy-2 plate materials 6515 and 6497 are given in Tables 5.3 and 5.4. The compositions of program plate materials were previously reported.⁽²⁾

As previously noted, the weight gains of all alloys tested are comparable at each flux position, they increase with increasing flux intensity, and there is no significant effect of cold work or cold work versus annealing on weight gain. The surface hardness of all coupons increased with increasing neutron exposure. The ratio of weight gain in-reactor to weight gain out-of-reactor increased from about two to one at the lowest fast flux intensity ($< 6 \times 10^{12}$ nv) to about five or six to one at the highest fast flux position ($> 6 \times 10^{13}$ nv), except for the Zircaloy-3 wt% Nb-1 wt% Sn alloy, which

Quarterly Progress Report - Metallurgy Research Operation - July, August, September, 1964, edited by J. J. Cadwell, HW-84281, September 15, 1964.

2. Quarterly Progress Report - Metallurgy Research Operation - October, November, December, 1962, edited by J. J. Cadwell, HW-76228, January 15, 1963.

TABLE 5. 1
BEHAVIOR OF PREAUTOCLAVED ZIRCONIUM ALLOYS
IN LOW-OXYGEN WATER^(a)

Neutron Flux (> 1 Mev), nv	Tempera- ture, F	Plate 6515			Plate 6497			NPR Zircaloy-2			Zircaloy-4			Nickel-Free Zircaloy-2			Zr-3 wt% Nb-1 wt% Sn		
		Weight ^(c) Gain, mg/dm ²	Hardness, Rockwell B	Hydrogen, % Theoretical	Weight Gain, mg/dm ²	Hardness, Rockwell B	Hydrogen, % Theoretical	Weight Gain, mg/dm ²	Hardness, Rockwell B	Hydrogen, % Theoretical	Weight Gain, mg/dm ²	Hardness, Rockwell B	Hydrogen, % Theoretical	Weight Gain, mg/dm ²	Hardness, Rockwell B	Hydrogen, % Theoretical	Weight Gain, mg/dm ²	Hardness, Rockwell R	Hydrogen, % Theoretical
0 ^(b)	536	3.1 ^{20(d)}	100	23	2.6 ²⁰	100	29	2.7 ⁸⁶	102	53	2.6 ₂	92	5	3.1 ₂	94	18	6.1 ₂	97	11
								2.7 ₂	96	14									
2.5 - 6 x 10 ¹²	520	4.8 ⁴⁰	102	54	4.5 ²⁰	--	56	3.1 ⁸⁶	--	94	3.8 ₂	--	35						
					4.8	96	103	3.3	--	37				4.6 ₂	--	19	--	--	--
2 - 6.6 x 10 ¹²	520	5.7 ²⁰	100	35	4.8 ²⁰	100	47	5.5 ⁸⁶	102	68	4.3 ₂	92	23	4.2 ₂	94	16	4.4 ₂	100	17
								6.0 ₂	98	31									
1.6 x 10 ¹³	523	6.9 ⁴⁰	104	47	6.8 ¹⁰	101	38	6.4 ⁸⁶	106	76	6.1 ₂	95	34	6.3 ₂	97	20	6.6 ₂	104	15
					6.4 ²⁰	102	36	6.6	101	24									
6.2 x 10 ¹³	534	16.7 ₂ ⁴⁰	104	35	14.8 ¹⁰	102	34	14.2 ⁸⁶	106	50	13.6 ₂	97	45	13.1 ₂	99	35	12.4 ₂	106	15
					14.2 ⁴⁰	106	45	13.0	102	9									
6.6 x 10 ¹³	532	20.0 ₂	101 ^(e)	38															
1.7-4.2 x 10 ¹³	530	40.7	--	18															

Average of data for 47 specimens with 19.2 days' exposure from Quarterly Progress Report - Metallurgy Research Operation - October, November, December, 1962, HW-76228.

(a) 16.5 days' exposure at indicated approximate temperatures.

(b) Zero flux data from exposure in out-of-reactor autoclave

(c) Indicated weight gains are in addition to preautoclave film averaging between 7.3 and 8.0 mg/dm² for the various alloys.

(d) Superscripts indicate per cent cold work if not annealed; subscripts indicate number of specimens averaged.

(e) Original plate hardness: 94

TABLE 5.2

COMPARISON OF THE EFFECT OF 16.5 DAYS' EXPOSURE IN THE ETR G-7 LOOP
ON THE BEHAVIOR OF ANNEALED ZIRCALOY-2 FROM DIFFERENT SOURCES^(a)

Neutron Flux (> 1 Mev), nv	Temperature, F	Plate	Hardness, Rockwell B	Hydrogen Gain, % Theoretical	Weight Gain, mg/dm ²	
					Preautoclaved ^(b)	Etched
0	536	6515	94	--	2.9 ₂	9.8 ₁
6.6 x 10 ¹³	532	6515	101	38 ₁	20.0 ₂	25.7 ₁
0	536	Bettis	88	--	2.5 ₃	10.0 ₁
6.6 x 10 ¹³	532	Bettis	98	29 ₁	16.6 ₃	24.2 ₁

(a) > 10 cc H₂ per kg of water; pH 10.0 LiOH

(b) Preautoclave films averaged 8.1 and 7.6 mg/dm²
for Plate 6515 and Bettis materials, respectively.

(c) Subscripts indicate number of specimens averaged.

TABLE 5.3

ZIRCONIUM ALLOY SPECIMEN COMPOSITIONS

Average Analysis of Ingot

Element	NPR Zircaloy-2 ^(a)	Zircaloy-4 ^(b)	Ni-Free Zircaloy-2 ^(b)	Zr-3 wt% Nb-1 wt% Sn ^(c)
Fe, wt%	0.109	0.22	0.14	0.055
Cr, wt%	0.107	0.09	0.09	0.005
Ni, wt%	0.045	<0.001	0.0035	<0.001
Nb, wt%	--	--	--	2.80
Sn, wt%	1.48	1.34	1.44	1.15
Al, ppm	44	25	30	40
B	<0.3	<0.2	<0.2	<0.2
C	142	<30	163	55
Cd	<0.3	<0.5	<0.3	<0.3
Co	<10	<5	<0.5	<5
Cu	<20	<25	<25	<20
H(d)	31	12	11	9
Hf	<125	72	70	80
Mg	<10	<10	<10	<10
Mn	<25	<10	<10	<10
Mo	<10	--	--	<10
N	30	35	55	25
O	900	--	--	915
Pb	<20	13	<5	<5
Si	47	70	50	66
Na	<10	--	--	<20
Ti	<20	<20	25	<20
W	<20	<10	<50	300
U	1	0.8	1.9	2.0
V	<10	--	--	<20

(a) Harvey Aluminum Company, Torrance, California

(b) Wah Chang Corporation, Albany, Oregon

(c) Oregon Metallurgical Corporation, Albany, Oregon

(d) Hot vacuum extraction hydrogen analyses at this laboratory.

TABLE 5. 4

ZIRCONIUM ALLOY SPECIMEN FABRICATION HISTORYNPR Zircaloy-2

Tube drawn at 1550 F to 0.4-in. wall thickness, followed by cold draw to nominal 0.25-in. wall. Tube wall section rolled at < 900 F to 0.072-in. thickness followed by cold rolling to 0.050-in. specimen thickness. Annealed specimens heated in vacuo 8 hr at 1400 F.

Zircaloy-4 and Ni-Free Zircaloy-2

Ingot forged at 1800 F to 4-in. slab followed by hot rolling at 1800 F to 2-in. slab. Strip hot rolled at 1450 F to 0.1-in. thickness followed by cold rolling to nominal 0.030-in. thickness. Strip vacuum annealed 1 hr at 1450 F.

Zircaloy-3 wt% Nb-1 wt% Sn

One-half-in. -thick arc-cast ingot button rolled to 0.060-in. thickness at 1200 to 1300 F with intermediate anneal at 1400 to 1475 F following each 40% reduction. Strip cold rolled from 60 to 40 mils. Specimens cut and annealed in vacuo at 1070 F for 24 hr. No fabrication abnormalities, embrittlement or edge splitting of rolled strip were observed.

showed no significant effect of flux on weight gain through 1.6×10^{13} nv (> 1 Mev) and a maximum weight gain ratio of only two to one at the highest flux position. The variation of estimated temperatures over the range of positions in the loop would not be expected to affect weight gain by an amount greater than 0.5 mg/dm^2 during the short exposure period.

Hydrogen cycle weight gain results which appeared in Figure 5.1 of the previous report⁽¹⁾ have been replotted to reflect actual flux data obtained from the counting of iron flux wires exposed with the specimens. The net effect is a slight increase in the slope of the curve, but the general comparison of the effects of hydrogen-bearing versus oxygen-bearing water environment in-reactor is not affected significantly. Hydrogen cycle (low-oxygen) weight gain results for the other alloys are shown in Figure 5.2 in comparison with out-of-reactor data obtained elsewhere at higher temperatures and at 536 F in autoclave facilities at this laboratory. In general, it appears that irradiation at 6.2×10^{13} nv (> 1 Mev) in 534 F hydrogen-bearing low-oxygen (<0.1 ppm) water results in oxidation rates greater than for out-of-reactor exposure to 680 F water. For comparison it may be recalled that in-reactor

1. Quarterly Progress Report, Metallurgy Research Operation - July, August, September, 1964, edited by J. J. Cadwell, HW-84281. September 15, 1964.

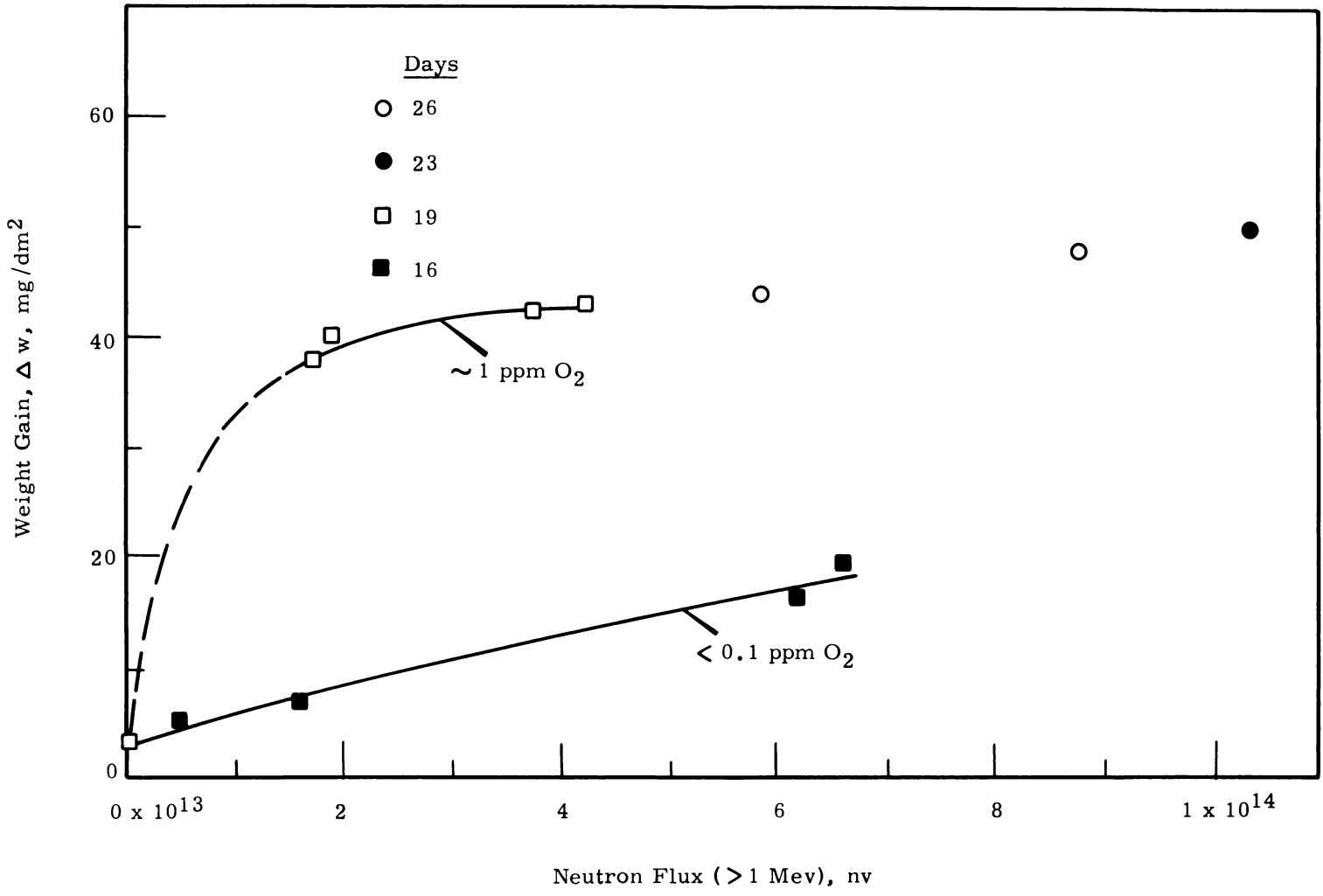


FIGURE 5.1
Environmental Effects on Oxidation of Zircaloy-2 ETR G-7 Loop

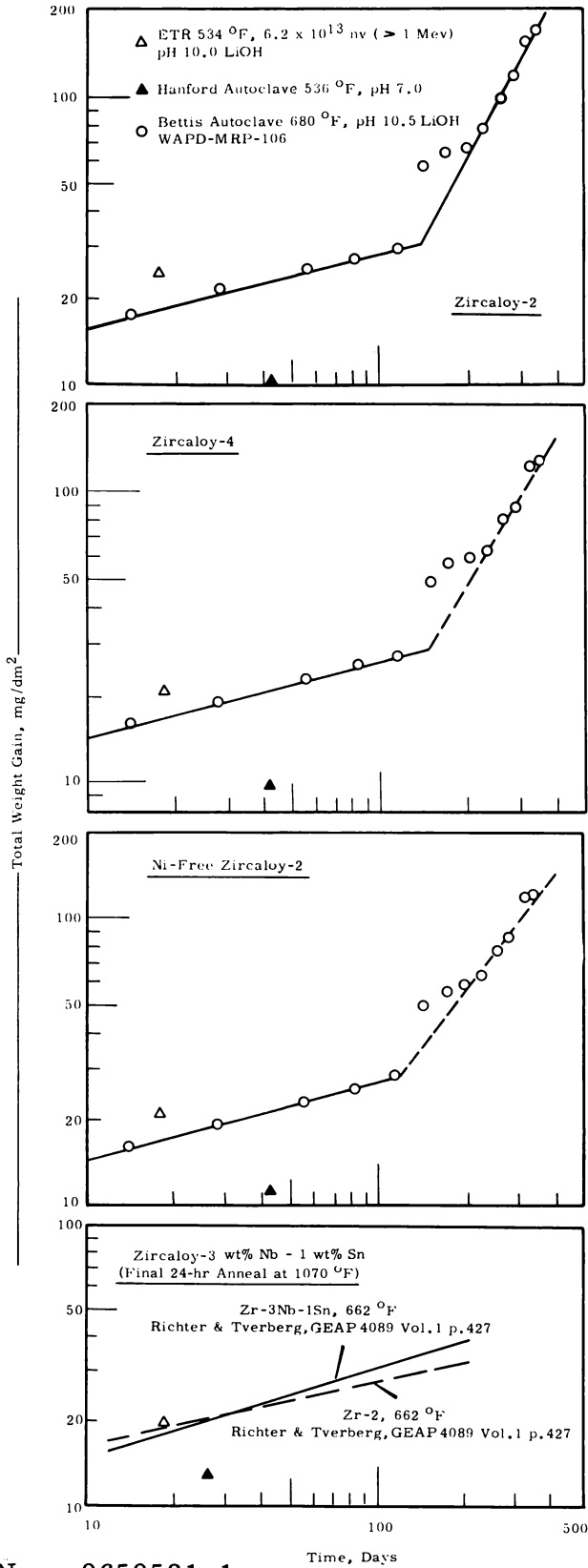


FIGURE 5.2
Comparison
of In- and Out-of-Reactor
Corrosion for Zirconium Alloys

weight gains previously reported by this laboratory for normal ETR G-7 loop water containing oxygen at the level of about 1 ppm indicated oxidation rates greater than for out-of-reactor exposure to 750 F steam.

Hydrogen pickup fractions during the hydrogen cycle experiment were generally higher for irradiated specimens of all alloys except Zircaloy-3 wt% Nb-1 wt% Sn. For this alloy there was no significant difference in the fractional pickup of theoretical corrosion hydrogen between out-of-reactor controls and irradiated material. This alloy also exhibited the lowest in-reactor pickup fraction of the test group: ~ 15%. In-reactor hydrogen pickup fractions for Zircaloy-2 during the hydrogen cycle were generally higher by a factor of about two than for the previous, higher oxygen condition. Hydrogen gain results for the Zircaloy-2, Zircaloy-4, and Ni-Free Zircaloy-2 alloys of this experiment are shown on Figure 5.3 in comparison with out-of-reactor data obtained elsewhere at higher temperatures. Hydrogen pickup data for a Zircaloy-Nb-Sn alloy of a composition and heat treatment and in an environment approximating that of the present experiment could not be found in the available literature for comparison purposes. However, data obtained elsewhere in steam, moist air, and water for alloy compositions varying to 2-1/2% Nb and to 1-1/2% Sn and for usually much longer exposure times show low hydrogen pickup—usually less than 10%—at the lower temperatures and particularly at small weight gains. (1, 2, 3)

In the case of NPR Zircaloy-2, the 86% cold-worked specimens showed higher hydrogen pickup fractions than any of the other materials tested, and there was an apparent marked effect of alpha annealing on

-
1. S. B. Dalgaard. The Corrosion Resistance of Zr-Nb and Zr-Nb-Sn Alloys in High-Temperature Water and Steam, CRMET-911. (AECL-993) Atomic Energy of Canada Limited. March 1960.
 2. B. Cox and J. A. Read. Oxidation of a Zr-2-1/2% Nb Alloy in Steam and Air, AERE-R-4459. Atomic Energy Research Establishment. Harwell, England, October 1963.
 3. B. Cox, P. G. Chadd, and J. F. Short. The Oxidation and Corrosion of Zirconium and its Alloys. XV. Further Studies of Zirconium-Niobium Alloys, AERE-R-4134. Atomic Energy Research Establishment. August 1962.

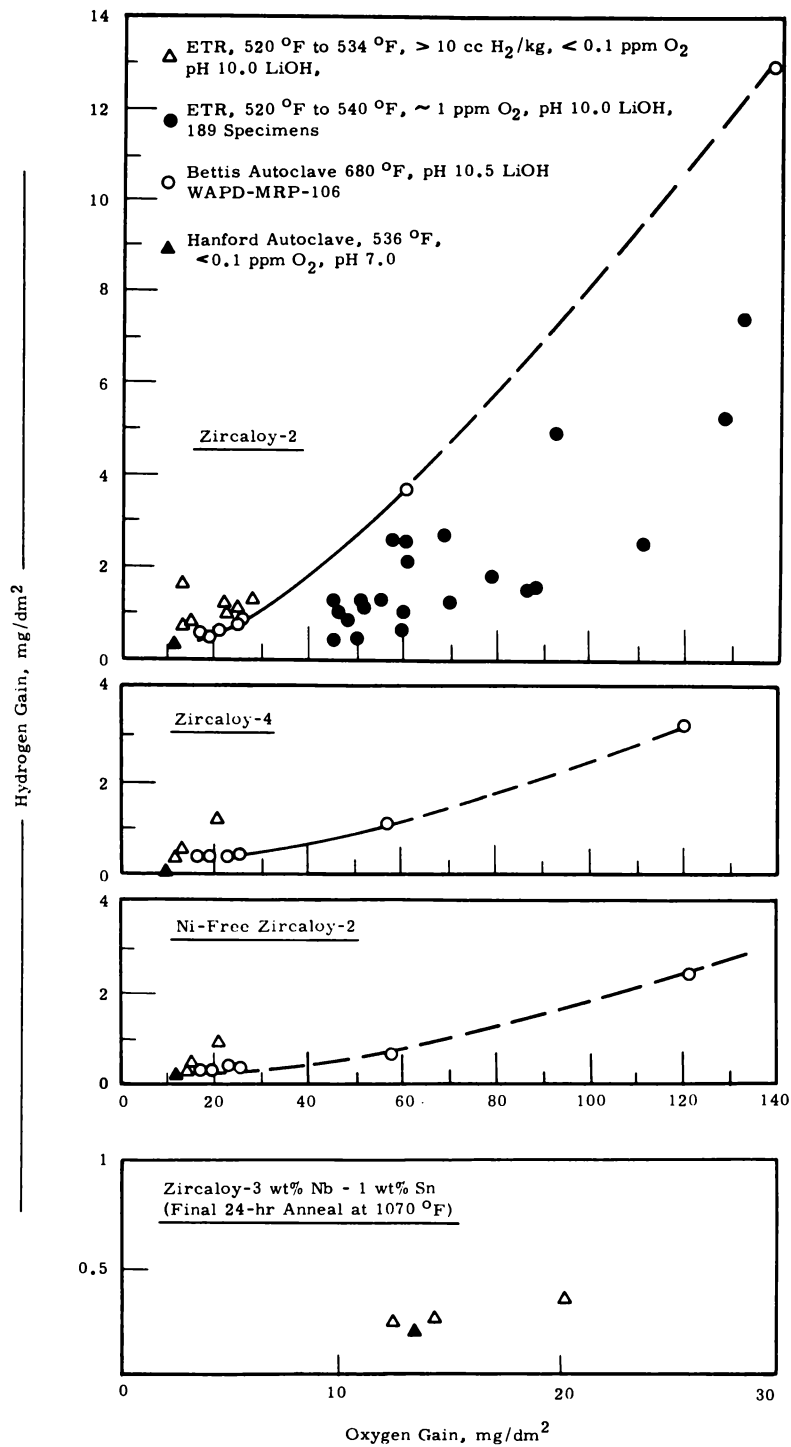


FIGURE 5.3

Comparison of Hydrogen Pickup
for Zirconium Alloys During Corrosion In- and Out-of-Reactor
Neg. 0650581-3

hydrogen pickup both in- and out-of-reactor. Pickup fractions for annealed NPR Zircaloy-2 specimens were, for the most part, comparable with pickup fractions for Irradiations Program Zircaloy-2 material but less than half those for specimens in the 86% cold-worked condition. However, this was the only heavily cold-worked material tested and the only material tested with coupons representing these extremely different metallurgical conditions. Consequently, no conclusions can or should be drawn on the basis of this experiment relative to the probable effect on hydrogen pickup of the lesser amount of cold work normally used in the fabrication of reactor components.

ATR GAS LOOP SUPPORT

Corrosion Studies - L. A. Charlot and R. E. Westerman

Stresses within an oxide resulting from phase changes or differences in thermal expansion of metal and oxide during heating and cooling cycles can cause spalling of a protective oxide film. Tests have been completed on Hastelloy X-280 and Haynes Alloy 25 in a severe oxidizing atmosphere, 25 torr oxygen, to determine the effect of thermal cycling from room temperature to 2048 F on the oxidation process. The weight changes of the samples were monitored by use of a recording microbalance. Each cycle consisted of a 3000 min (~2 days) oxidation at temperature (2048 F) followed by a furnace cool to room temperature. The oxidizing atmosphere was maintained during the furnace cool. In general, the cooling time consisted of approximately 2 hr for the temperature to drop from 2048 to 950 F, followed by an additional 3 to 4 hr to reach room temperature. At the end of each cycle, the sample was brushed lightly to remove all but the most tenacious oxide film. Nine such cycles were completed for each alloy. At the start of each cycle, a fresh 25 torr oxygen atmosphere was introduced into the reaction tube.

Figures 5.4 and 5.5 show graphically the effect of thermal cycling on both alloys. It is apparent that Haynes Alloy 25 loses more metal than Hastelloy X-280, considering only the weight change data. For the nine cycles, total metal weight loss from the Haynes Alloy 25 sample was 83 mg/cm², compared with 11.1 mg/cm² metal loss for Hastelloy X-280. Note that the oxidation rate of Haynes Alloy 25 increases rapidly after the fifth cycle, while the oxidation rate of Hastelloy X-280 continually decreases.

One possible explanation for the observed spalling of Haynes Alloy 25 is deformation of an oxide film by phase change. For a Co-20 wt% Cr alloy, cobalt monoxide will be a dominant oxide specie at 2048 F in an

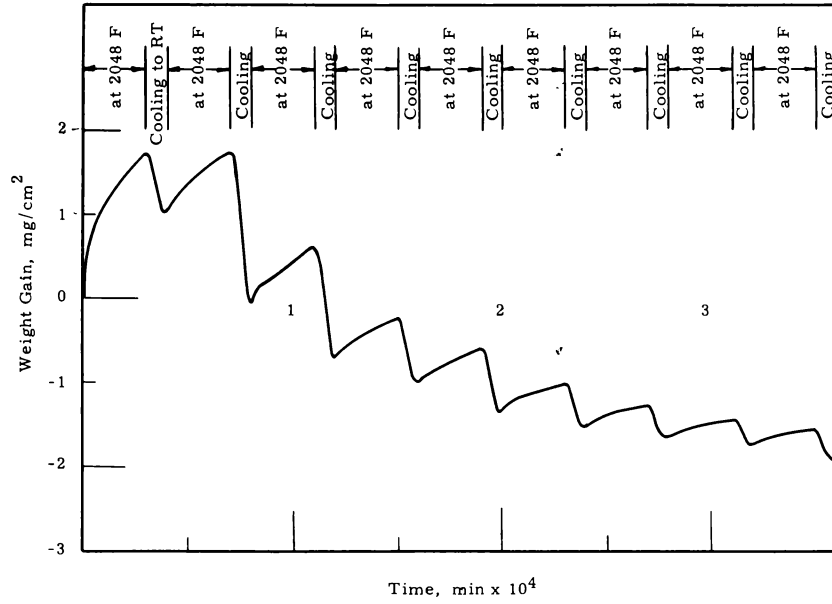


FIGURE 5. 4

Thermal Cycling of Hastelloy X-280 Static Test in 25 Torr O₂

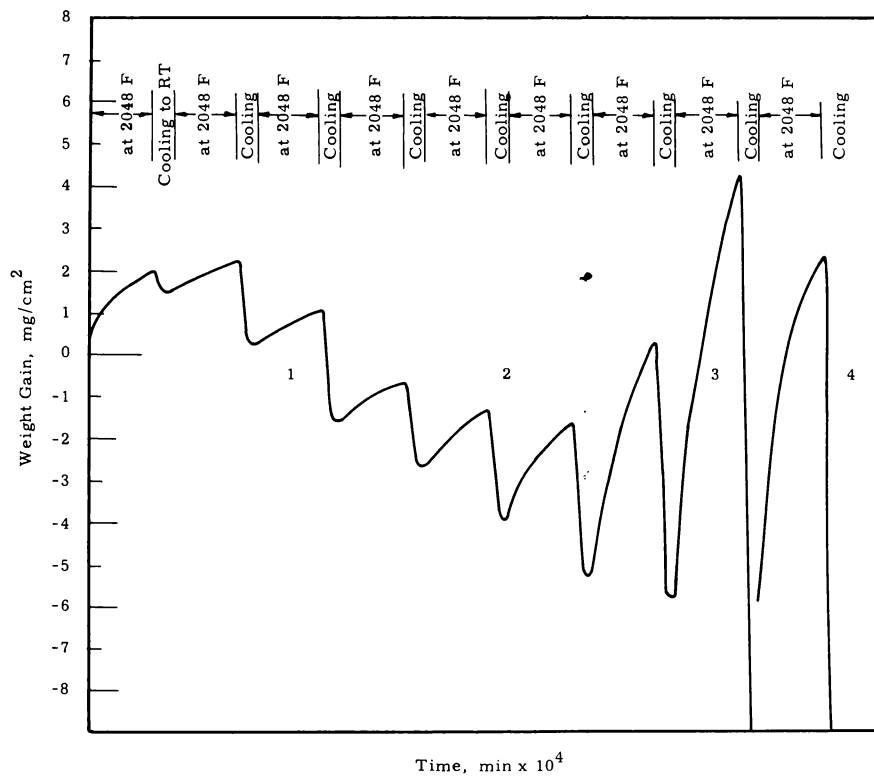


FIGURE 5. 5

Thermal Cycling of Haynes Alloy 25 Static Test in 25 Torr O₂

oxidizing atmosphere.⁽¹⁾ However, Co_3O_4 which has about three times the volume of CoO is stable and has been observed in scales formed at 1650 F.⁽¹⁾ The stresses induced by an oxide phase change on cooling of the sample along with those induced by material strength, thermal diffusivity and thermal expansion, could increase the spalling tendency which would, in turn, increase the oxidation tendency.

The microstructure of both alloys at the end of nine thermal cycles is being examined. Metallography should indicate the extent of alloy depletion and intergranular oxidation for these two alloys.

1. F. R. Morral. "Identification of Corrosion Products on Cobalt and Cobalt Alloys," Corrosion, vol. 18, pp. 421t-423t.. 1962..

Corrosion of Super Alloys in High Temperature, High VelocityHelium - R. A. Thiede and R. E. WestermanEquipment Status

The numerous small changes in the loop controls (Dynamic Materials Testing Apparatus) have been satisfactory and stable operation is now possible. The greatest source of operating problems appears to be:

1. A good gas-tight fit of the alumina test section into the Pt-10% Rh test section holder. If the fit at the tapered seat is not tight or if the alumina cracks, the temperature in the test section cannot be made uniform.
2. Rupture of the diaphragm on the diaphragm compressor. According to the manufacturer, diaphragm change after 600 to 1000 hr of operation will almost entirely eliminate the possibility of a diaphragm rupture. A running time meter has been installed to accomplish this objective.

At the present time, difficulty (1) has been resolved and the temperatures in the test section are uniform. The compressor diaphragms are now changed after 1000 hr service. A small sintered-metal filter has been placed in the line following the test section, so that the oxide which spalls off of the sample can be collected for examination.

Runs completed to date and not previously reported are summarized in Table 5.5.

During Run Number 4 the diaphragm of the diaphragm compressor ruptured and introduced oil into the loop. When the loop was opened and the test section removed, it was apparent that considerable oil vapor had been "cracked" and had left a very black deposit on the ceramic beads. The sample, however, was "bright" and did not appear to have much scale. The oil appeared to be mainly in the check valves on top of the compressor head and in connecting tubing. The affected parts were cleaned with acetone and blown out with compressed air. Metallographic examination of the sample showed thorough carburization, with a complete network of carbides through the grain boundaries.

Run Number 5 was made with a ceramic dummy in the test section, and with air purposely introduced into the loop gas. This procedure appeared to effectively clean up the residual oil contamination.

TABLE 5.5
SUMMARY OF EXPERIMENTS
IN THE DYNAMIC MATERIALS TESTING APPARATUS

<u>Run Number</u>	<u>Temperature, F</u>	<u>Sample Number</u>	<u>Sample Material</u>	<u>Hours at Temperature</u>
3	2050	2	Haynes Alloy 25	189 $\frac{1}{2}$
4	2050	2	Haynes Alloy 25	151
5	2050	Ceramic Dummy	---	113 $\frac{1}{2}$
6	2050	2	Haynes Alloy 25	406
7	2050	Ceramic Dummy	---	42 $\frac{1}{2}$
8	2050	3	Hastelloy X	240
9	2050	3	Hastelloy X	237

All of the runs have been made in Grade A helium at 350 psi and at gas velocities on the order of 525 fps. Some clean gas is introduced periodically to make up for leaks and gas sampling for the chromatograph.

Run Number 6 was made to determine the behavior of the carburized Haynes Alloy 25 in a "clean" loop gas atmosphere. After 406 hr the sample showed only a small excess of carbides over the "as-received" material, i. e., decarburization was rapid in the typical loop gas.

Run Number 8 was the first run made using a Hastelloy X sample. The sample was exposed to the helium atmosphere for 240 hr at 2050 F. The oxide formed on the sample was not as tenacious as that formed on coupons in static oxygen atmospheres. Only about 25% of the total oxide formed was retained. The sample lost a total of 10.5 mg of metal/cm² during the run. Assuming a probably oxide composition, this amounts to an equivalent oxygen "weight gain" of 3.5 mg/cm². Extrapolating data obtained at the same temperature in a static oxygen atmosphere of 18 μ pressure,*

* An oxygen pressure of 18 μ would be approximately equivalent to 1 vpm oxygen in the gas loop helium.

a weight gain of 3.6 mg/cm^2 is obtained, in excellent agreement with the "weight gain" found in the dynamic system. There is no evidence to date that the high flow rates influence the oxygen-metal reaction kinetics.

The results of Run Number 9 have not been completely evaluated.

In general, during a "clean" run, the gas atmosphere shows the following characteristics:

Hydrogen - Hydrogen is undetectable when the loop is first filled.

The concentration builds up slowly during the run, and may attain concentration up to values of 50 ppm.

Oxygen - When the loop is first filled, oxygen is usually 2-3 ppm.

With the loop at temperature, oxygen is undetectable.

Nitrogen - Nitrogen usually remains constant during the run at 3-4 ppm.

Methane - Methane is usually undetectable at less than 0.1 ppm.

The next series of experiments scheduled for the DMTA will evaluate columbium samples in Grade A helium, largely to compare scaling tendencies with Haynes Alloy 25 and Hastelloy X. On completion of this study a gas clean-up system will be inserted in the system to evaluate ATR structural metals in a more favorable environment.

ZrO₂ - Oxygen Probe - D. W. Shannon

The calcia stabilized zirconia electrolytic oxygen probe reported last quarter has been modified to use air as a reference oxygen partial pressure. The use of air avoids complicated seals used with the Ni-NiO reference discussed previously. Also it was found that hydrogen in the test gas could seriously damage the Ni-NiO reference, probably by reducing the NiO. A probe designed as in Figure 4.6(a) followed the theoretical voltage very closely as shown in Figure 5.7. A simplified design as shown in Figure 5.6(b) has also been found to be satisfactory and design 5.6(b) is to be incorporated into a portable instrument for analysis of reactor helium.

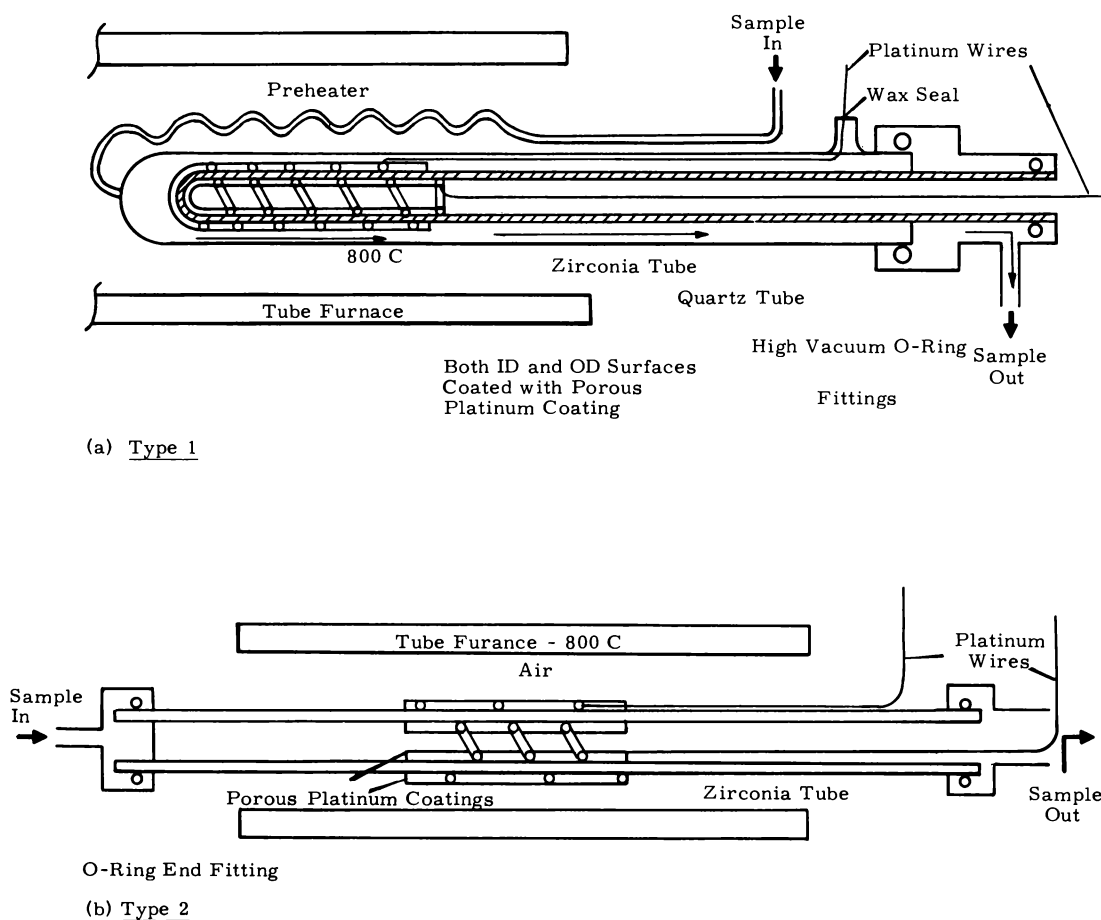


FIGURE 5.6

Zirconia Oxygen Probes Stabilized with 7-1/2 wt% CaO

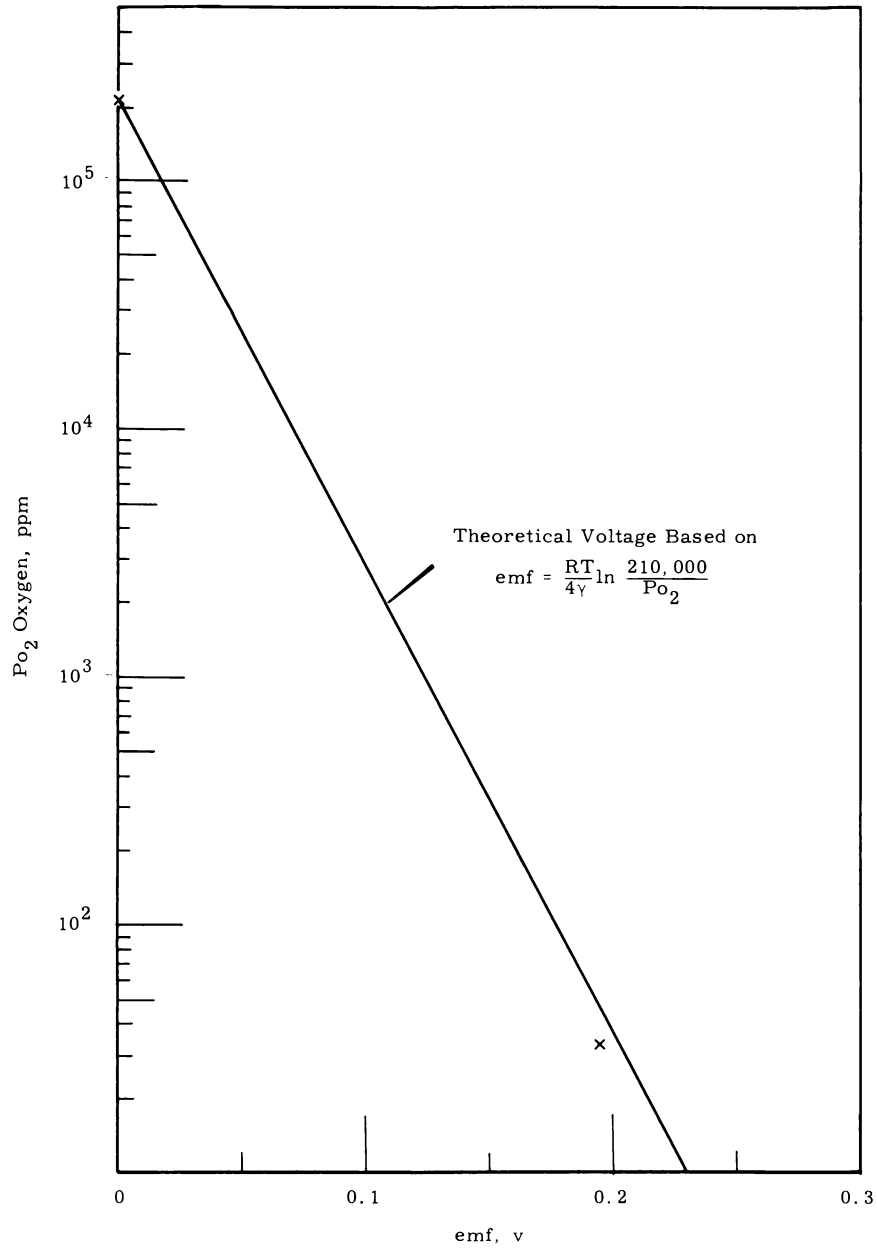


FIGURE 5.7
Response of Zirconia Oxygen Probe, 800 C

PRP MATERIALS DEVELOPMENTIn-Reactor Corrosion of PRTR Fuel Sheathing - H. C. Bowen and B. Griggs

A coupon rod is undergoing irradiation in the PRTR to determine the radiation effect on Zircaloy corrosion in the PRTR. The coupon rod replaces a fuel rod on a PRTR 19-rod cluster fuel element. Alternate Zircaloy-2 and Zircaloy-4 coupons with three different pretreatments are included on the rod.

The rod has now been exposed a total of approximately 2000 hr at reactor operating conditions (pH-10 lithiated D₂O, 275 C, 1050 psi). Examination of the rod after about 1400 hr exposure showed no unexpected effects. Oxides on the first few coupons on the inlet end were still in the interference color range. All the rest were black or gray. The element was recharged and is undergoing further exposure.

PRODUCTION REACTOR CORROSION AND COATING STUDIES

Corrosion of High Silicon Aluminum Alloys - H. C. Bowen

A program to determine the corrosion resistance of aluminum alloys containing 7 and 10 wt% silicon plus nickel and/or magnesium in comparison to 8001 aluminum (1 wt% Ni, 0.5 wt% Fe) is continuing. The alloys are being tested in 140 C high and low flow process water under isothermal and nonisothermal conditions, in 360 C water, and 400 C, 100 psi steam. Galvanic couples of the experimental alloys with Zircaloy-2, 8001 aluminum, 1245 aluminum and AISI 304 SS and stress samples of the experimental alloys are being tested in 140 and 50 C process water. The nominal compositions of the experimental alloys are: HDA-1; 10 wt% Si, 1 wt% Ni, 1 wt% Mg; HDA-2; 7 wt% Si, 1 wt% Ni, 1 wt% Mg; HDA-3; 10 wt% Si, 1 wt% Mg; and HDA-4; 10 wt% Si, 1 wt% Ni.

In the nonisothermal high flow (25 fps) test the HDA-1 alloy lost about 1/3 less metal than 8001 aluminum under the same conditions after 2 months' exposure. The test is being run at 140 C with a ΔT of 70 C through the loop. The results are in agreement with data reported by Videm for similar alloys.⁽¹⁾ Under these test conditions 8001 aluminum forms a very highly stressed film which spalls badly when dried. The silicon alloy retained almost twice the amount of oxide as 8001 aluminum. There is insufficient exposure on the other experimental high silicon alloys to determine their corrosion resistance under these conditions.

In 140 C high flow (25 fps) isothermal process water HDA-3 corrodes about 20 wt% less than the other alloys after 2 months' exposure. HDA-1, 2, and 4, and 8001 aluminum were about equivalent in corrosion resistance in this test. In low flow 140 C process water HDA-3 again shows about 20 wt% less corrosion than the rest of the alloys which have about the same

1. K. Videm. Aluminum Alloys with Improved Corrosion Resistance in High Temperature Water, KR-19, Kjeller Research Establishment, Lillestrøm, Norway. May 1962.

penetrations. All the silicon alloys pitted when galvanically coupled with stainless steel. The worst pitting appeared on HDA-3. No evidence of stress corrosion in this test was seen after 1 months' exposure.

In 360 C high-purity water HDA-3 was destroyed in less than 10 days. HDA-1, 2, and 4 were attacked to approximately the same degree as 8001 aluminum after 1 month, but after 2 months' exposure the silicon alloys were blistered, HDA-1 and 2 severely.

Except for HDA-3 the silicon alloys were more resistant to 400 C, 100 psi steam than 8001 aluminum. HDA-3 samples were destroyed in less than 5 days. After 1 month 8001 aluminum was blistering but the silicon alloy surfaces were still uniform. Metallography of the samples showed void formation throughout the entire sample of 8001 aluminum but no void formation was seen in the silicon alloys.

The 50 C process water galvanic couples and stress coupons have not yet received sufficient exposure for comparative evaluation.

N-REACTOR CORROSION AND HYDRIDING

Nickel-Plated Aluminum for High Temperature Aqueous

Environments - A. B. Johnson and K. D. Hayden

Three nickel-plated Pu-Al fuel elements and five plated 8001 aluminum dummy elements were exposed in the C-1 loop in-reactor for approximately 1 month in pH 5.5 to 7.3 water at a water temperature of 260 C. The nickel plate was chemically deposited in thicknesses of 0.8 mil on the fueled elements and 0.8 and 0.4 mils on the dummy elements. The elements were heat treated in air at 400 C for 2.5, 10, and 40 hr.

Weight losses on the fueled elements represented 35 to 50% of the nickel weight. Metallography showed considerable attack on the outer nickel layer. However, the attack proceeded only to the inner Ni-Al diffusion layer.

On dummy elements with 0.8 mil plate, the plate was nearly intact. Weight losses were 1 to 11% of the total nickel weight. Metallography showed less than 3 mils penetration into the aluminum cladding at an intentional defect in the plate and minimal undercutting of the nickel plate. Behavior of the 0.4 mil plate was less favorable; weight losses corresponded to 55 to 75% of the nickel weight.

A thermocouple inserted in one of the plated fuel elements registered 280 C through the exposures, in contrast to cyclic temperature increases (up to ~ 400 C) observed in previous C-1 loop tests on unplated elements. In summary, the test indicated:

1. Plate retention and low corrosion rates on the surfaces of unfueled elements with 0.8 mil plate.
2. Plate retention, with higher corrosion rates on the fueled elements, the attack being contained by the Al-Ni diffusion layers.
3. Light attack and little undercutting at intentional defects in plate on an unfueled element.

4. Improved heat transfer compared to fueled, unplated elements.
5. Insufficient protection by 0.4 mil plate on unfueled elements.

Out-of-reactor tests at 330 C indicate that nickel corrosion rates are lower in pH-10 NH_4OH than at neutral pH; corrosion rates of unclad aluminum in pH-10 NH_4OH are comparable to rates at neutral pH after 20 days. An in-reactor evaluation of nickel-plated aluminum-clad fuel in ammoniated water seems justified.

MATERIALS ENGINEERING

GAS LOOP DEVELOPMENT

Model Gas Loop Heater and Piping Redesign - D. R. Doman

A new model gas loop heater is being designed to incorporate and investigate salient design details of the compact two-stage heater presently being considered for the ATR gas loop. The model loop heater uses an outer ring of 12 Ni-Cr tubes to heat the gas from 1500 to 1800 F with a flow reversal to an inner ring of six molybdenum tubes to produce the 2100 F outlet temperature. Alumina surrounds all tubes to act as combination electrical insulator and flow block to force the majority of the gas through the inside of the heated tubes. Metallic foil type insulation around the heater tube assembly reduces the temperature of the pressure-bearing shell to less than 1000 F.

Design calculations on the heater are 95% complete and detail drawings 15% complete. Most major components have been submitted for suppliers' bids. Some material is on-site and fabrication will begin upon completion of the detailed drawings.

The present double-contained model gas loop piping is being redesigned to also incorporate metallic-foil type insulation which is proposed for the ATR gas loop use. This system will permit single-containment of the high purity, high temperature gas. Scoping drawings have been completed and a stress analysis of the redesigned system is being prepared for digital computer solution.

Helium Purification System - J. H. Hoage

The high pressure helium purification system was activated in November by Engelhard, Inc. The system produced helium with less than 0.1 ppm of the following: H₂, N₂, O₂, CH₄, CO, and CO₂. Moisture was less than 2 ppm but it is believed to be due to moisture on the wall of the sample lines.

A bypass cleanup system consisting of charcoal and 13X molecular sieve, all at the temperature of liquid nitrogen, was placed in service on the gas loop utilizing the pressure available from the gas system. The system is unable to reduce the hydrogen content as it must be oxidized to form water for removal. During a typical run lasting 29 hr, the gas analyses were as follows:

	<u>GAS ANALYSES IN ppm</u>					
	<u>H₂</u>	<u>O₂</u>	<u>N₂</u>	<u>CH₄</u>	<u>CO</u>	<u>H₂O</u>
Start	<0.1	1.8	5.8	<0.1	<0.1	33
10 hr	10.5	<0.1	<0.1	<0.1	<0.1	5.2
23 hr	80	<1	<1	<1	<1	2.5
23.5 hr*	150	<1	<1	<1	<6	4.4
29 hr	280	25	3.2	<1	<1	12.6

* Breakthrough of absorbing beds

The installation of a copper oxide bed together with larger dual low temperature beds would permit the system to operate with an analysis of 2.0 ppm H₂O and <1 ppm total other impurities.

Weld Embrittlement - D. R. Ireland

The construction of the ATR gas loop will require the welding of dissimilar metals. Both of the two candidate weld filler metals, Hastelloy X and Hastelloy W, indicate a sharp loss in tensile test ductility at temperatures between 1200 and 1600 F. This loss in ductility is associated with a precipitation phenomenon and therefore is a function of time as well as temperature. The purpose of this part of the program is to determine the effect of time and temperature on the ductility of the two candidate filler metals. The relative age embrittling or loss in ductility of the weld filler metals will be determined from "free-bend" tests of longitudinal weld specimens. The weld specimens were made according to standard thick wall pressure vessel welding procedures and by qualified welders. All welds have been radiographically inspected according to Section VIII of the ASME boiler and pressure vessel code for unfired pressure vessels. The unaged bend and tensile properties have been established and the aging of the other weld specimens is in progress. The aging times are 500, 1000, and 5000 hr. The aging temperatures are 1000 and 1200 F for the AISI SS joints and 1400 and 1600 F for the Haynes 25 joints.

The test procedure and criterion for failure in these bend tests is in accordance with standard ASTM practices. The bend test will indicate where the lowest ductility material will be located (base metal, heat affected zone, or weld metal) for a given dissimilar metal joint. The base metal combinations being investigated are AISI 316 SS to Hastelloy X and Haynes 25 to Hastelloy X.

The ductility of the weld metal will be measured from the elongation of 1/4 in. square grids inked on the tension surface of the bend specimens and from measurements of the bend radius. The bend test specimens are large enough, 1/2 in. thick, 3 in. wide and 9 in. long, to have 1-1/8 in. gage length tensile specimens cut from undeformed weld metal at both ends after being bent to a 180° bend. These weld metal tensile tests will be used to verify the bend tests.

PRTR PRESSURE TUBES

In-Reactor Monitoring - P. J. Pankaskie

The Zircaloy-2 pressure tubes in the PRTR are periodically and nondestructively inspected in situ to assist in evaluating their performance. Beginning this quarter, these inspections consist of a visual examination to detect and measure the extent of localized corrosion or mechanical damage that may arise from reactor operation.

During this quarter, 43 inspections were made in 38 process channels. The results of these inspections showed relatively little new fretting corrosion. These inspections disclosed the presence of a new 15 mil deep fretted area associated with the single rod wire wrap of a fuel element in the pressure tube in process channel 1653. In all other instances, fretting was only minor in severity.

An analysis of the inspections throughout the past year showed that the incidence and severity of fretting is now about as low or lower than previously experienced in the PRTR. During the past year, three fretted areas with depth of 10 mils or greater and about 12 fretted with depths of 5 to 10 mils were observed. In no instance did fretting corrosion constitute any near term hazard to reactor operation. Based on these results and the results of inspections during 1963, a reduction in the number of pressure tube inspections has been proposed. This proposed inspection program reduces the number of tubes to be inspected each year by one-half and eliminates gas gap and ID measurements from routine inspections.

Properties of Irradiated PRTR Pressure Tubes - M. C. Fraser

A report concerning strength, ductility, zirconium hydride concentration and crack propagation characteristics of specimens taken from irradiated and discharged PRTR Zircaloy-2 pressure tubes has been written. It has been entitled "Postirradiation Evaluation of Zircaloy-2 PRTR Pressure Tubes - Part III," HW-84540. This is the third report on this subject to be written about work performed for the pressure tube surveillance portion of the Plutonium Recycle Program.

The conclusions in this report state that: Burst test hoop strength and elongation data show that tubes having fast neutron exposure of 10^{21} nvt or less have high strength with ductility; furthermore, the curves indicate that increasing exposure by a factor of two will not substantially change these conditions. Crack propagation data for tubes having fast neutron exposure of 5×10^{20} nvt or less show that resistance to crack propagation is unaffected by the neutron exposure; and that the crack length necessary for propagation at PRTR operating pressure is about 10 in. Hydride concentration data indicate general levels of hydride concentration are low, but at flaws high hydride concentrations have been found. When tested the worst combined effect of flaw plus hydride produced a strength reduction of 25%.

Irradiated Tube Testing Facility - P. M. Jackson

The new facility for postirradiation evaluation of reactor process tubing has been in constant operation during the quarter. Six burst tests and two stress rupture tests were completed during this period and an additional three stress rupture tests are currently in progress. These three tests have accumulated the following hours at elevated temperature and pressure conditions - PRTR 2683 hr, KER 3618 and 825 hr. Results of the completed tests are reported elsewhere in this report.

Movement of Zirconium Hydride in Zircaloy-2 - R. J. Evans

A strip of Zircaloy-2, hydrided to 275 ppm hydrogen, was placed between the electrodes of a direct current power supply to determine the effects of a direct current on zirconium hydride. The initial experiment applied 1.3 volts and 55 amps to a Zircaloy-2 strip. This current maintained 400 ± 50 C on the surface of the strip. After 3 days the sample overheated and melted. Metallography indicated a massive buildup of hydride at the negative end (cathode) of the strip and a depletion of hydride at the positive end (anode) (See Figure 6.1). A second strip was connected to the electrodes through a quartz "T" with helium directed at the center of the strip. After 100 hr at conditions similar to that of the first strip, metallography indicated that hydride was being lost from the ends and concentrated in the cool center of the strip. The cathode retained slightly more hydride than the anode (See Figure 6.2). The strip was then connected to the electrodes through a quartz tube with helium directed at the ends of the strip. After approximately 100 hr metallography indicated a massive buildup of hydride at both ends of the strip and a depletion of hydride from the center. More hydride can be seen at the cathode than at the anode (See Figure 6.3).

These qualitative studies indicate a small amount of hydride movement toward the cathode due to the effect of a direct current and a very large movement of hydride from a hot zone to a cool zone.

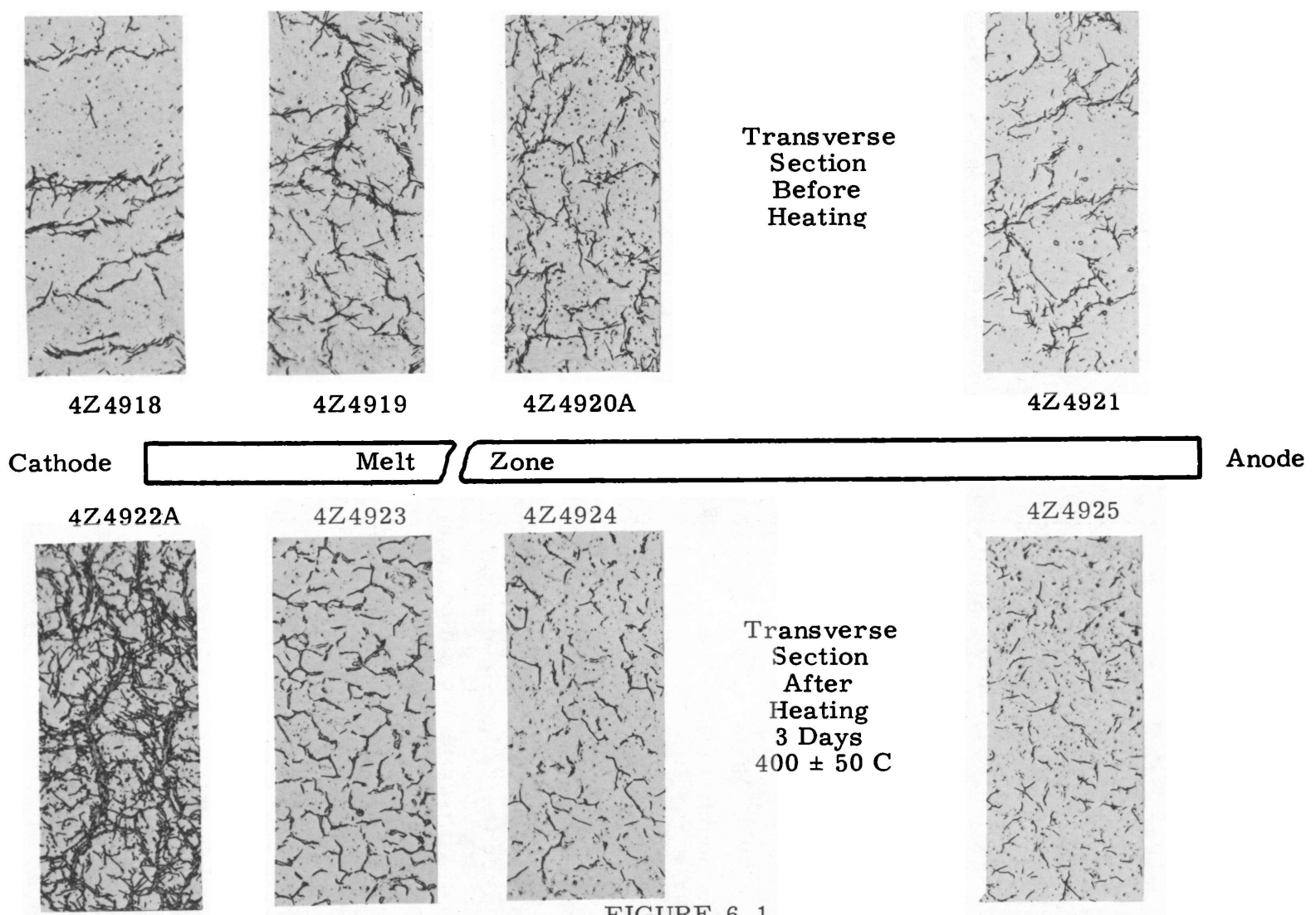
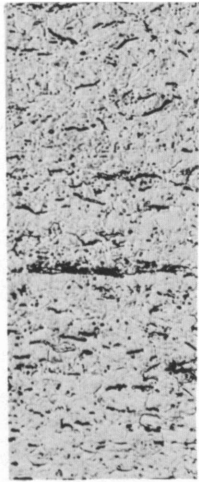
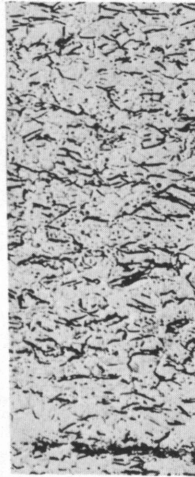


FIGURE 6.1

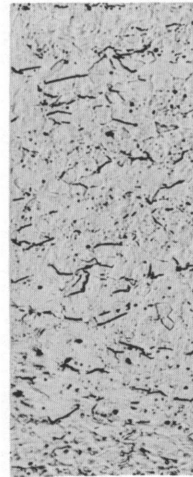
Transverse Section Before and After Heating (250X)



5Z-5324-A



5Z-5324-B



5Z-5324-C

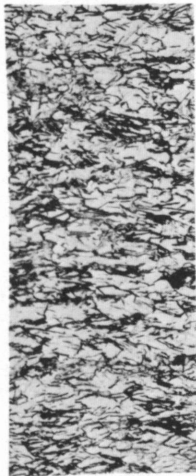
FIGURE 6.2
Center Cooled
by Helium for 100 hr
at 400 ± 25 C
(250X Longitudinal Section)

Cathode



Anode

565-5029A



565-5029B



565-5029C

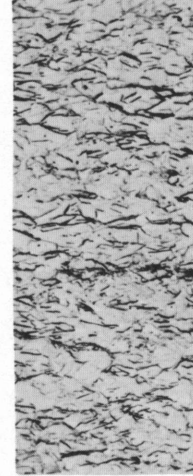


FIGURE 6.3
Ends Cooled
by Helium for 100 hr
at 400 ± 30 C
(250X Longitudinal Section)

N-REACTOR PRESSURE TUBESZr-Nb Pressure Tubing - L. J. Defferding

An order of 84 ft Zr-2.5 wt% Nb pressure tubing was received from Harvey Aluminum Company. The tubing is 2.375 in. OD with a 0.180 in. wall. The extrusion billets were reduced using a "Rockrite Tube Reducing" machine with one-half of the order having 33% cold work, and the remainder having 50% cold work. Difficulty was encountered in producing the 33% cold worked tubing, with cracks developing on one portion of the inner surface during final reduction after an intermediate anneal at 1200 F. The cause of the cracking has not been determined at this time. The burst and crack propagation properties of the tubing will be determined after nondestructive testing has been completed.

PROPERTIES OF IRRADIATED STEEL STRUCTURESLow Alloy Steel Pressure Vessels - D. R. Ireland

This part of the program is concerned with the crack propagation and burst test properties of ASTM A212 B pressure vessels. At the present time pressure vessels of the KER tube size of 2 in. ID and approximately 1/4 in. wall thickness are being investigated. The irradiated specimens will be obtained from GEH-10 baskets having a central 2 in. ID tube length of 45 in. The baskets will be used by R. K. Marshall in the P-7 and M-3 locations of the ETR at Arco, Idaho.

Since A212 B is only available in plate form the tubes are being made by press braking 3/8 in. thick plate, welding two longitudinal seams, and machining to size. The tubes are given a stress relieving heat treatment before being used as baskets. The baskets have been fabricated and the first one will be used in the ETR sometime during the first half of 1965. The unirradiated properties will be determined from tubes made by the same fabrication procedures as the baskets and these tubes are currently being fabricated. Testing procedures for obtaining multiple crack propagation data points from a single specimen are currently being investigated.

INTERNAL DISTRIBUTIONCopy Number

1	F. W. Albaugh - H. M. Parker
2	T. W. Ambrose
3	J. A. Ayres
4-5	T. K. Bierlein
6	S. H. Bush
7	J. J. Cadwell
8	T. T. Claudson
9	D. L. Condotta
10	L. L. Crawford
11	D. H. Curtiss
12	D. R. de Halas
13	R. L. Dickeman
14-15	R. L. Dillon
16	K. Drumheller
17	E. A. Eschbach
18	E. A. Evans
19	T. W. Evans
20	J. C. Fox
21	J. M. Fox, Jr.
22	L. A. Hartcorn
23	H. Harty
24	W. M. Harty
25	R. S. Kemper
26	G. A. Last
27	M. C. Leverett
28	C. G. Lewis
29	L. M. Loeb
30	J. E. Minor
31	W. N. Mobley
32	R. D. Nelson
33	J. W. Nickolaus
34	R. E. Nightingale
35	R. Nilson
36	D. P. O'Keefe
37	R. E. Olson
38	R. S. Paul
39	J. W. Riches
40	W. E. Roake
41	F. A. Smidt
42-43	J. C. Tobin
44	F. W. Van Wormer
45	E. E. Voiland
46	M. T. Walling
47-48	R. G. Wheeler
49	O. J. Wick
50-51	Technical Publications
52-56	Extra
57	300 File Copy
58	HAPO Document Transfer and Accountability

EXTERNAL DISTRIBUTION (Special)Number of Copies

2	Atomic Energy Commission, Washington Division of Research Attn: Don K. Stevens Dorothy Smith
2	Atomic Energy Commission, Washington Division of Reactor Development Attn: W. R. Voigt J. M. Simmons
1	Battelle Memorial Institute Radiation Effects Information Center Attn: W. H. Veazie
3	Center for Nuclear Studies at Saclay P. O. Box #2 Gif-sur-Yvette (Seine-et-Oise), France Attn: Thomas de Montpreville
1	Dow Chemical Company, Rocky Flats Attn: Robert D. Forest
1	European Atomic Energy Community (Euratom) 51-53 rue Belliard Brussels, Belgium Attn: Pierre Kruys
2	G. E. Technical Data Center, Schenectady
1	H. J. Pessl Route 1, Box 892 Hood River, Oregon
2	Richland Operations Office Attn: R. K. Sharp Technical Information Library
1	University of California, Berkeley Attn: J. F. Dorn
1	University of Florida Metallurgical Research Laboratory College of Engineering Attn: R. T. de Hoff
1	University of Michigan Attn: M. J. Sinnott

Ptd.	Standard Distribution	Ptd.	Standard Distribution
3	ABERDEEN PROVING GROUND	1	BUREAU OF SHIPS (CODE 1500)
2	AEROJET-GENERAL CORPORATION	1	CARBORUNDUM COMPANY
1	AEROJET-GENERAL NUCLEONICS	1	CHICAGO PATENT GROUP
2	AERONAUTICAL SYSTEMS DIVISION	1	COMBUSTION ENGINEERING, INC.
1	AEROPROJECTS INCORPORATED	1	COMBUSTION ENGINEERING, INC. (NRD)
		1	DEFENCE RESEARCH MEMBER
1	AIR FORCE INSTITUTE OF TECHNOLOGY	1	*DEL ELECTRONICS CORPORATION
		1	DENVER RESEARCH INSTITUTE
1	AIR FORCE RESEARCH AND TECHNOLOGY DIVISION	1	DOW CHEMICAL COMPANY, ROCKY FLATS
		4	DU PONT COMPANY, AIKEN
1	ALLIS-CHALMERS MANUFACTURING COMPANY	1	DU PONT COMPANY, WILMINGTON
1	ALLIS-CHALMERS MANUFACTURING COMPANY, BETHESDA	1	FRANKFORD ARSENAL
1	ALLISON DIVISION-GMC	1	FRANKLIN INSTITUTE OF PENNSYLVANIA
10	ARGONNE NATIONAL LABORATORY	1	FUNDAMENTAL METHODS ASSOCIATION
1	ARMY ENGINEER RESEARCH AND DEVELOPMENT LABORATORIES	2	GENERAL ATOMIC DIVISION
		2	GENERAL DYNAMICS/FORT WORTH
1	ARMY MATERIALS RESEARCH AGENCY	2	GENERAL ELECTRIC COMPANY, CINCINNATI
1	ARMY MISSILE COMMAND	1	GENERAL ELECTRIC COMPANY, PLEASANTON
1	ARMY RESEARCH OFFICE, DURHAM	6	GENERAL ELECTRIC COMPANY, RICHLAND
1	ARMY TANK-AUTOMOTIVE CENTER	1	GENERAL ELECTRIC COMPANY, SAN JOSE
1	ATOMIC ENERGY COMMISSION, BETHESDA	1	GENERAL NUCLEAR ENGINEERING CORPORATION
1	AEC SCIENTIFIC REPRESENTATIVE, BELGIUM	1	GOODYEAR ATOMIC CORPORATION
1	AEC SCIENTIFIC REPRESENTATIVE, FRANCE	1	IIT RESEARCH INSTITUTE
1	AEC SCIENTIFIC REPRESENTATIVE, JAPAN	1	INTERNATIONAL BUSINESS MACHINES CORPORATION
3	ATOMIC ENERGY COMMISSION, WASHINGTON		
4	ATOMIC ENERGY OF CANADA LIMITED	2	IOWA STATE UNIVERSITY
		2	JET PROPULSION LABORATORY
2	ATOMIC ENERGY OF CANADA LIMITED, WHITESHELL	1	JOHNS HOPKINS UNIVERSITY
4	ATOMICS INTERNATIONAL	3	KNOLLS ATOMIC POWER LABORATORY
1	AVCO CORPORATION	1	LING TEMCO YOUGHT, INC.
4	BABCOCK AND WILCOX COMPANY	1	LOCKHEED-GEORGIA COMPANY
2	BATTELLE MEMORIAL INSTITUTE	1	LOCKHEED MISSILES AND SPACE COMPANY (NASA)
2	BEERS (ROLAND F.), INC.	3	LOS ALAMOS SCIENTIFIC LABORATORY
1	BERYLLIUM CORPORATION	1	M & C NUCLEAR, INC.
1	BLUME (JOHN A.) AND ASSOCIATES	1	MALLINCKRODT CHEMICAL WORKS
2	BROOKHAVEN NATIONAL LABORATORY	1	MARE ISLAND NAVAL SHIPYARD
1	BUREAU OF MINES, ALBANY	1	MARITIME ADMINISTRATION
1	BUREAU OF NAVAL WEAPONS	1	MARTIN-MARIETTA CORPORATION

Ptd.	Standard Distribution	Ptd.	Standard Distribution
1	*MINNESOTA MINING AND MANUFACTURING COMPANY (BRANDT)	1	REACTIVE METALS. INC.
1	MOUND LABORATORY	1	REACTIVE METALS. INC., ASHTABULA
		1	RENSSELAER POLYTECHNIC INSTITUTE
1	NASA LEWIS RESEARCH CENTER	1	SAN FRANCISCO OPERATIONS OFFICE
		2	SANDIA CORPORATION, ALBUQUERQUE
1	NASA MANNED SPACECRAFT CENTER	1	SANDIA CORPORATION, LIVERMORE
2	NASA SCIENTIFIC AND TECHNICAL INFORMATION FACILITY	1	SOUTHWEST RESEARCH INSTITUTE
		1	STANFORD UNIVERSITY (SLAC)
		1	SYLVANIA ELECTRIC PRODUCTS, INC.
2	NATIONAL BUREAU OF STANDARDS	1	TENNESSEE VALLEY AUTHORITY
1	NATIONAL BUREAU OF STANDARDS (LIBRARY)	1	TRW SPACE TECHNOLOGY LABORATORIES (NASA)
2	NATIONAL LEAD COMPANY OF OHIO		
1	NAVAL POSTGRADUATE SCHOOL	1	UNION CARBIDE CORPORATION, CLEVELAND
3	NAVAL RESEARCH LABORATORY	2	UNION CARBIDE CORPORATION (ORGDP)
		5	UNION CARBIDE CORPORATION (ORNL)
1	NRA. INC.		
1	NUCLEAR MATERIALS AND EQUIPMENT CORPORATION	1	UNION CARBIDE CORPORATION (PADUCAH PLANT)
1	NUCLEAR METALS, INC.	2	UNITED NUCLEAR CORPORATION (NDA)
1	NUCLEAR UTILITY SERVICES, INC.	1	U. S. GEOLOGICAL SURVEY, DENVER
1	OFFICE OF ASSISTANT GENERAL COUNSEL FOR PATENTS (AEC)	1	U. S. GEOLOGICAL SURVEY, MENLO PARK
		1	U. S. GEOLOGICAL SURVEY, WASHINGTON
2	OFFICE OF NAVAL RESEARCH	1	U. S. PATENT OFFICE
1	OFFICE OF NAVAL RESEARCH (CODE 422)	2	UNIVERSITY OF CALIFORNIA, BERKELEY
1	OHIO STATE UNIVERSITY	2	UNIVERSITY OF CALIFORNIA, LIVERMORE
1	PETROLEUM CONSULTANTS	1	UNIVERSITY OF PUERTO RICO
4	PHILLIPS PETROLEUM COMPANY (NRTS)	1	WESTERN RESERVE UNIVERSITY (MAJOR)
1	PHYSICS INTERNATIONAL, INC.	4	WESTINGHOUSE BETTIS ATOMIC POWER LABORATORY
1	PICATINNY ARSENAL	1	WESTINGHOUSE ELECTRIC CORPORATION
1	POWER REACTOR DEVELOPMENT COMPANY	1	WESTINGHOUSE ELECTRIC CORPORATION (NASA)
3	PRATT AND WHITNEY AIRCRAFT DIVISION		
1	PURDUE UNIVERSITY	325	DIVISION OF TECHNICAL INFORMATION EXTENSION
1	RADIOPTICS, INC.		
1	RAND CORPORATION	75	CLEARINGHOUSE FOR FEDERAL SCIENTIFIC AND TECHNICAL INFORMATION

*New listing or change in old listing.

